GENERALIZED HYDRODYNAMIC DESCRIPTION OF DUSTY PLASMAS

By

SANAT KUMAR TIWARI

PHYS06200704020

Institute for Plasma Research, Gandhinagar

A thesis submitted to the
Board of Studies in Physical Sciences

In partial fulfillment of the requirements

For the Degree of

DOCTOR OF PHILOSOPHY

of

HOMI BHABHA NATIONAL INSTITUTE

August, 2013

Homi Bhabha National Institute

Recommendations of the Viva Voce Board

As members of the Viva Voce Board, we recommend that the dissertation prepared by **Sanat Kumar Tiwari** entitled "Generalized Hydrodynamic description of dusty plasmas" may be accepted as fulfilling the dissertation requirement for the Degree of Doctor of Philosophy.

PKaw -- **Date :** 29. 10. 2013

Chairman : Prof. Predhiman Kaw

Amita Das. -- **Date :** 29- 10 - 2013

Convener : Prof. Amita Das

Abhijit -- **Date :** 29-10-2013

Member : Prof. Abhijit Sen

-- **Date :** 29-10-2013

Member : Dr. Sudipsen Gupta

Final approval and acceptance of this dissertation is contingent upon the candidate's submission of the final copies of the dissertation to HBNI.

I hereby certify that I have read this dissertation prepared under my direction and recommend that it may be accepted as fulfilling the dissertation requirement.

Amita Das -- **Date :** 29- 10 - 2013

Guide : Prof. Amita Das

STATEMENT BY AUTHOR

This dissertation has been submitted in partial fulfillment of requirements for an advanced degree at Homi Bhabha National Institute (HBNI) and is deposited in the Library to be made available to borrowers under rules of the HBNI.

Brief quotations from this dissertation are allowable without special permission, provided that accurate acknowledgement of source is made. Requests for permission for extended quotation from or reproduction of this manuscript in whole or in part may be granted by the Competent Authority of HBNI when in his or her judgment the proposed use of the material is in the interests of scholarship. In all other instances, however, permission must be obtained from the author.

Sanat Kumar Tiwari

Sanat Kumar Tiwari

DECLARATION

I, hereby declare that the investigation presented in the thesis has been carried out by me. The work is original and the work has not been submitted earlier as a whole or in part for a degree/diploma at this or any other Institution or University.

Sanat Kumar Tiwari

Sanat Kumar Tiwari

To my family

ACKNOWLEDGEMENTS

It gives me great pleasure to pay my sincere thanks to all those who supported and inspired me all along the journey of thesis completion and I hope they will continue to do so in future. Words may not be sufficient to express my gratitude towards my teachers, friends, family and to the Almighty but I learnt keep trying during my thesis period.

Foremost, I would like to express my sincere gratitude to my thesis supervisor Prof. Amita Das for her excellent guidance, help and the time she spent throughout my period of association with her. She always encouraged me for everything I tried to attempt and gave me freedom to learn as much as I could have. The positive attitude I learnt from her will remain with me for ever. Madam, though hard to acknowledge your contributions, I thank you for everything you did for me to make my Ph.D. a success.

I am extremely grateful to Prof. Predhiman Kaw for all academic discussions during my thesis period. Each time I discussed, I learnt a lot and got enriched with several novel ideas. Meeting with you was always an experience for me.

I would like to thanks Prof. Abhijit Sen and Dr. Sudipsen Gupta for their useful suggestions which helped me to improve my thesis. A special thanks to Prof. Sen for those encouraging "Good"s which kept me always at high spirits.

I wish to thanks Prof. R. Singh, Dr. Prabal Chattopadyay, Dr. Joydeep Ghosh, Dr. Subrato Mukharji, Dr. R. Ganesh, Dr. Mrityunjay Kundu, Dr. Asim Chattopadyay, Dr. Surya P. Pathak, Prof. Ajai Kumar, Dr. S. Pradhan and Dr. L. M. Awasthi for their support and encouragement during my Ph.D. tenure. I would also like to convey my sincere thanks to IPR library, IPR administration and computer center staff for their kind support during my thesis period.

Thanks to my seniors (Dr.) Pintu, Manas, Rajneesh, Bhaskar, Kishore, Ritu and Maya P. N., Sharad, Sunita Negi, Jugal, Satya, Sekhar for providing me a homely atmosphere in hostel and all the support whenever I needed. I would like to thanks Gurudatt, Vikram Narang, Prabal, Ujjawal, Khitish, Ashwin, Sayak, Manjit, Neeraj, Roopendra, Vibhu, Akanksha, Vidhi, Deepa, Mangilal, Harish, Megharaj, Sandeep, Dushyant, Dr. Swati, Dr. Sanjay, Dr. Satish and Dr. Sarveshwar for their wonderful company in Hostel and institute. I enjoyed games, hot debates, light moments and discussions (society relevant topics dominated) with them as it helped me to overcome the pulses of frustration during Ph.D. Thanks to Piyush, Sapna, Akshay, Amit, Pratibha madam and Jasraj for making the IPR atmosphere very friendly and pleasant to me.

A special thanks to Dr. Vikrant and Dr. P. N. Maya for their support while initial stage of Ph.D., the time, I am sure they showed lot of patience and taught me the alphabets of plasma and linux. My sincere thanks to Dr. Bhavesh who is responsible for most of numerical knowledge I gained in my later years of Ph.D. I enjoyed working on variety of physics problems and numerical techniques with Vikram Dharodi, Dr. Sita, Dr. Bhavesh, Dr. Sunil, Deepa, Chandrasekhar, Gaurav, Mriganka and Piyush as it all added a lot of intellectual property to my knowledge beyond my specific Ph.D. topic. Thanks to Dr. Gurudatt, Dr. Sita, Sushil and Vikram Dharodi for extended discussions on different physics issued which always helped me to get rid of my confusions and in a clear understanding of those topics. I am indebt to Avadhesh for all his technical support and all other official supports as it helped me to focus primarily on my research work.

My colleagues and friends from theory room Dr. Sita, Vikram Dharodi, Avadhesh and Dr. Bhavesh are always special to me. They were around me in all my good, bad and ugly days and their unconditional support took me out of all hardships during thesis tenure. Thanks for being special to me and I wish never to forget you all.

Bach-mates are always special as they give us freedom to share everything from academic topics to very personal things. I will thanks Sushil, Rameshwar and Pravesh for their support and making Ph.D. life easier and full of light moments. Thanks to Sushil and G. Veda Prakash for being too supportive, being true critic and for always listening me with all their patience.

Thanks to Pragya, Rishi, Sandeep, Amrendra, Niharika, Anchal, Saurabh and Aditya Roshan for listening me at the times when I really needed to be listened. My family, Yes indeed it is your faith in me that finally made me to come upto this moment and this is your unconditional and selfless support which will encourage me to come out of all sort of odds in my life.

Don't worry God, I haven't forgotten you. Thanks for all this you gave me and much more awaited for me in your time plan !

Contents

Abstract

A plasma impregnated with heavier macroscopic sized dust particles, is termed as a dusty plasma when the charged (due to electron/ion impingement on the dust surface) dust species behaves in a collective manner. The typical low thermal velocity and high charge density on the macroscopic dust species often renders such a dusty plasma medium in a strongly coupled state. Such dusty plasmas can be prepared artificially and/or get formed inherently in certain laboratory situations, for example in Tokamaks, rocket exhausts, plasma torches etc. In addition they are also ubiquitously present in astrophysical environments such as Planetary ring systems, Stars, Solar nebulae etc.

In recent years, the dusty plasma medium has attracted a lot of attention due to its variety of applications and the possibility of it being able to address several interesting fundamental physics issues in a simpler setting. One of the main attributes in the case of the dusty plasma medium is the ease with which it can be prepared/found in a strongly coupled regime. In this regime, the dusty plasmas can mimic the physical characteristics of a broad range of fluids (simple viscous as well as elastic nature are exhibited) and crystalline solids as well. The description of such a fluid behavior (visco - elastic features) has been in the past provided by the Generalized Hydrodynamic (GHD) formulation for the understanding of the linear response of the medium. Such a study has revealed existence of a modified dispersion characteristics of dust acoustic waves and the existence of the transverse shear waves. These predictions have been experimentally verified and have also been reproduced by the MD (Molecular Dynamics) simulations.

The GHD model has been employed in this thesis to carry out investigations of the dusty plasma medium in the nonlinear regime. In particular the 1-D response of

the medium has been explored by studying the permissible coherent solutions and their evolution. In 2-D the characteristics of shear flow driven Kelvin - Helmholtz (KH) instability has been studied extensively for this particular medium. The observation of small scale structure formation in the context of KH evolution has led us to a detailed investigation on studying spectral evolution of the turbulent fluctuations for this medium.

Some highlights of our investigation are:

- The observation of readily accessible and stable singular cusp structures dithering at the wave breaking point in our 1-D simulations for weakly coupled dusty plasma system.

- The weakly nonlinear strong coupling 1-D dusty plasma system has been shown to follow a novel paradigm of Hunter Saxton (HS) equation in contrast to the usual KdV equation followed by the system in the weak coupling limit. The HS equation is known not to permit smooth soliton solutions. The equations instead permit both conservative and dissipative singular shock solutions. This is a characteristic feature of elasticity in the medium. The evolution of the GHD equations in strong coupling 1-D limit also demonstrate the formation of shocks.

- In 2-D, the properties of the shear flow driven Kelvin - Helmholtz (KH) instability has been studied in detail. The compressibility and dispersion effects in the weak coupling case show a reduction in the growth rate and the domain of the unstable mode wave numbers are also found to shrink. These features are borne out in the nonlinear simulations. In the nonlinear state, the coalescence of smaller vortices ultimately lead to the formation of long scale vortex structures.

- In the strong coupling limit the growth rate curve is bound between the two curves involving the inviscid and viscous cases (with infinitesimal relaxation time) of the weak coupling case. These features of the growth are borne out in the simulations. In contrast to the weakly coupled case the nonlinear regime of the strongly coupled medium shows a novel phenomena of recurrence in which there is a repetitive formation of long scale structures interrupted by the appearance of short scales again and again. This observation show that the process of spectral cascade in the strong coupling regime has to be fairly complex.

- The spectral cascade features were studied by employing an initial spectrum of random fluctuations around specific regions of the wave numbers. It is observed that unlike the turbulent spectra of normal fluids, in this case, there cannot be any characterization in terms of a single power law. Instead one observes a break in the spectra, with different regions exhibiting different forms. The evolved spectrum also does not show any universality and has dependence on the initial content of the spectral excitations. These features are understood in terms of the memory relaxation parameter intrinsic to the GHD equation.

It is important to carry out further studies on the GHD depiction of the medium and constitutes the future scope of the thesis. Experimental confirmation of our observations would be interesting and important. The recent observation by Teng *et al.*, on the singular cusp solutions are in line with our simulation studies [1]. However, other phenomena related to turbulent spectral cascade properties can be experimentally investigated.

List of Figures

List of Tables

List of Publications

Publications in Peer Reviewd Journals:

- **Sheared flow driven instability in Visco-Elastic fluids**,

  Sanat Kumar Tiwari, Vikram Singh Dharodi, Amita Das, Bhavesh G. Patel and Predhiman Kaw

  Submitted

- **Turbulence simulation in visco-elastic medium**,

  Sanat Kumar Tiwari, Vikram Singh Dharodi, Amita Das, Bhavesh G. Patel and Predhiman Kaw

  To be submitted

- **Exact propagating nonlinear singular disturbances in strongly coupled dusty plasmas**,

  Amita Das, Sanat Kumar Tiwari, Predhiman Kaw and Abhijit Sen

  Under communication, New Journal of Physics

- **Observation of sharply peaked solitons in dusty plasma simulations**,

  Sanat Kumar Tiwari, Amita Das, Predhiman Kaw and Abhijit Sen

  New Journal of Physics 14, 063008 (2012)

- **Kelvin-Helmholtz instability in a strongly coupled dusty plasma medium**,

  Sanat Kumar Tiwari, Amita Das , Dilip Angom , Bhavesh G. Patel , Predhiman K. Kaw

  Physics of Plasmas 19, 073703 (2012)

- **Kelvin - Helmholtz instability in a weakly coupled dust fluid**,
  Sanat Kumar Tiwari, Amita Das, Predhiman Kaw and Abhijit Sen
  Phys of Plasmas 19, 023703 (2012)

- **Longitudinal singular response of dusty plasma medium in weak and strong coupling limits**,
  Sanat Kumar Tiwari, Amita Das, Predhiman Kaw and Abhijit Sen
  Physics of Plasmas 19, 013706(2012)

- **Nonlinear wave propagation in strongly coupled dusty plasmas**,
  B. M. Veeresha, S. K. Tiwari, A. Sen, P. K. Kaw, and A. Das
  Physical Review E 81, 036407 (2010)

Conferences/Schools:

International Participation

- Observation of cusp structures in 1-D dusty plasma simulations. (Talk)
  Sanat Kumar Tiwari, Amita Das, Abhijit Sen and Predhiman Kaw
  ICOPS, Chicago, Illinois, 26th - 30th June, 2011.

- Kelvin Helmholtz Instability in dusty plasmas.(Poster)
  Sanat Kumar Tiwari, Amita Das, Abhijit Sen and Predhiman Kaw
  ICPDP,Garmisch-Partenkirchen, Germany 15th - 20th May, 2011.

- Elastic Turbulence: In context of dusty plasmas. (Poster)
  Sanat Kumar Tiwari, Vikram Singh Dharodi, Amita Das, Bhavesh G. Patel and Predhiman Kaw
  ICCPPNDS, IPR, Gandhinagar, India November 2012.

- Sheared Flow Instability in Dusty Plasmas: Fluid and Particle Approach. (Poster)

  Sanat Kumar Tiwari, Amita Das, Bhavesh G. Patel and Predhiman Kaw

  School on Hands-On Research in Complex Systems, ICTP, Italy, 1-12 July 2013.

National Participation

- Nonlinear Studies of strongly correlated dusty plasma system.(Talk)

  Sanat Kumar Tiwari, Amita Das, Abhijit Sen and Predhiman Kaw

  24th National Symposium On Plasma Science and Technology, 8-11 Dec, 2009, Hamirpur, India.

- Observation of various nonlinear structures in 1-D dusty plasma simulations. (Poster)

  Sanat Kumar Tiwari, Amita Das, Abhijit Sen and Predhiman Kaw

  1st Scholar's Colloquium, IPR, Gandhinagar, India April 2011.

- 2-D Turbulence in Strongly Coupled Dusty Plasmas. (Poster)

  Sanat Kumar Tiwari, , Vikram Singh Dharodi, Amita Das, Bhavesh G. Patel and Predhiman Kaw

  National Symposium on Plasma Science and Technology- Plasma-2012, Pondicherry University, India, December 2012.

- Solitary structures Near wave breaking point in dusty plasmas. (Talk and Poster)

  Sanat Kumar Tiwari, Amita Das, Abhijit Sen and Predhiman Kaw

  1st PSSI-Plasma Scholars Colloquium, IPR, Gandhinagar, India July 2012.

1

Introduction

1.1 Introduction

In a regular electron ion plasma, the presence of heavier (typical mass of 10^{-10} – 10^{-15} Kg), macroscopic (typically micron sized) particles often act as a third component of the plasma. The constant impingement of electrons and ions on the surface of these heavy particles causes it to acquire charge thereby making it act as third charged species in the plasma. Such a plasma is termed as *Dusty Plasma* medium. The dusty plasmas possess a variety of interesting properties which have motivated considerable theoretical as well as experimental interest in this area [9–17]. The relevance of such studies is evident from the ubiquitous presence of dusty plasma. The dusty plasmas are found as natural plasmas (planetary ring systems, stars, cometary tails, lightening, ionosphere of Earth, Solar nebulae, Zodiacal lights etc) as well as artificially produced plasmas (experimental dusty plasma devices, tokamaks, Rocket exhaust, plasma torches, industrial plasma applications etc) [11,13,15,18–21].

The features unique to the dust component are its large size, mass (in comparison to electron and ion species) and high charged state. The massive sized dust particles introduce a host of collective phenomena of slow time scales and larger length scales. The high charge state often ensures that the dust component in the plasma is in a strong coupling regime, wherein the interparticle potential energy exceeds the thermal kinetic energy of the dust species. The dusty plasma, thus, can often be found in a crystalline state. Even when it is in fluid regime, as the coupling parameter Γ (ratio of electrostatic potential energy to average thermal energy) increases, the medium shows behavior similar to the complex fluids. It aquires elastic properties as the coupling parameter is increased, a property that is innate to complex fluids. These properties directly relate the dusty plasma medium with other areas of physics, e.g. condensed matter, complex fluids systems etc [9, 22]. Furthermore, an additional advantage in the context of dusty plasma is due to the macroscopic size of the dust species. It ensures that the dusts as well as its collective dynamics can be easily visualized by simple cameras. Thus, the physics associated with kinetic effects occurring at atomistic levels which are normally impossible to visualize, in this case, can be seen and explored by simple economic experiments. These advantages have been recognized and have contributed to an increased research activity in this area lately.

A wide range of coupling parameter can be observed in simple laboratory experiments of dusty plasma medium, wherein it displays features as diverse as that ranging from simple charged fluid to complex non Newtonian elastic fluids and even crystalline solids. Such a diverse behavior has posed theoretical challenge for its description. At very high values of the coupling parameter where the dusty plasma medium behaves like a crystalline solids, concepts of condensed matter physics can be borrowed and applied. However, in the intermediate regime of coupling parameter where the medium neither behaves like a solid and/or a freely flowing fluid, the difficulty arises. In this domain, lately, there have been attempts at using a Generalized Hydrodynamic (GHD) prescription for the depiction of the dust fluid. In the GHD description the strong coupling effects are mocked up as a relaxation time parameter of the medium. A normal fluid has an instantaneous response. The finite values of the relaxation time parameter are suggestive of the elastic properties of the medium. Thus, using the GHD description one hopes to mock up the entire domain from normal fluid to a complex visco-elastic fluid. This model has predicted a host of properties associated with the linear normal mode of the system. The changed dispersion curve for the longitudinal acoustic mode and the existence of transverse shear modes being some such features. These predictions have been successfully verified in the experiments [23, 24]. Keeping this in view it is then important to understand the nonlinear implications of the GHD model description. This is the prime objective of the studies carried out in this thesis. In the next section of this Chapter we introduce some concepts and parameter definitions associated with the dusty plasma medium. We also discuss in some quantitative detail wherein the dusty plasma medium would be in the strong coupling parametric domain to behave as a complex fluid. In section 1.3, we briefly survey some of the model descriptions that have adopted for the description of this medium. This includes the Generalized Hydrodynamic (GHD) description of the dust species. The GHD model being a basis of the nonlinear studies of the thesis has been discussed in detail in Chapter 2. A brief review of earlier works on the dusty plasma medium has been provided in section 1.4. Section 1.5 summarizes the salient aspects of the thesis.

1.2 Dusty Plasmas

The presence of micron sized dust particles (macroscopic in comparison to the electron and ion species) in a conventional electron - ion plasma can lead to the formation of a dusty plasma medium. The macroscopic particles get charged by the constant bombardment of electron and ion fluxes on its surface and act as an additional species in the plasma. When conditions for these additional species to behave in a collective fashion are satisfied, the system is identified as a dusty plasma. The accumulation of charges on the dust species can be as high as 10^4 electronic charges. The random thermal fluctuation of these particles can, however, be quite small. This additional species can, therefore, be easily in strong coupling regime, as Γ, the coupling parameter can be quite high for these species. The traditional plasma is characterized by certain parameters such as temperature associated with the species, the number density etc. Often, instead of directly talking about these parameters one mentions certain length and time scales dependent on these parameters, which define the characteristic features of the plasma. For instance length scale such as Debye length $\lambda_D = \sqrt{\frac{\lambda_{de}^2\lambda_{di}^2}{\lambda_{de}^2+\lambda_{di}^2}}$ (Here, $\lambda_{de,i}^2 = \frac{k_B T_{e,i}}{4\pi n_{0e,i}e^2}$), electron plasma frequency $\omega_{pe} = \left(\frac{4\pi n_{0e}e^2}{m_e}\right)^{1/2}$ and acoustic speed $c_s = \lambda_D\omega_{pe}$ etc., (which are dependent on temperature and number density) are invoked to represent a traditional plasma. These scales have specific physical implications (e.g. Debye length defines the characteristic screening length of a charge species and the plasma frequency indicates the response time scale of the medium to electric fields). In a similar fashion the dusty plasma is also characterized by certain parameters and the associated scales. We discuss about them now.

The scales, dust radius (r_d), inter-dust separation (a_d) and plasma Debye length (λ_D) decide the role of charged dust grains in plasma. If $r_d << \lambda_D < a_d$, the dust grains get shielded by opposite charge species and will not participate in collective dynamics of plasma and occasionally known as "Dust in plasma", while for $r_d << \lambda_D > a_d$, the charged dust grains show a collective behavior and hence the medium is called dusty plasmas. Because of inclusion of charged dust species, the plasma becomes even richer with several additional new modes arising solely due to the collective behavior of charged dust grains. The Dust Acoustic Wave (DAW), Dust Ion Acoustic Wave (DIAW), Dust Acoustic Solitons (DAS), Dust Ion Acoustic Solitons (DIAS) , Dust shocks are among those novel modes. For DAW's, the inertia comes from dust species while the restoring force comes from electrons and ions. Contrary to this, for DIAW's, the ions provide inertia (As dusts are assumed to be stationary) and restoring force comes from electrons while the dust effects introduced through Poisson's equation. The length and time scales associated with these modes are very large and typically of the order of millimeter in length scales and several milliseconds in time scales.

The dust grains are intrinsically neutral heavy and large sized particles. Once the grains are introduced in a typical electron-ion plasma, they face heavy flux of electrons and ions over its surface. As the mobility of electrons is higher than that of ions, the dust grains gets negatively charged. The typical charge on dust grains is 10^2e-10^5e . In some occasions, when the dust particles undergo emission of electrons because of radiation sources like ultraviolet lights, secondary electron emission, thermionic emission, field emission etc., the dust grains may also be found to be positively charged. The charges on dust species fluctuate because the electrons/ions may leave the surface of dust grains in course of collision with other ions or dust grains, because of thermal effects or other radiative processes in plasma.

The dust grains experience variety of forces in plasma medium. The Drag forces (specially ions and neutrals), Electromagnetic forces, Gravitational force, Polarization force, Radiation pressure forces and Therophoretic force are of quite interest in the context of dust fluid. As the scope of present thesis is to study collective nonlinear phenomena and effect of strong coupling over such phenomena, the inclusion of all such forces is avoided to keep the dynamical equation simple yet suitable enough to study prime interest of thesis.

A very interesting feature of dust grains is that they could be found in crystalline form under suitable conditions. It is observed in several naturally occurring dusty plasma mediums [25] as well as in laboratory plasmas [26, 27]. The heavily charged dust particles often feel the presence of other dust particles because they are not completely shielded in plasma (as $\Gamma \geq 1$). Because of this, they are often found to be in strong coupling regime and form crystalline structures as in most of solids.

The coupling of plasma species is measured with the *coupling parameter* Γ which is the ratio of average Coulomb energy to average kinetic energy of particles in plasma. When the value of Γ exceeds unity, the species are termed to be strongly coupled. For a classical one component plasma (OCP) with charge Ze on its particles,

$$\Gamma_{OCP} = \frac{(Ze)^2}{4\pi\epsilon_0 a k_B T} \tag{1.1}$$

Here, a is the average interparticle separation between particles in OCP. The plasma normally contains more than one charged species like electrons, ions with multiple charges, charged dusts etc. It has been estimated in Ichimaru *et al.* that for densities of order $10^{11} - 10^{16} cm^{-3}$ and temperature ranging from $10^4 K$ to $10^8 K$ with $Z \sim 1$, the possible range of Γ parameter is $10^{-7} - 10^{-3}$. In nature and laboratory experiments, we occasionally find the plasmas of same order of density and temperature of electrons and ions. This is the reason, the classical plasmas are found to be in weak coupling regime hence explaining their thermodynamical proximity with ideal gases [28].

The coupling of plasma species could increase if they are highly charged or they are compressed so hard that the effect of interparticle coulomb interaction enhance significantly. There are some examples in astrophysical scenario when such conditions are found to be achieved. It was observed that inside evolved stars whose inner core is highly compressed, the ion species were in strongly coupled state with coupling parameter ranging from 10 to 200 even though they are in classical regime [29].

With the advent of laser technologies, it is now possible to generate highly compressed plasmas with density upto $\sim 10^{26} cm^{-3}$. In this density regime, even the electrons could be found to be strongly coupled [30].

The strongly coupled electrons and ions could also be found in ultracold plasmas. The plasmas with $T_e \sim 100mK$ and $T_i \sim 10\mu K$ with density of order $10^9 cm^{-3}$ had been created for which the coupling parameters for electrons and ions were found $\Gamma_e \sim 30$ and $\Gamma_i \sim 10^5$ respectively causing the electrons to behave as strongly coupled liquids while the ions will behave as *Wigner* solid [31,32].

Strongly coupled dusty plasmas

In contrast to two component electron-ion plasma, the dust species are frequently found to be in strong coupling regime. As the dust particles get shielded with electrons and ions in plasmas, the coupling parameter can be redefined as the ratio of Yukawa potential energy to kinetic energy of particles [10,31].

$$\Gamma = \frac{(Z_d e)^2}{4\pi\epsilon_0 a_d k_B T_d} exp\left(-\frac{a_d}{\lambda_D}\right) \tag{1.2}$$

The ratio a_d/λ_D is known as screening parameter κ which takes care of shielding due to background plasma. The high dust charge (typically $10^2 e - 10^5 e$) and low dust temperature makes the coupling parameter $\Gamma > 1$ even at lower dust density. Thus the dusty plasmas could be found in gaseous, liquid as well as ordered crystalline phase. Also, it is found that the phase transition occur under suitable physical condition [26].

1.3 Model description for dusty plasma medium

The conditions for strong coupling can easily be satisfied in the context of dusty plasma medium. This makes the task of its description fairly challenging. We briefly summarize some attempts at its description in this particular section.

1.3.1 Quasilocalized Charge Approximation (QLCA) approach

The dusty plasmas, as described earlier, could be found in gaseous, liquid or solid phase depending upon the coupling parameter Γ. While the weakly coupled dusty plasmas ($\Gamma << 1$) are close to fluid like and Vlasov description of plasmas, the strongly coupled plasmas behave like crystals ($\Gamma \rightarrow \infty$). The collective modes in fluid plasmas come from its continuum behavior and the same come from phonons interactions in crystals. The QLCA approach assumes the localization of dust particles (within the limits of relaxation time). The sites of localization are assumed to evolve over time scales longer than relaxation time to new equilibrium locations. This is the reason these dust species are assumed as *Quasilocalized*. A detailed description of this approach could be found in *Kalman et al.* [33] and references therein. In the QLCA approach, the particles are assumed to be trapped in fluctuating potential wells, distributed at random locations in system. These random locations of potential wells are correlated with each other. The trapped particles oscillate in the momentary potential wells and cause the excitation of phonon. These potential wells further dissolve into different configuration after an average lifetime, hence, causing the trapped particles to diffuse from its temporary locations [33, 34]. The QLCA approach also assumes that the amplitude of the excursion of oscillations as well as excursion due to external perturbations should remain smaller than the interparticle separation. This assumption is in accordance with the harmonic approximation for phonon excitations but also limits the QLCA approach only upto linear response studies in strongly coupled plasmas. Also, by the definition, QLCA approach does not explain the weak coupling regime of plasmas. The QLCA approach is reliable for higher $\Gamma(\geq 10)$, i.e., at the onset of localization. The model successfully explains the longitudinal and transverse modes in Coulomb and Yukawa systems of particles [35, 36].

1.3.2 Molecular Dynamic (MD) simulation approach

In MD approach, the exact dynamics of each particle is governed through some known form of interaction potential. The dusty plasmas typically consist of three different charged species (of different densities) interacting through Coulomb potential. However, it is computationally very expensive to study such systems. It is found that the electrons and ions, compared to dust mass, behave like inertia-less medium and merely provide the shielding effect over dusts collective dynamics. Hence, if the electrons and ions are assumed to serve only as the shielding background for dust species, the dusty plasma could be considered as a system with only dust species interacting through a shielded Yukawa potential.

$$U(r) = \frac{(Z_d e)^2}{r} exp(-r/\lambda_D) \tag{1.3}$$

This assumption makes the MD simulations feasible for realistic dust density. The MD simulations have been performed to study DAWs, propagation of shock, melting of dust crystals, elastic properties of dusty plasmas, viscosity measurements etc, in dusty plasma medium treating them as Yukawa system [37–40]. Such simulations typically require few thousands of dust particles and hence are economic in computation. Apart from these small scale simulations, there have also been few attempts to study fluid instabilities and other collective phenomena in dusty plasmas treating them as Yukawa fluids [41, 42]. Molecular Dynamic simulations are based on the particles dynamics which is governed by their interaction potential. Most of MD simulations carried out in context of dusty plasmas assume the charged dust species interact with each other through *Yukawa* potential.

1.3.3 Particle In Cell (PIC) simulations approach

In this method, the plasma is approximated by substitution of original number of plasma particles with substantially smaller number of super-particles. The charge and mass of these super-particles are proportionally larger than that of original plasma particles. However, the ratio of charge to mass remains the same, hence, PIC method makes it feasible to simulate plasma systems with large number of particles. Thus, in principle, the dusty plasmas could be studied using PIC simulation, with all three charged species i.e. electrons, ions and dusts. The phenomena related to collective dynamics of electrons, ions and dust species have a large variation in terms of time scales which ranges from electron plasma period (ω_{pe}^{-1}) to dust plasma period (ω_{pd}^{-1}). To simulate a dusty plasma medium where the time scales of all three species could be resolved, will again require lots of computational resources as well as time. It again makes the PIC technique less practical to simulate the dusty plasmas. However, a hybrid approach could be adopted where the electrons could be assumed as negatively charged fluid while the ions and dust species could be assumed as particles. This would help us study the more exact description of dusty plasmas taking ion dynamics into the consideration.

1.3.4 Generalized Hydrodynamic (GHD) approach

The GHD approach assumes the continuum fluidity primarily responsible for the collective modes in dusty plasmas. The solid like elastic properties have been coupled with viscous nature of dust fluid phenomenologically. In this way, the model describes the dusty plasmas as *Visco-Elastic* fluids. The coupled fluid and soild properties of such plasmas have been incorporated in terms of *Visco-Elastic* nature of dusty plasma fluid. This model has been of prime focus to present thesis work. More detailed description on the adoption of this model to study nonlinear phenomena in dusty plasma has been provided Chapter 2.

1.4 Review of earlier works

We now briefly review earlier studies that have been made to understand the system of dusty plasma medium. There have been both theoretical and experimental activities towards understanding this particular medium. Most theoretical studies have been directed at understanding the features of linear and/or weak nonlinear response of this medium in weak coupling regime. In experimental work strongly nonlinear response as well as strong coupling regime of this medium has also been explored.

1.4.1 Theoretical work

The study related to dusty plasmas have been of prime interest for long time because of its strong presence in astrophysical scenario. Previously, the studies have been carried out considering dust species only as a neutralizing background to the typical e-i plasma. For example, Angelo *et al.* has studied the Kelvin-Helmholtz instability in astrophysical plasmas treating dust species as neutralizing background for electron-ion plasma in external magnetic field [18].

It was first time at the beginning of $90's$ when Rao *et al.* first presented a theoretical description for the existence of DAW's solely due to collective dynamics of dust species in plasma [43]. The existence of DIAW's has been first presented by Shukla *et al.* [44]. The concept of DA shocks has been stated by Eliasson *et al.* [45] in weakly coupled dusty plasma medium. The formation of shocks has been predicted for the case of strongly coupled dusty plasmas using a GHD model by Shukla *et al.* [46]. However, the nonlinear adaptation of GHD model by the authors does not preserve the Galilean invarience. More on this will be discussed in Chapter 2. The nonlinear coherent DA solitons has been predicted theoretically by Rao *et al.* as the solution of Korteweg-DeVries (KdV) equation in one dimension which is obtained by integrating fluid equations along with Poisson's equation in weak nonlinearity regime [43]. Since then, the study of these localized nonlinear structures have been of prime interest in 1-D nonlinear studies of dusty plasmas [47–49].

Apart from studies of collective modes in plasma due to dust species, lot of effort have been made to study various type of forces acting on dust species. Because of high dust charge and large mass, many kinds of force have significant response on them, whereas they are often negligible for electron-ion plasma. The presence of Polarization force on dust grains in a nonuniform plasma medium is first stated by Farouki *et al.* [50]. Later the effect of Polarization force on DAW and DA solitons has also been studied [51, 52]. The plasma drag forces has been first studied by Northrop *et al.* because of coulomb collisions [53]. Recently a fully self consistent ion drag force calculation has been made for dust in collisionless plasma in the presence of external electric field [54].

Charging of dust particles is also an important phenomena as because of change in physical conditions, the charge on dust species varies [55]. Effect of dust charging has been studied on DAWs [56] and Rayleigh-Taylor instability in dust fluids [57].

The strongly coupled dusty plasmas have been extensively explored through various analytical models and simulation techniques such as Molecular dynamic (MD) simulations and Particle in Cell (PIC) simulations. While analytical models have been given by Kalman *et al.* based on Quasi Localized Charged Approximation (QLCA) approach, Murillo *et al.* based on Dynamic Local Field Correction (DLFC) and Kaw *et al.* based on Generalized Hydrodynamic approach [35, 58, 59]. The strongly coupled dusty plasmas (or Yukawa liquids) has been explored using MD simulations by Murillo in his many articles covering from excitation of acoustic wave and study of strong coupling effects on these modes, existence and properties of transverse shear waves, viscosity measures for strongly coupled yukawa fluids/dust fluids etc [37, 38, 60–62].

It was first Ikezi who predicted theoretically the existence of dust solids [63].

The Dust Lattice Waves (DLW) has been first studied by Melandso *et al.* [64].

The generalized Hydrodynamic model has been proposed to study the dynamics of strongly coupled dusty plasmas [59] which predicted the phase reversal phenomenon in longitudinal dispersion and existence of transverse shear waves in such plasmas. Since then, the model has been used to look over the strong coupling effects on DAW and DA shock waves [46, 65].

The fluid instabilities in dusty plasma medium has also been studied in past. The Kelvin - Helmholtz (KH) instability has been analyzed with significant details in past. The instability arises due to sheared flow velocity in fluids [66, 67]. Angelo *et al.* first time introduced the sheared flow instability in a magnetized dusty plasma [18]. Birk *et al.* and Wiechen *et al.* presented the simulation studies of K-H instability in astrophysical scenario [12, 68]. They have studied extensively the nature of instability in noctilucent clouds with magnetized, partially ionized, different polarity of charge. The KH instability has also been studied in Yukawa liquids with strong coupling effects using MD simulation technique [41].

1.4.2 Experimental studies

First experimental observation of DAWs and DIAWs have been made by Barken *et al.* [6, 69]. Since then many experimental observations of DAW's have been made in weakly as well as strongly coupled dusty plasma [24, 70, 71]. The Dust Ion Acoustic (DIA) Solitons and DIA Shocks has been observed experimentally by Nakamura *et al.* [72, 73]. These observations also show the damping of solitary waves due to ion-dust collisions and kinematic viscosity. The DA shocks has been observed in experiments by Merlino *et al.* [74] and the experimental observation of DA solitons has been made by Pintu *et al.* [4]. The first experimental study of DA shocks under microgravity condition has been presented by Samsonov *et al.* [75] and then further, the author also studied the melting of shock waves in 2-D dusty plasma crystals [76]. The existence of transverse shear waves and phase reversal phenomenon of DAWs in strongly coupled dusty plasmas have been observed experimentally by Pramanik *et al.* and Pintu *et al.* [4, 23] which was the verification of earlier such prediction using GHD description of dusty plasma [59]. Nunomura *et al.* has also observed the transverse shear waves in a monolayer suspension of charged dust species [77]. They have also calculated the charge on dust particle by comparison of experimental results with a theoretical result based on Yukawa description of dusty plasmas. The

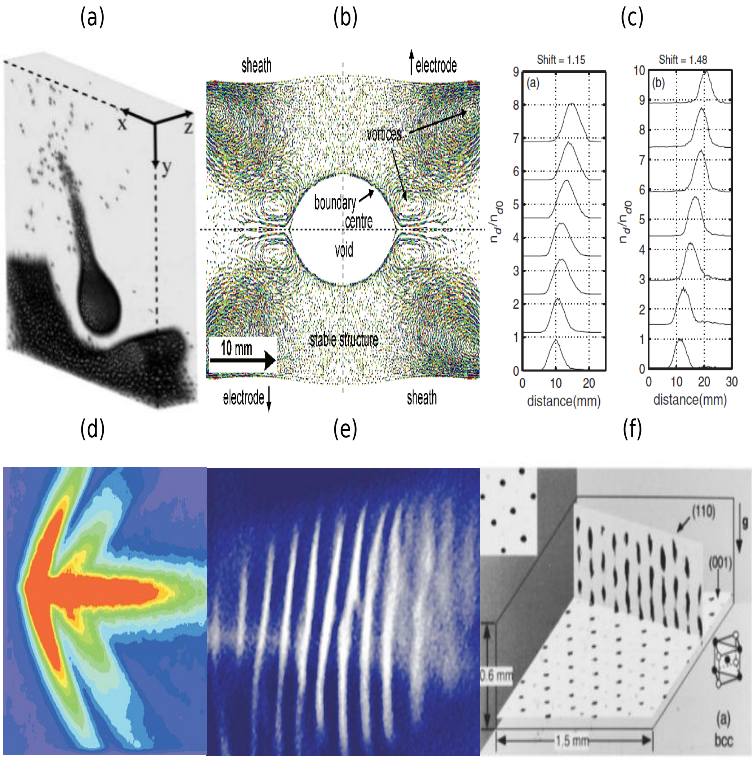

Figure 1.1: Experimental observations in dusty plasmas for (a) Blobs and bubbles by Schwabe *et al.* [2], (b) Dust void and formation of vortices by Nefedov *et al.* [3], (c) Dust solitary wave propagation by Pintu *et al.* [4],(d) Mach cones observed by Melzer *et al.* [5], (e) Excitation of dust acoustic waves from Barken *et al.* [6] and (f) 3-D dust crystal formation by Pieper *et al.* [7].

different kind of forces acting on dust particles have also been studied extensively. The Thermophoretic force acts on dust species because of a temperature gradient in neutral gas. The thermophoresis has been found to counteract gravity and lifting up (suspending) the dust particles in Rothermel *et al.* [78]. The experimental verification of existence of polarization force came with Melzer *et al.* [79]. Nitter *et al.* gave a nice description of drag forces on dust particle in rf and DC glow discharge plasmas [80].

The first experimental observations of dust crystals have been reported by Chu *et al.* and Thomas *et al.* [3, 26, 27, 81]. Further, some elaborated studies made about the properties of 2-D and 3-D dust crystals in plasma [7]. Experimental observations of longitudinal dust lattice waves have been reported by Homann *et* *al.* [82]. Further, the author has also studied the screening length of dust particles excitation of lattice waves through lasers [83].

Selwyn *et al.* has encountered the dust as contamination suspending at the sheath boundaries [84]. Charged dust species has also been found in many industrial and laboratory devices such as plasma torches and magnetic fusion machines like tokamaks [85]. Winter *et al.* discusses the different mechanisms for dust formation in fusion devices and the growth of dust particulates during plasma discharge process [86].

The KH instability manifests in nature viz. oceans, clouds, Saturn's rings, solar corona, Jupiter's red spots etc as well as its study is applicable in inertial confinement fusion, Q-Machines etc [87–89]. Most of astrophysical scenarios where KH instability has been observed, belong to dusty plasmas. The first experimental observation for KH instability in dusty plasmas has been made by Luo *et al.* [20]. Several dusty plasma experiments also report the dust flows and rotations. Konopka *et al.* shows the rotation of dust crystals in a vertically aligned magnetic field. They have shown the dust rotation as a rigid body as well as sheared flow rotation [90]. The Rayleigh-Taylor instability has also been observed experimentally in dusty plasma experiments [91].

1.5 Thesis organization

The Generalized Hydrodynamic (GHD) description for the dynamics of dust species has been successful in providing the description of the linear response of the dusty plasma medium. It is, therefore, important that the nonlinear implications of such a model description be investigated. This is the prime motivation of the work carried out in this thesis. We have investigated various nonlinear features predicted by the GHD model.

In Chapter 2, we describe the adaptation of the Generalized Hydrodynamic model (GHD) for the description of the dusty plasma medium. Issues such as the preservation of the Galilean invariance, which have been overlooked in previous nonlinear adaptation of this particular model, have been addressed suitably by us. This model is then employed for numerical simulation and theoretical analysis.

Chapter 3 discusses the 1-D studies carried out on a weakly coupled dusty plasma system. These studies could be categorized in three regimes of nonlinearity. Primarily, in linear regime, small sinusoidal perturbations of various wave numbers have been evolved numerically and the phase velocity for each mode has been evaluated. In this way, the linear dispersion of DAW has been verified numerically with the analytical dispersion relation. Then, in weakly nonlinear regime, the perturbative approach has been used to study the nonlinear coherent solutions in weakly coupled dusty plasmas. The standard *Korteweg-de-Vries*(KdV) form of evolution equation is obtained. The KdV equation has the standard Soliton solutions, which form because of the balance of nonlinearity with the dispersion of medium. Apart from dusty plasmas, solitons have also been observed and studied in variety of fields e.g. optical fibers, oceans, as low frequency modes in proteins and DNA, in magnets, laser plasma interaction etc. The solitons are used as signal carriers in communication systems [92] and are also known for the transport of energy to the core of fuel in inertial fusion experiments [93]. At small amplitude (in weakly nonlinear regime), the exact localized solutions of weakly coupled dusty plasma systems match with the solitons obtained as the solutions from KdV equation. Further, the standard propagation and collision characteristics of the DAS were reproduced in our simulations. An interesting observation of our numerical studies in this context is that when the initial amplitude of the perturbation (whether localized or a periodic pattern) is significantly high, it eventually evolves towards solutions having singular cusp structure in density, velocity and potential fields. Theoretical analysis reveals that these are essentially the DAS at their wave breaking amplitude limit [94]. These structures are thus found to be fairly stable and robust and continue to dither at the wave breaking limit. The wave breaking may take different forms. It may appear as crash of gravity waves at sea shores where all the energy given to the particles and wave disappears. Also, it may appear adiabatically as a sharp crest at the top of wave [95]. The highly peaked structures dithering at wave breaking limit observed in our simulations may belong to the latter form of wave breaking scenario. Such high amplitude structures dithering at wave breaking point can be utilized as energy carriers and are also important in particle acceleration. It is interesting to note that the structures are in strong resemblance with those found in experiments recently by Teng *et al* [1].

Further, in Chapter 4, we have explored the existence and evolution of 1-D coherent structures in strongly coupled dusty plasma. Again the linear dispersion relation of the longitudinal mode has been verified through simulation studies for benchmarking purpose [37, 59]. The weakly nonlinear regime is explored using the theoretical reductive perturbative scheme and also via numerical simulations. We have shown that the reductive perturbation calculation with the correct Galilean invariant form for the strongly coupled plasma does not reduce to the standard KdV form of equation, instead an equation with one additional term is obtained. The additional term is a positive definite integral and bars formation of smooth nonlinear localized and/or periodic solutions. In the parameter regime, where the elastic effects due to correlation dominate over Boltzmann screening and thermal dispersion effects, one can ignore the potential and pressure contribution and the above mentioned equation (with KdV and an extra term) takes a new form. We show that the new equation has the form of the *Hunter-Saxton* (HS) equation [8,96]. These equations have previously been invoked for the study of the directors field in liquid crystals. These equations are known to support singular shock solutions of both conservative and dissipative variety. These HS equation has step like shock solutions with a slope and step size that are time dependent. The solutions have a remarkable feature that as the left and right corners of linear segment having negative slope collide for the creation of a shock wave with infinite slope (which may lead to wave breaking), the spatial support in real space diminishes to zero size as the step approaches verticality, the energy can remain conserved. At complete verticality, the HS solutions has no step size and that is why it is sometimes called as "shock wave of zero strength".

In subsequent Chapter 5 to 6, we have concentrated on 2-D nonlinear features associated with the GHD model. In Chapter 5, we have studied the sheared flow instability for the case of weakly coupled dusty plasma. The dusty plasma medium supports the compressible dust acoustic mode in the weak coupling limit. The role of this particular mode on the KH mode vis a vis the incompressible hydrodynamic fluid in both linear and nonlinear regimes have been identified [97]. We have presented a perturbative description along with exact linear stability analysis to study the role of compressibility over the growth rate of KH instability which shows the reduction in growth rate of instability with increasing compressibility. It has also been observed that the dispersive effects further reduce the growth rate of this instability.

When the medium is in strong coupling regime a transverse shear mode is also supported by the medium along with the dust acoustic mode. In Chapter 6, it is observed that the combined effects of transverse shear waves and compressibility cause formation of small scale vortices in contrast to the 2-D inverse cascade feature associated with the incompressible hydrodynamic flows [98]. The simulations also reflect recurrence of KH instability during its evolution. In this phenomenon, the velocity shear layer forms the vortices which lengthened again to form a new shear layer. The process recurs many times and finally stabilizes in form of a shear layer along with some small scale vortices.

The short scale formation in 2-D for the KH mode motivated the investigation for the understanding of the nonlinear evolution of the random turbulent spectra for the strongly coupled dusty plasma medium which has been presented in Chapter 7. The simulations suggest that the inverse cascade is not the preferred way to transfer energy for different modes in such systems unlike 2-D hydrodynamic systems where the energy and enstrophy both are conserved. There is also a tendency for transfer of energy to smaller scales (i.e. forward cascade). The nature of such kind of 2-D decaying turbulence has been studied for strongly coupled dusty plasmas with various kind of phase randomized initial spectral profiles. The evolution shows a distinct scale separation in the evolved power spectra, the slope of which depends on the choice of length scales for initial power injection into the system as well as on the parameters related to the strong coupling effects.

Finally, the Chapter 8 provides a summary of thesis work and discusses the possible implications of our results for future work in dusty plasmas.

An equation means nothing to me unless it expresses a thought of God.

S. Ramanujan

2 Generalized Hydrodynamic Model

The dusty plasma medium, as already elucidated in previous Chapter 1, can behave like a solid, liquid and gas depending upon the value of the coupling parameter Γ. In the weak coupling regime ($\Gamma \leq 1$), the dust remains in gaseous or liquid state and hence the dynamics of dust plasma could be explained with fluid description. The dynamical evolution in this case can typically be understood by the help of continuity and momentum equations coupled with the Poisson equation, the electromagnetic effects being negligible in most situations. As usual, the equation of state is used for closure. At very high values of the coupling parameter $\Gamma = \Gamma_c > 173$, the dust species in the plasma crystallizes. In this case, concepts from condensed matter systems can be invoked. However, there is an intervening interesting regime of the coupling parameter, viz., $1 < \Gamma < \Gamma_c$, where the dust particles are neither fixed at specific lattice locations like crystal nor can they freely move like a fluid. The particles are mobile but they tend to retain a certain memory of their past locations. This leads to the medium exhibiting certain elastic characteristics. It has, therefore, been felt that a visco - elastic fluid description may suitably be applied for the dusty plasma medium [99]. In this regard a Generalized Hydrodynamic (GHD) description of a visco - elastic fluid has successfully been invoked for the study of linear modes of the dusty plasma system [59, 62]. However, nonlinear regime of such a model description has largely remained unexplored so far. There have been attempts at employing reductive perturbative schemes to study the weakly nonlinear regime. However, even in these studies the GHD model that was adopted did not satisfy the criteria of Galilean invariance in the nonlinear regime [46, 65]. In this thesis, we focus on studying the weak as well as strong nonlinear regime for the correct Galilean invariant GHD model description of the system.

This Chapter has been organized to introduce such a model description and discuss the numerical procedure that has been adopted for simulating it. A brief introduction of the visco - elastic fluids has been provided and it is shown how the dusty plasma system can also be looked upon as such a medium. The GHD model employed for the description of visco - elastic fluids are then adapted for the dusty plasma system for the restricted case of unmagnetized plasma and for the description of electrostatic phenomena. The plasma effects thus enter through electrostatic fields, which have to be evaluated self consistently through Poisson's equation. The numerical scheme for simulating the coupled GHD - Poisson set of equation is also discussed in detail.

2.1 Visco - elastic fluids

A *Visco - elastic fluid*, as reflected from its nomenclature exhibits both viscous and elastic traits. A pure elastic system when displaced from its equilibrium position, tends to oscillate around and ultimately relax back to its original location, once the perturbing stress is removed. In some systems, however, the memory of the equilibrium location fades with time. If a stress is applied for a time interval longer than the memory relaxation time, such a system is unable to relax back to its original location. For an ideal elastic medium the memory never fades and hence the memory relaxation time τ_m is infinite. The other limit is that of fluids described by the Navier Stokes equation, where the fluid elements respond immediately to any stress and display no tendency of returning back towards their original position. The fluid element continues to flow in response to any stress and stops only when viscous effects damp its flow velocity. The instantaneous response of the Navier Stokes fluid shows that for them the memory relaxation time τ_m is infinitesimal small, almost zero. The intermediate regime for which τ_m is finite is an interesting one where the medium exhibits both elastic and viscous behavior.

The response of the medium whether viscous or elastic and/or a combination of the two is thus dependent on the time scale of the phenomena one is concerned about. For instance if the typical time scale of a phenomena under consideration is much longer than τ_m the medium will typically behave like a normal fluid, the elastic effects being negligible under these conditions. On the other hand if the phenomena of interest occurs at time scales faster than the memory relaxation time of the medium, the elastic traits would be dominant. A unified description for the visco - elastic fluid is desirable which can be invoked to study regimes right from the extreme limit of viscous Navier Stokes fluid to the pure elastic system.

Numerous approaches have been attempted to provide a unified model description. These models are essentially based on the special forms of the constitutive equation relating shear and strain rates. For instance, the Maxwell's model [99,100] chooses the summation of the Newton's viscous stress and Hooke's elastic stress in the constitutive equation. The constitutive equation in this case is linear and a definite memory relaxation time is chosen in this model. There are also various differential and Integral forms of the constitutive relations [100]. There are models in which the relaxation time itself is dependent on the stress etc., The Generalized Hydrodynamic (GHD) Model, about which we will discuss in the subsequent part of the Chapter, is primarily based on the Maxwell model and provides a unified description for the evolution of visco - elastic fluids.

In the context of neutral systems, the visco - elastic fluid behavior has been explored extensively through both experimental and theoretical studies [100–103]. Mostly macromolecular fluids like polymer fluids, biological fluids (for example synovial fluids found in joints) and other soft matters belong to category of visco - elastic fluids. Studies of such systems have yielded a host of interesting observations from fluid dynamics point of view and they also have considerable applied relevance. Experiments have shown that these fluids can withstand shear stresses. The behavior of vortex, wake formation, bubble shapes, siphon action etc., are all quite distinct for such fluids. Moreover, the transport properties, for fluid and heat also get significantly altered in the visco - elastic limit.

The dusty plasma medium in the parametric domain of $1 < \Gamma < \Gamma_c$, has been lately modeled as a charged visco - elastic fluid. The attempts in this direction have been fruitful as the predictions of the linear modes made on the basis of such a modeling has suitably been confirmed by experiments. The present thesis is now aimed at exploring the possible nonlinear collective phenomena that the dust plasma system should exhibit when considered as a visco - elastic system.

2.2 Dusty plasma as visco - elastic fluids

When the micron sized dust particles are sprinkled in a normal electron ion plasma, the dust species get heavily charged (mostly negative) by the constant bombardment of ions and electrons hitting its surface.

The high value of charge accumulated on the surface of dust particles, causes the interparticle dust potential energy to be quite large. This potential energy often easily becomes comparable and/or higher than the random kinetic energy of the dust particle associated with its temperature. Thus, it is very easy to have a dusty plasma medium in a strong coupling state. Hence, the dusty plasma medium offers a unique possibility of studying the strong coupling regime of plasma in a simple laboratory environment. Experiments have confirmed liquid and solid like characteristics of the dusty plasma medium. In the regime where the coupling parameter $1 < \Gamma < \Gamma_c$, the dust particles are neither crystallized nor behave like a freely flowing fluid. In fact experiments have shown and evaluated the average time spend by a dust particle at a particular location [104]. The results suggest that there is a finite memory relaxation time beyond which information of any particular configuration of the medium is lost. It is observed that the dust species tend to oscillate along a shifted location when a perturbing stress is applied. These studies suggest that the dusty plasma medium can be looked upon as a charged visco - elastic fluid. The magnetic field requirement to magnetize the dust species being typically high, most terrestrial experiments have been confined to the unmagnetized dust and have dealt with only electrostatic response. We will also adhere to these restrictions in this thesis.

In section 2.3, a Generalized Hydrodynamic model description with the above mentioned considerations have been provided.

2.3 Generalized Hydrodynamic model for dusty plasmas

For the visco - elastic fluids the stress - strain relationship is provided by the constitutive relationship. This modifies the conventional momentum equation describing any fluid. The Generalized Hydrodynamic (GHD) Model of visco - elastic fluids is a phenomenological model replacing the conventional momentum equation of the fluids. The stress - strain relationship of the *Maxwell's* model coupling the properties of Newtonian fluids with Hookian solid forms the basis of this model.

A proper Galilean invariant form of the GHD model for the dust species can be written as follows:

$$\left[1+\tau_m\left(\frac{\partial}{\partial t}+\vec{v_d}\cdot\nabla\right)\right]\left[\left(\frac{\partial}{\partial t}+\vec{v_d}\cdot\nabla\right)\vec{v_d}+\frac{\nabla P}{n_d}-\nabla\phi\right]=\eta\nabla^2\vec{v_d}+\left(\frac{\eta}{3}+\zeta\right)\nabla\left(\nabla\cdot\vec{v_d}\right) \tag{2.1}$$

The variables, $n_d, \vec{v_d}$ and ϕ are the density, velocity and electrostatic potential of dust fluid respectively. The pressure is calculated with equation of state $P = \mu_d n_d k_B T_d$. Here T_d is the dust temperature. Here, τ_m is the memory relaxation time of the medium, and η and ζ are the Kinematic viscosity and the Shear viscosity (divided with density) of the dusty plasma medium respectively. In the limit $\tau_m \frac{d}{dt} < 1$, i.e. in weak coupling limit ($\Gamma < 1$), the equation (2.1) turns in to standard Navior Stokes form of momentum equation, thus showing that the weakly coupled dusty plasma could be explained with typical fluid model. In contrast limit, i.e. $\tau_m \frac{d}{dt} > 1$, the equation becomes second order in time and represents the oscillatory mode of the solid.

It should be noted that in contrast to the neutral visco - elastic fluid the electrostatic field in addition to pressure also appears in the equation. The electrostatic field has to be self consistently evolved along with the motion of dust species. This can be achieved by coupling the Eq. (2.1) above, with the continuity equation and the Poisson's equation.

$$\frac{\partial n_d}{\partial t}+\nabla\cdot(n_d\vec{v_d})=0 \tag{2.2}$$

$$\nabla^2\phi = n_d+\mu_e exp(\sigma_i\phi)-\mu_i exp(-\phi) \tag{2.3}$$

Here, $\mu_e = \frac{n_{e0}}{Z_d n_{d0}}, \mu_i = \frac{n_{i0}}{Z_d n_{d0}}$ and $\sigma_i = \frac{T_i}{T_e}$. The mass of dust species is many orders higher than that of electrons and ions present in plasma. Thus, the electron and ion fluids are assumed to be inertialess compared to the time scale of dust dynamics. These inertialess species, provide a Boltzmann response having the following form

$$n_e = n_{e0}exp(\frac{e\phi}{k_BT_e}); \qquad n_i = n_{i0}exp(\frac{-e\phi}{k_BT_i}) \tag{2.4}$$

which has been substituted in the Poisson's equation (Eq. (2.3)) for the electron and ion densities. The plasma being quasineutral, the equilibrium density of the three species, satisfy following relation:

$$n_{e0} + Z_d n_{d0} = n_{i0} \tag{2.5}$$

The Eqs. (2.1,2.2, 2.3) are written in their normalized form. The potential, length and time are normalized by $e\phi/k_BT_i, L_D = \sqrt{\frac{k_BT_i}{4\pi Z_d n_{d0} e^2}}$ and ω_{pd}^{-1} respectively.

The parameters τ_m, $\eta^* = (4/3\eta + \zeta)$ and μ_d appearing in the evolution equations above are not all free but satisfy the following constraining relationships.

$$\begin{aligned}
\frac{\eta^*}{\eta_0} &= 0.0051\frac{\Gamma_m}{\Gamma} + 0.374\frac{\Gamma}{\Gamma_m} + 0.022 \\
\Gamma_m(\kappa) &= 171.8 + 82.8(\exp(0.565\kappa^{1.38}) - 1) \\
\tau_m &= \frac{\eta^*}{\lambda_D^2}\frac{1}{1 - \gamma_d\mu_d + \frac{4}{15}u(\Gamma)} \\
\mu_d &= 1 + \frac{u(\Gamma)}{3} + \frac{\Gamma}{9}\frac{\partial u(\Gamma)}{\partial\Gamma}
\end{aligned} \tag{2.6}$$

The parameter η_0 is the characteristic viscosity [105]. $u(\Gamma)$ has two forms depending on the value of Γ

$$u(\Gamma) \approx -\frac{\sqrt{3}}{2}\Gamma^{3/2}; \qquad \Gamma \leq 1$$

$$u(\Gamma) = -0.89\Gamma + 0.95\Gamma^{1/4} + 0.19\Gamma^{-1/4} - 0.81; \qquad \Gamma > 1$$

These relationships have been obtained by extensive molecular dynamic simulations which have been described in references [35, 62, 105, 106]. Experimentally, the relaxation parameter τ_m has been calculated with estimation of the phase shift between the stress and the shear rate in oscillatory tests [101]. We have chosen the screening parameter κ as zero in our studies.

2.4 Numerical methods

Present thesis primarily focused on the nonlinear aspects of dusty plasma dynamics. In addition, however, linear studies have also been performed in certain scenarios which have resulted in providing interesting new insights. In this section, we briefly describe the numerical techniques that have been employed to carry out the investigation presented in the thesis.

2.4.1 Linear stability analysis

Apart from nonlinear simulations, we have also performed the linear stability analysis numerically for 2-D K-H instability. Here, for example, we have chosen the case of incompressible strongly coupled dusty plasma fluid (refer to Chapter 6, section 6.3). The equations have been Fourier transformed in y direction (flow direction which is periodic) and in time domain. In this process, we obtain the linearized differential form of equations (with derivatives in x direction which is direction of shear).

$$
\begin{aligned}
&-i\left(\omega - k_y v_{y0}\right) v_{1x} + p_1^{'} = \psi_x \\
&-i\left(\omega - k_y v_{y0}\right) v_{1y} + v_{1x} v_0^{'} + i k_y p_1 = \psi_y \\
&-i\tau_m\left(\omega - k_y v_{y0}\right) \psi_x = \eta\left(v_{1x}^{''} - k_y^2 v_{1x}\right) \\
&-i\tau_m\left(\omega - k_y v_{y0}\right) \psi_y = \eta\left(v_{1y}^{''} - k_y^2 v_{1y}\right) \\
&v_{1y} = \frac{i v_{1x}^{'}}{k_y}
\end{aligned}
\tag{2.7}
$$

Here, ($'$) is the derivative in x direction. Also, $\psi_x, \psi_y, v_{1x}, v_{1y}, p_1$ are coupled variables as function of ω, k_y and x. $v_0(x)$ is the equilibrium flow velocity as function of x. Further, the above set of Eqs. (2.7) will be solved numerically as eigen value problem.

$$
\begin{aligned}
&\left(k_y^2 v_{1x} - v_{1x}^{''}\right)\omega = k_y^3 v_{1x} v_{y0} - k_y v_{1x}^{''} v_{y0} + k_y v_{1x} v_{y0}^{''} - k_y \psi_y^{'} + i k_y^2 \psi_x \\
&-i\tau_m \psi_x \omega = -i k_y v_{y0} \tau_m \psi_x + \eta\left(v_{1x}^{''} - k_y^2 v_{1x}\right) \\
&-i\tau_m \psi_y \omega = -i k_y v_{y0} \tau_m \psi_y + \frac{i\eta}{k_y}\left(v_{1x}^{'''} - k_y^2 v_{1x}^{'}\right)
\end{aligned}
\tag{2.8}
$$

Each of above equations then discretized in following form

$$\begin{aligned} & \omega\left(l_1 v_{1x}^{i-1} + l_2\psi_x^{i-1} + l_3\psi_y^{i-1} + l_4 v_{1x}^{i} + l_5\psi_x^{i} + l_6\psi_y^{i} + l_7 v_{1x}^{i+1} + l_8\psi_x^{i+1} + l_9\psi_y^{i+1}\right) \\ = \; & r_1 v_{1x}^{i-2} + r_2\psi_x^{i-2} + r_3\psi_y^{i-2} + r_4 v_{1x}^{i-1} + r_5\psi_x^{i-1} + r_6\psi_y^{i-1} + r_7 v_{1x}^{i} + r_8\psi_x^{i} + r_9\psi_y^{i} \\ + \; & r_{10} v_{1x}^{i+1} + r_{11}\psi_x^{i+1} + r_{12}\psi_y^{i+1} + r_{13} v_{1x}^{i+2} + r_{14}\psi_x^{i+2} + r_{15}\psi_y^{i+2} \end{aligned} \tag{2.9}$$

These equations now could be written in matrix form [A] and [B] whose coefficients are l_{1-9} and r_{1-15} respectively.

$$[A][X] = \omega[B][X] \tag{2.10}$$

The Eq. (2.10) is then solved numerically using *Eig* function of MATLAB or using ZGGEV subroutine from LAPACK package.

2.4.2 Exact nonlinear solutions

To look in to the possibility of existence of localized solutions for 1-D dusty plasma medium, we transformed the coupled set of equations (as an example, for the case of weakly coupled dusty plasma system Eqs. (4.1,4.2,4.5)) in a moving frame with a constant velocity β. Thus, we have transformed to a stationary frame $\xi = x - \beta t$ and $\tau = t$ such that,

$$\frac{\partial}{\partial x} = \frac{\partial}{\partial \xi}; \;\; \frac{\partial}{\partial t} = -\beta\frac{\partial}{\partial \xi} \tag{2.11}$$

As $\partial/\partial\tau = 0$ for the solutions in time stationary frame. The transformed set of equations is as follows:

$$\begin{aligned} & \frac{\partial}{\partial \xi}\left(-\beta n_d + n_d v_d\right) = 0 \\ & \frac{\partial}{\partial \xi}\left(-\beta v_d + \frac{v_d^2}{2} + \alpha\log n_d - \phi\right) = 0 \\ & \frac{\partial^2\phi}{\partial \xi^2} = n_d + \mu_e e^{(\sigma_i\phi)} - \mu_i e^{(-\phi)} \end{aligned} \tag{2.12}$$

Now, with appropriate boundary conditions for localized solutions, i.e. as $\xi \to \infty$, $n_d \to 1$ and $v_d \to 0$, the above coupled set of Eqs. (2.12) finally reduce to

$$\begin{aligned} \phi &= \frac{1}{2}\left[\beta^2\left(\frac{1}{n_d^2}-1\right)+2\alpha log(n_d)\right] \\ \frac{\partial^2\phi}{\partial\xi^2} &= \left[\frac{3\beta^2}{n_d^4}-\frac{\alpha}{n_d^2}\right]\left[\frac{\partial n_d}{\partial\xi}\right]^2+\left[\frac{-\beta^2}{n_d^3}+\frac{\alpha}{n_d}\right]\frac{\partial^2 n_d}{\partial\xi^2} \end{aligned} \tag{2.13}$$

Eqs. (2.13) have further been solved using any of popular numerical techniques to solve differential equations (for example RK-4 method) as an initial value problem.

2.4.3 Exact nonlinear simulations

The Generalized momentum equation and continuity equation (Eqs. (2.1,2.2)) have been modeled numerically (fully nonlinear evolution) using Flux Corrected Transport (FCT) Finite Difference scheme. We have employed a package of subroutines LCPFCT to evolve the Eqs. (2.1,2.2) using such scheme [107]. The LCPFCT routines solve the equations of Generalized Continuity Equation form. The subroutines are specifically written in 1-D, but could be employed for 2-D and 3-D dimensions easily. Also, the routines are written for Cartesian, Cylindrical as well as Spherical coordinate systems. The LCPFCT routines employ Runga-Kutta-2 method for evolution in time while the space derivatives have been solved with central different scheme.

While the continuity equation can directly be evolved with FCT routines, the generalized momentum equation have been split to a form of two coupled convective equations which were then evolved using FCT set of routines.

$$\begin{aligned} \left(\frac{\partial}{\partial t}+\vec{v_d}\cdot\nabla\right)\vec{v_d}+\frac{\nabla P}{n_d}-\nabla\phi &= \vec{\psi} \\ \left(\frac{\partial}{\partial t}+\vec{v_d}\cdot\nabla\right)\vec{\psi} &= -\frac{\vec{\psi}}{\tau_m}+\frac{1}{\tau_m}\left[\eta\nabla^2\vec{v_d}+\left(\frac{\eta}{3}+\zeta\right)\nabla\left(\nabla\cdot\vec{v_d}\right)\right] \end{aligned} \tag{2.14}$$

To solve nonlinear Poisson equation for our case, we have employed a successively relaxation method based (Storey's scheme) for periodic boundary conditions. To solve the Poisson equation with Storey's method, the Eq. (2.3) is written as

$$\frac{d\phi_i^{n+1}}{dh} = \nabla^2\phi_i^{n+1} - n_d^n - \mu_e exp(\sigma_i\phi_i^n) - \mu_i exp(-\phi_i^n) \tag{2.15}$$

Here, dh is a parameter responsible for relaxation of ϕ profile and should be chosen appropriately to get a desirable result in few iteration. i and n are the index parameters for space grid location of profile and number of iterations of profile respectively. Further, the Eq. (2.15) has been written as

$$\frac{\phi_i^{n+1}}{dh} - \nabla^2\phi_i^{n+1} = \frac{\phi_i^n}{dh} - n_d^n - \mu_e exp(\sigma_i\phi_i^n) - \mu_i exp(-\phi_i^n) \tag{2.16}$$

As we know the initial profile of ϕ, to get the solution at higher time steps, we use the previous ϕ profiles and take the Fourier transform of both side of Eq. (2.16) in spatial coordinate system. Then, we rearrange the equation and take inverse Fourier transform of following equation to obtain ϕ^{n+1}.

$$\phi_{ik}^{n+1} = \left[-\frac{1}{dh} - k^2\right]\left[\frac{\phi_{ik}^n}{dh} - n_{dk}^n - \mu_e exp(\sigma_i\phi_{ik}^n) - \mu_i exp(-\phi_{ik}^n)\right] \tag{2.17}$$

The iteration remains continue until the difference of previous and advance iteration profiles achieve a permitted tolerance.

The complete dynamics of dusty plasmas have been performed by simultaneously solving Continuity equation, Generalized momentum equation and Poisson equation. The results in linear regime have been obtained by keeping initial amplitude of perturbation very small such that the nonlinear term does not play significant role. While for nonlinear studies, the amplitude of perturbation has been kept higher.

In this Chapter, we have provided a brief description of the necessary tools in lines of governing equations and the numerical approach towards extracting physical insights on the dusty plasma medium when viewed as a visco - elastic system.

3

Coherent solutions in weakly coupled dusty plasmas in 1-D

The nonlinear aspects of the weak coupling limit (i.e. $\Gamma \leq 1$) of the coupled GHD - Poisson equation in 1-D are investigated. This corresponds to choosing $\eta = \tau_m = 0$ in the Eqs. (2.1,2.2,2.3) and hence in this limit the dusty plasma system behaves like a weakly coupled hydrodynamic system. Such a system has been investigated in considerable detail for the study of linear as well as weak nonlinear response. The linear mode supported by such a system is the compressible Dust Acoustic Wave (DAW). In the weak nonlinear limit the reductive perturbative analysis carried out by several authors [47, 48] have shown that the equation reduces to the KdV form and supports the Dust Acoustic Solitons. In this Chapter, we have sought the possibility of analytical solutions for arbitrary amplitude. Furthermore, we have carried out exhaustive studies on nonlinear simulation of weakly coupled dusty plasma medium. An important observation is the existence, stability and accessibility of the soliton structures at the wave breaking limit, where the density and velocity fields acquire a singular cusp form.

3.1 Introduction

The linear and nonlinear characteristics of collective oscillations in a dusty plasma system have been the subject of much theoretical and experimental studies in recent years [10, 108]. The dust acoustic wave (DAW), in particular, has received a great deal of attention. This low frequency longitudinal mode is an analogue of the ion acoustic mode found in normal electron-ion plasmas with the massive dust particles now providing inertia and the pressure contributions for sustaining the wave coming from both electrons and ions [43]. Its linear propagation characteristics are well understood theoretically and have also been widely confirmed experimentally [109, 110]. There is also an extensive theoretical literature on the subject of nonlinear evolution of DAWs mostly centered on the idea of excitation of solitons [4, 43, 47, 72, 111]. These localized one dimensional pulse structures belong to a class of exact solutions of integrable nonlinear partial differential equations (PDEs), such as the Korteweg-DeVries (KdV) equation (and its generalizations) and have been applied in a wide variety of physical systems. The one dimensional idealization holds good in many practical situations where the time scale for the breakup of the soliton due to bending instabilities in the perpendicular direction are quite long compared to the propagation time of the soliton over an experimental length. Likewise, collisional effects and other damping mechanisms can be effectively controlled by varying the plasma parameters ensuring that the solitons have a long life time. Consequently, KdV solitons and similar other one dimensional solitons have been experimentally studied by many researchers (see [112] for a detailed review) ever since the first laboratory observations by Ikezi *et al.* [113]. More recently such pulses have also been observed in dusty plasmas [4]. Other nonlinear structures that have been studied in the context of DAWs are shock waves and two dimensional vortices.

An important class of nonlinear solutions that has not received much attention in a dusty plasma is that of sharply peaked solitons. These solutions occur near the wave breaking amplitude and have a spatial structure that is distinctly different from the smooth pulse soliton solutions. Mathematically, these sharply peaked solitons, dithering at the wave breaking amplitude, are singular in nature and may exhibit singularities in the field and/or its higher derivatives at its maximum amplitude [114]. They are similar to singular structures observed in other situations such as slowly propagating envelope solitons in laser plasma interactions. The physical mechanism responsible for the excitation of such structures is the incident laser pulse produced ponderomotive pressure driving the ion waves to near wave breaking amplitudes [115]. Similar nonlinear states involving upper hybrid waves have also been reported for theoretical studies of electron-ion magnetized plasmas [116–118] and in numerical simulations [119] of the Jaulent Miodek equations [120]. More recently such singular structures have been observed in experiments with dusty plasmas. Schwabe *et al.* [2] have observed cusp like structures on the surface of voids formed in a dusty plasma system created in a microgravity environment of outer space . Teng *et al.* [1] have carried out wave breaking experiments in the laboratory and have seen cusp-like structures in the bulk of a compressible dusty plasma fluid.

The work in present Chapter is motivated to some extent by these recent experimental observations and by a desire to theoretically explore the accessibility and evolution of sharply peaked solitons for DAWs. To achieve this goal we have carried out large scale 1-D numerical simulations of bulk longitudinal oscillations in a dusty plasma using a standard three fluid model that has been widely used in the literature for solitonic studies. Our simulations show the spontaneous excitation of a single sharply peaked propagating structure or a chain of sharply peaked pulses when large amplitude initial perturbations in the form of a single pulse or a wave train are imposed on the system. These structures are quite long lived (over several dust acoustic frequency periods) and are accessible from a range of initial conditions.

Our simulation results show a remarkable resemblance to the cusp like structures observed in the above mentioned recent experiments and may provide important insights into the role of such structures in the wave breaking and wave-particle interaction processes of dusty plasma systems.

3.2 Governing equations

Our simulation model equations describing the dusty plasma medium in 1-D are

$$\frac{\partial n}{\partial t} + \frac{\partial (nv)}{\partial x} = 0 \tag{3.1}$$

$$\frac{\partial v}{\partial t} + v\frac{\partial v}{\partial x} + \frac{\alpha}{n}\frac{\partial n}{\partial x} - \frac{\partial \phi}{\partial x} = 0 \tag{3.2}$$

$$\frac{\partial^2 \phi}{\partial x^2} = n + \mu_e e^{(\sigma\phi)} - \mu_i e^{(-\phi)} \tag{3.3}$$

The above set of equations are in normalized units and the electrons and ions were assumed to follow Bolzmannian distribution, as per description given in previous

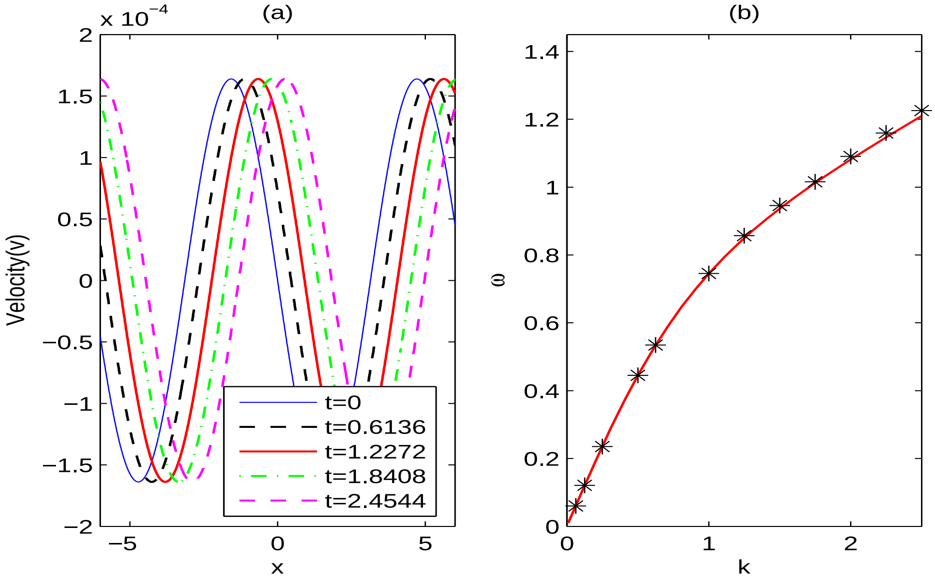

Figure 3.1: (a) A small amplitude sinusoidal DA perturbation (linear regime) in velocity has been evolved in time. (b) The linear dispersion relation plotted numerically (stars) and analytically (line). The parameters chosen for simulation are $\mu_e = 0.1$, $\mu_i = 1 + \mu_e$, $\sigma = 1.0$ and $\alpha = 0.1$.

Chapter 2. Also, the subscript d has been dropped from dust density and velocity for simplicity. We would like to remind that the parameter $\alpha = v_{thd}^2$ in normalized units.

Equations (4.1) and (4.2) are numerically solved by the flux corrected scheme of Boris *et al.* [107]. At each time step the scalar potential ϕ is determined from the Poisson equation (4.5). The latter is solved by employing a successive relaxation scheme. Fig. 3.1(a) shows the evolution of $k = 1$ mode of DA sinusoidal small amplitude perturbation. It is observed that as expected in linear regime, the DA mode does not decay in amplitude and if we calculated the phase velocity of DA mode for different k values, we can plot a dispersion relation numerically. Fig. 3.1(b) gives a comparison between numerically obtained dispersion relation and one plotted analytically and both were found to match exactly. In this way, our numerical code has been appropriately benchmarked in the small amplitude limit to accurately agree with the linear dispersion relation of the dust acoustic wave. The analytical dispersion relation for DAW could be obtained by linearizing the Eqs. (4.1-4.5) and replacing other variables in terms of single variable. The dispersion relation for DAW is,

$$\omega^2 = \alpha k^2 + \frac{k^2}{k^2 + \mu_e \sigma + \mu_i} \tag{3.4}$$

3.3 The KdV DA solitons

The existence of DA solitons was first predicted by Rao *et. al.* [43] by obtaining an analytically solvable KdV form of partial differential equations in weak nonlinearity regime. To obtain KdV form of equation, we have expanded the variables n, v and ϕ using standard reductive perturbative method in terms of a small parameter ϵ as,

$$\begin{aligned} n &= 1 + \epsilon n^{(1)} + \epsilon^2 n^{(2)} + \epsilon^3 n^{(3)} + \dots \\ v &= \epsilon v^{(1)} + \epsilon^2 v^{(2)} + \epsilon^3 v^{(3)} + \dots \\ \phi &= \epsilon \phi^{(1)} + \epsilon^2 \phi^{(2)} + \epsilon^3 \phi^{(3)} + \dots \end{aligned} \tag{3.5}$$

Taking stretched co-ordinate system $\xi = \epsilon^{1/2}(x - \lambda t)$ and $\tau = \epsilon^{3/2} t$ we can write the derivatives as,

$$\frac{\partial}{\partial x} = \epsilon^{\frac{1}{2}} \frac{\partial}{\partial \xi} \quad ; \quad \frac{\partial^2}{\partial x^2} = \epsilon \frac{\partial^2}{\partial \xi^2} \tag{3.6}$$

$$\frac{\partial}{\partial t} = -\lambda \epsilon^{\frac{1}{2}} \frac{\partial}{\partial \xi} + \epsilon^{\frac{3}{2}} \frac{\partial}{\partial \tau} \tag{3.7}$$

Expanding Eqs. (4.1-4.5) using above expansion, collecting the lowest order terms from each equation and then replacing each other, we finally get a equation of KdV form as,

$$\frac{\partial^3 \phi_1}{\partial \xi^3} + \frac{2\lambda}{(\lambda^2 - \alpha)^2} \frac{\partial \phi_1}{\partial \tau} + \left((\mu_i - \mu_e \sigma^2) - \frac{3\lambda^2 + \alpha}{(\lambda^2 - \alpha)^3} \right) \phi_1 \frac{\partial \phi_1}{\partial \xi} = 0 \tag{3.8}$$

Here, ϕ_1 is same as $\phi^{(1)}$ and is the first order amplitude of ϕ in terms of small parameter ϵ. Now this KdV form of equation is exactly solvable by transforming it again from $\xi, \tau \rightarrow \zeta$ frame using transformation $\zeta = \xi - M\tau$, the Eq. (3.8) could be written as a differential equation as,

$$\frac{\partial^3 \phi_1}{\partial \zeta^3} - Ma\frac{\partial \phi_1}{\partial \zeta} + b\phi_1 \frac{\partial \phi_1}{\partial \zeta} = 0 \tag{3.9}$$

Where a and b are the coefficient of $\partial\phi_1/\partial\tau$ and $\phi_1\partial\phi_1/\partial\xi$ in Eq. (3.8) respectively. Now with appropriately choosing boundary (or initial) conditions, the final solution could be written as,

$$\phi_1 = \frac{3Ma}{b} sech^2 \left[\frac{\zeta - \zeta_0}{(Ma)^{1/2}/2}\right] \tag{3.10}$$

Here, ζ_0 is the constant of integration.

3.4 Exact solutions

The KdV equation obtained under the ansatz of weak nonlinearity is an approximate solution of the complete set of equations, which clearly will not hold in the high amplitude limit. Here, we obtain exact solutions for the complete set of equations which is valid for any amplitude. This is achieved by seeking seeking stationarity in a moving frame for the full set of Eqs. (4.1) - (4.5). Assuming that all dependent variables are functions of $\xi = x - \beta t$ only, we can reduce the full set of equations to the following ordinary differential equation (ODE) in n as

$$\frac{1}{2}\left(\frac{\partial n}{\partial \xi}\right)^2 + V(n) = 0 \tag{3.11}$$

Where

$$V(n) = \left[\frac{2}{(-2\beta^2/n^3 + 2\alpha/n)^2}\right] \times \left[2\beta^2\left(\frac{1}{n} - 1\right) + 2\alpha\,(n-1) + \frac{2\mu_e}{\sigma}\left\{\exp\left(\sigma\phi\right) - 1\right\} + 2\mu_i\left\{\exp\left(-\phi\right) - 1\right\}\right]$$

with

$$\phi = \frac{1}{2}\left(\beta^2\left(\frac{1}{n^2} - 1\right) + 2\alpha \log n\right) \tag{3.12}$$

The Fig. 3.2(a) is the low amplitude localized solution of Eqs. (3.11-3.12) while

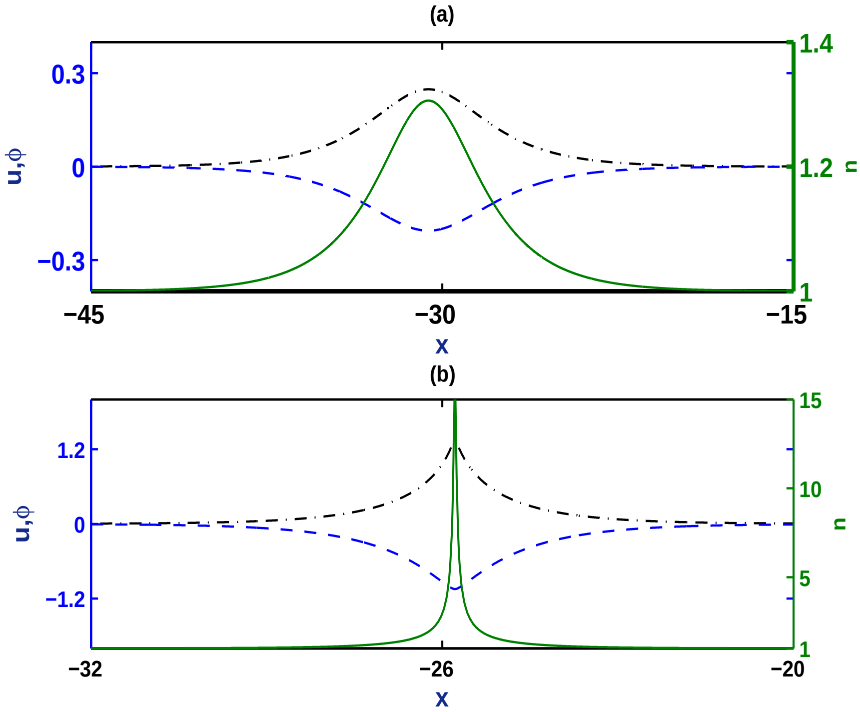

Figure 3.2: (a) The numerical solutions of Eqs. (3.11-3.12) obtained by shooting scheme illustrating the conventional Soliton solution and (b) Cusp structures at the wave breaking point for the dusty plasma system. The parameters of simulation are $\mu_e = 0.1$, $\mu_i = 1+\mu_e$, $\sigma = 1.0$ and $\alpha = 0.0$.

the solution shown in Fig. 3.2(b) is the extream end of solutions where the localized structures become singular in nature. Such limit of localized solutions are categorized as "Cusp" solutions. This could also be understood from the expression for $V(n)$ that it blows up when the denominator of the first bracket goes to zero. This occurs when $n = n_{max} = \beta/v_{thd}$ and here clearly the first derivative in density $\partial n/\partial \xi$ blows up from Eq. (3.11). Also from the continuity equation we have $n = \beta/(\beta - v)$; thus at this point we would have $v = v_{max} = \beta - v_{thd}$, as observed in our simulations studies. Similarly an expression for ϕ_{max} can be obtained from Eq. (3.12). The analytical values corresponding to these expressions for n_{max}, v_{max} and ϕ_{max} have been tabulated for various cases in Table 5.1.

Table 3.1: Cusp solutions

S. No.	v_{thd}	β^{anal}	v_{max}^{anal}	ϕ_{max}^{anal}	n_{max}^{anal}	β^{sim}	v_{max}^{sim}	ϕ_{max}^{sim}	n_{max}^{sim}
1	0.0	1.5090	1.5090	-1.1385	∞	1.5057	1.456	-1.033	10.2
2	0.2236	1.3316	1.1080	-0.7724	5.9553	1.3484	1.164	-0.7778	7.423
3	0.3162	1.3018	0.9856	-0.6558	4.1167	1.3094	1.047	-0.6348	5.068
4	0.3873	1.2917	0.9044	-0.5786	3.3352	1.2970	0.9719	-0.5634	4.023
5	0.4472	1.2908	0.8436	-0.5211	2.8863	1.2936	0.9152	-0.5023	3.42

3.5 A comparison amidst approximate KdV and exact solutions

Here, we provide a comparison between the approximate KdV solitons and those exact solutions which are obtained for the complete set of equations.

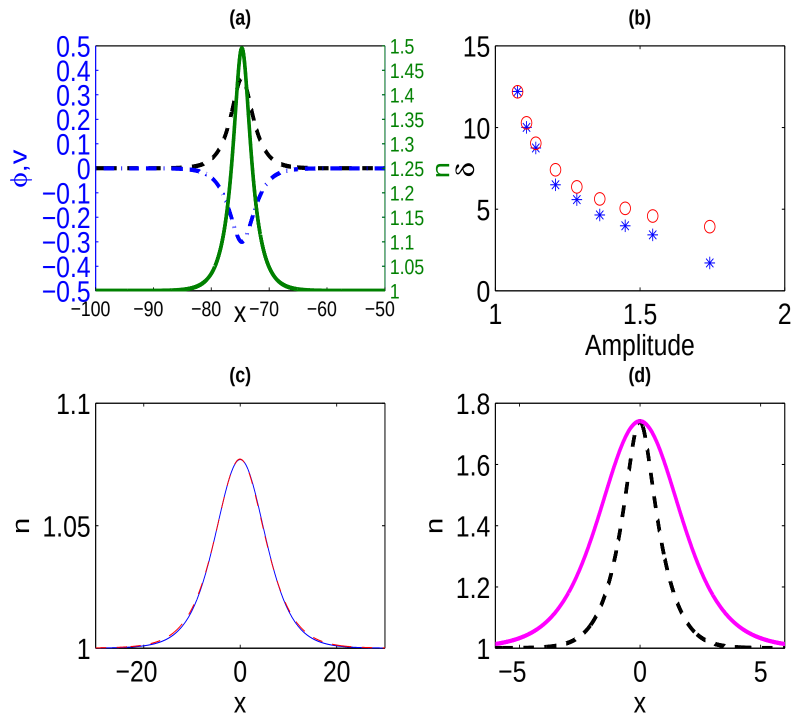

Figure 3.3: (a) Exact solutions of Eq. (3.11), (b) A comparison between exact solutions (filled circles) and KdV soliton structure ($*$), (c) The matching of exact localized solutions (red dashed line) with KdV soliton solutions (solid blue line) in low amplitude limit and (d) distinction between the two at high amplitudes.

The profiles of density n, potential ϕ and velocity v for exact localized solutions have been shown in the Fig. 3.3(a). The structure deviates from the KdV soliton profile at high amplitudes. This can be seen from the comparison with the KdV form provided in the other subplots of the figure. In Fig. 3.3(b) we have compared the width of the KdV solutions with the exact solutions obtained by numerically integrating Eq. (3.11). The exact solutions with similar amplitude are wider compared to KdV solution with increasing amplitude. The width keeps increasing as one increases the amplitude. In subplot (c) we show that at lower amplitude there is complete overlap between the KdV form and that of the exact solution. However, subplot (d) shows that the higher amplitude the form of the two solutions differ considerably. We observe that these higher amplitude solutions also show stable propagation when chosen as initial condition in our numerical evolution code which has been elaborated in following section.

Fig. 3.4 shows the collision of two oppositely moving low amplitude exact localized solutions while evolving it with time through Eqs. (4.1 - 4.5). It is found that such solutions not only move stably in time but also propagate through each other without any change in momentum, hence showing the property of solitons. The exact solutions of such low amplitude belong to the category of DA KdV solitons. Unlike soliton solutions, however, when two of these solutions are made to collide they are not able to preserve their identity. It can be seen from the plots of Fig. 3.5 that a significant amount of perturbed field appears as an aftermath of such a collisional interaction. Thus these localized solutions are not solitons in the true sense but can be looked upon as localized stable solutions permitted by the system.

3.6 Evolution studies

In previous sections, we have studied the possibility of existence for different possible coherent solutions in weakly coupled dusty plasma medium under observation. In the present section, we have observed not only the evolution of exact localized solutions with full set of model equations defining system but also observe the formation and evolution of coherent structures spontaneously appear during the course of evolution of various kind of high amplitude initial perturbations.

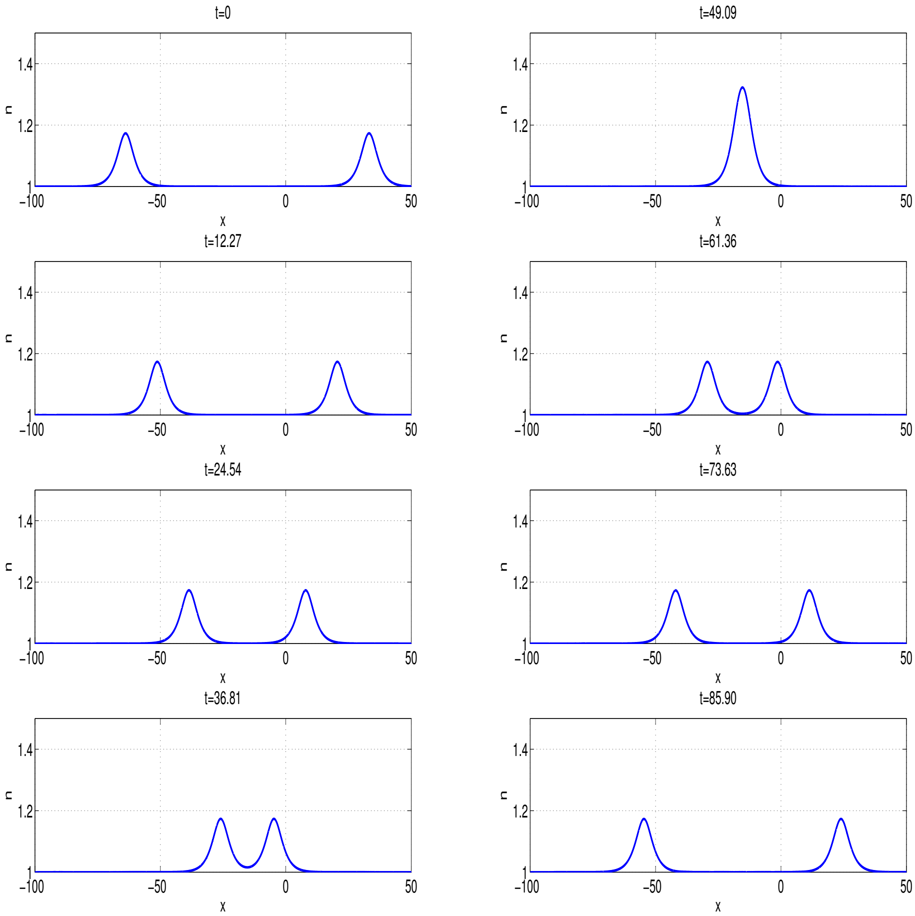

Figure 3.4: Evolution and collision of low amplitude exact stationary localized solutions with time in different subplots.

If we increase the amplitude of the initial perturbations gradually, we observe the excitation and evolution of the usual KdV soliton solutions that have been analytically predicted before. For a further increase in the amplitude we observe the excitation of both a smooth soliton and a sharply peaked soliton. This is shown in Fig. 3.6 where an initial large amplitude Gaussian pulse Fig. 3.6(a) is seen to split up into two oppositely propagating pulses Fig. 3.6(b) and as we follow the evolution of the right propagating pulse it is seen to separate into a smooth small amplitude soliton and a large amplitude sharply peaked solution (Fig. 3.6(c) and Fig. 3.6(d) show this at various stages in time). In Fig. 3.7, we have shown the spatial structures of the density n (solid line), the velocity v (dashed dot line) and the potential ϕ (dash line) of the soliton solution. The plots clearly reveal

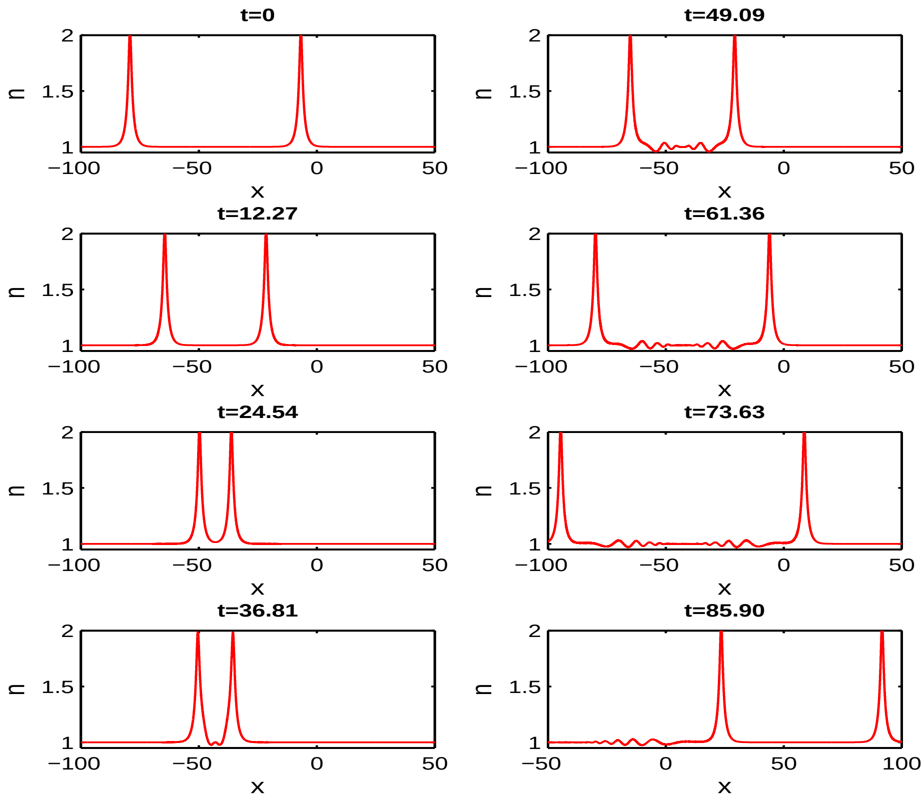

Figure 3.5: Evolution and collision of high amplitude exact stationary localized solutions with time in different subplots.

the development of a singular structure. For these simulations the dust species was assumed to be cold, *i.e.* $\alpha = v_{thd}^2 = 0.0$. The zero temperature case is, however, a mathematical idealization. Keeping this in view we have also carried out simulations of an initial Gaussian pulse for the case of finite dust temperature. We show the results of the finite temperature case in Fig. 3.8. (the inset in Fig. 3.8 shows the splitting of Gaussian pulse in opposite directions.) In this case also the singular characteristics, namely a cusp formation in density profile can be observed clearly. We note from our simulations that the profiles and the maximum value of the fields v and ϕ of the sharp structures that finally form are insensitive to any refinements in the grid resolution both for the zero as well as the finite temperature cases. The density profile and its maximum value are, however, insensitive to grid

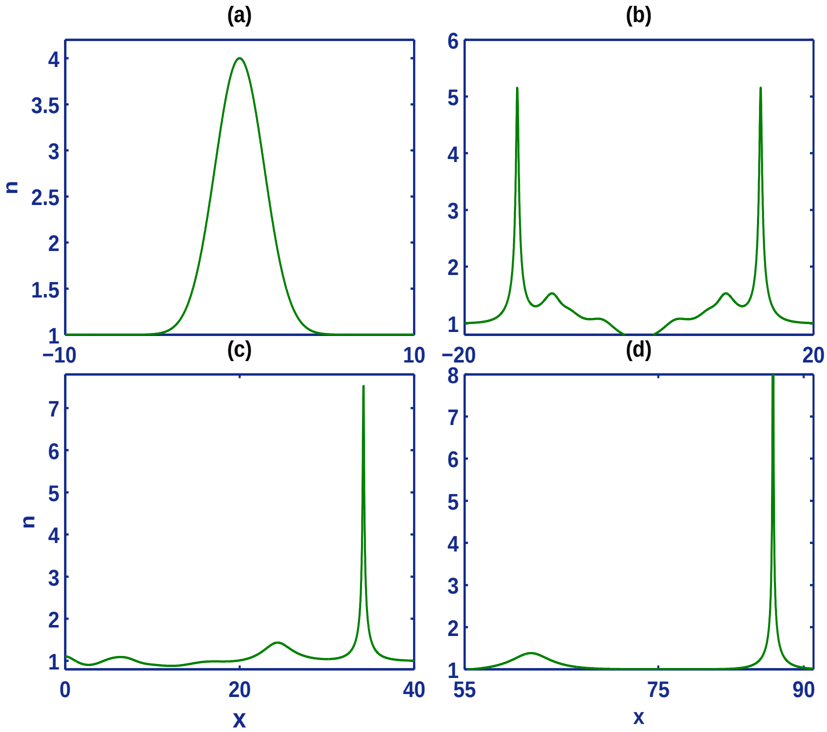

Figure 3.6: Emergence of soliton and cusp soliton solutions from an initial Gaussian density pulse (subplot (a) at $t = 0$). The pulse generates two oppositely propagating similar structures as shown in (b)for $t = 9.817$. The evolution of right going pulse has been shown in (c) and (d) at $t = 24.54$ and $t = 61.36$ respectively. It is evident that it evolves into a small amplitude soliton and a large amplitude sharply peaked soliton. The parameters of simulation are $\mu_e = 0.1$, $\mu_i = 1 + \mu_e$, $\sigma = 1.0$ and $\alpha = 0.0$.

resolution only for the finite temperature case. When the dust temperature is chosen as zero the maximum of the density is dependent on the choice of the grid resolution. We would show that in this case one expects the theoretical value of the density to shoot off to infinity, which obviously can never be captured, no matter how much the grid is refined. The sharply peaked soliton and the regular soliton move apart in time as their propagation velocities are different because of the difference in their respective amplitudes. We also observe from our simulations that the maximum value of the dust fluid speed $v = v_{max}^{sim}$ (which occurs at the cusp point) is close to $(\beta - v_{thd})$ where β is the sharply peaked soliton propagation speed and v_{thd} is the dust thermal velocity. This is seen from data gathered and consolidated from several simulations and summarized in Table 5.1. We also show the maximum values of the density, velocity and potential fields observed in the

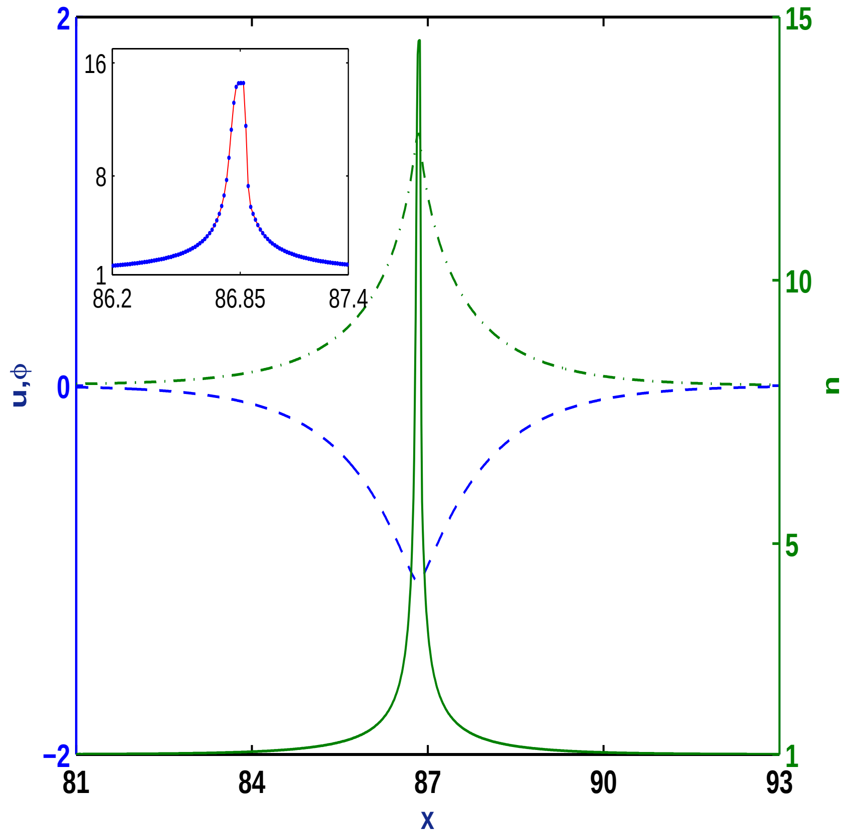

Figure 3.7: The plot of density n (green solid line), velocity v (dot dashed green line) and potential ϕ (blue dashed line) for the cusp solutions observed finally in Fig. 3.6(d). The inset shows the expanded form of the density profile of the structure.

simulation, for the sharp pulse that eventually forms spontaneously from a given large amplitude Gaussian initial condition. We observe that for v_{max} and ϕ_{max} there is a good agreement between the analytical estimation and observations obtained from simulations. The estimates and the observed values of the density in simulations show slight differences. For the cold dust ($T_d = 0$), the density can be infinite for the cusp solutions, which as stated earlier cannot be captured in simulations. In any case the simulations for $T_d = 0$ is only a mathematical idealization. We also wish to state that the choice of $\sigma = T_i/T_e = 1.0$ made in our simulations, though unrealistic, does not influence the cusp behavior, which is the main theme of this paper. The cusp occurs at the point where $V(n)$ blows up, i.e. when the denominator of the first factor in Eq. (5) (which does not depend on σ

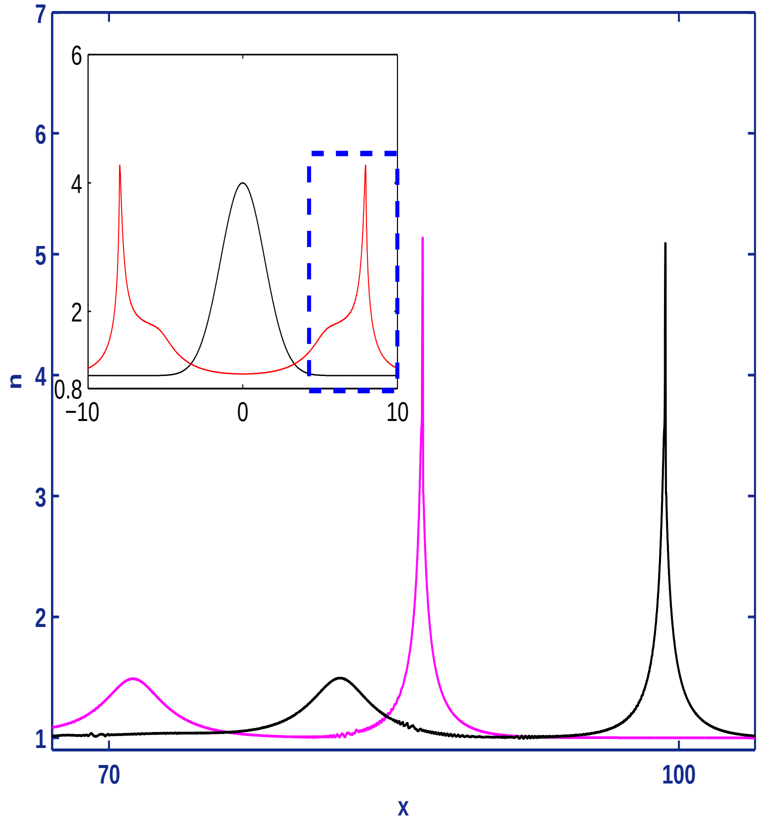

Figure 3.8: The evolution of an initial Gaussian density pulse for the case of finite dust temperature. The evolution of the right pulse enclosed by blue dashed box in the inset has been shown in the main frame of the figure at times 63.81 (solid magenta line) and 73.63 (solid black line) respectively. The parameters in this simulation are $\mu_e = 0.1$, $\mu_i = 1 + \mu_e$, $\sigma = 1.0$ and $\alpha = 0.1$.

) goes to zero. Furthermore, basically the realistic condition of $Ti << Te$ would simply make ion shielding more important. Charge density on the dust changes the electron density, influencing the electron Debye length and again enters through shielding effects only.

We also choose to consider different initial conditions for our simulations. For instance we have chosen the fields corresponding to the regular large amplitude solitons and the cusp solutions obtained from Eq. (3.11) as initial conditions. The regular soliton solutions and the cusp structure for a particular set of parameters have been shown in Fig. 3.2(a) and Fig. 3.2(b) respectively. In Fig. 3.9(a) the evolution of regular soliton structure of Fig. 3.2(a) has been shown. As expected the undistorted propagation of the soliton is captured well by our simulation. The choice of the cusp structure of Fig. 3.2(b) as our initial condition, again leads to a stable propagation. The evolution of the profiles of density n and velocity v are shown in Fig. 3.9(b) and Fig. 3.9(c) respectively. It should be noted that we had specifically chosen to show here the pathological case of $T_d = 0$ for which ideally the density solution should blow off to infinity. Clearly, the density profile for this case can not be accurately represented in the numerical solution chosen as initial condition and/or its simulation. The evolution, therefore, shows fluctuations in the amplitude of density. However, we would like to point out that even for this case, the velocity evolution shows a very stable propagation as has been demonstrated in the plots of Fig. 3.9(c). For those simulations for which the dust temperature is finite even the evolution of density shows no perceptible change in its amplitude. It appears that when a sharply peaked structure forms, the gradients in density and velocity become large close to the peak. These are smoothed by the numerical integration schemes at the grid scale which may be interpreted as viscosity/hyperviscosity operating on the soliton peak. This keeps the amplitude dithering close to the wave breaking amplitude. In reality, these numerical effects will be replaced by collisional effects or wave particle interaction effects in collisionless plasmas. To further test the accessibility and excitation conditions of the cusp solitons we have next changed the initial conditions to be in the form of a sinusoidal perturbation. This is also close to the experimental conditions of [1]. Again for very small amplitudes the wave train remains sinusoidal and propagates with a phase velocity given by the linear dispersion relation of the DAW. When the amplitude of the initial sinusoidal perturbation is chosen to be large, we observe that in the beginning the sinusoidal perturbations get steepened to form a periodic train of shocks. These shock structures then eventually evolve into a chain of cusp like sharply peaked structures which are stable and survive over hundreds of DAW periods. These stages of evolution have been illustrated in Fig. 3.10 and Fig. 3.11 for a cold and finite temperature dusty plasma system respectively. The evolutionary stages of a sinusoidal perturbation leading to the emergence of a train of sharply peaked structures bear a remarkable resemblance to the experimental findings of Teng *et al.* [1] where a self excited DAW is found to

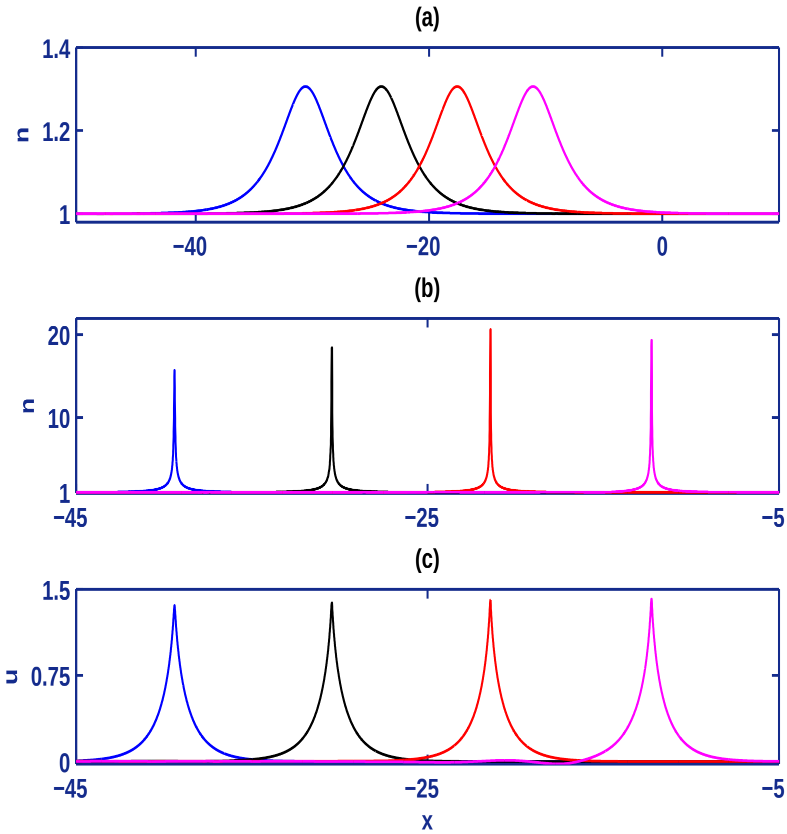

Figure 3.9: The evolution of exact solutions of Fig. 3.2 used as initial conditions of (4.1) - (4.5) has been shown. The subplot (a) shows the evolution of density profile for the initial condition of regular soliton of Fig. 3.2 and subplot (b) and (c) show the evolution of density and velocity profiles for the Cusp solution. The structures from left to right correspond to $t = 0.0$, $t = 6.135$, $t = 12.27$ and $t = 18.41$ respectively.

grow in amplitude till it approaches the wave breaking condition. The measured dust density profiles in that stage appear as a series of propagating cusp profiles. These steepened structures are seen to then significantly influence the dust micro-dynamics leading to particle trapping and disordered motion that brings about a phase transition from a liquid state of the dust fluid to a gaseous state. Our simple model simulations, based on a fluid model, cannot reproduce the wave particle dynamics observed in the experiment but does seem to capture well the emergence of propagating cusp structures that are close to wave breaking conditions. One further shortcoming of our model is that it is valid in the weakly coupled regime of

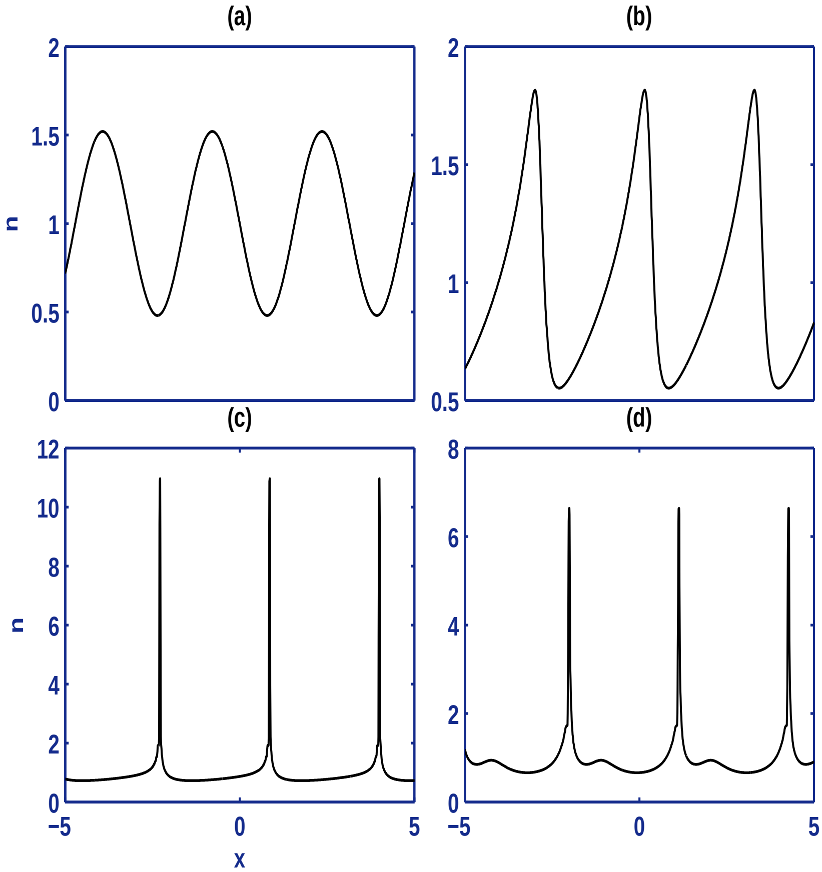

Figure 3.10: Evolution of a sinusoidal wave train perturbation has been shown. Subplot (a) shows the initial density profile. The profile develops into a series of shock structure shown at $t = 1.227$ in subplot (b), which eventually form a chain of cusp structures shown at $t = 3.067$ and $t = 60.132$ in subplot (c) and (d) respectively. The other parameters of simulation are $\mu_e = 0.1$, $\mu_i = 1 + \mu_e$, $\sigma = 1.0$ and $\alpha = 0.0$.

a dusty plasma where correlation effects arising from strong dust-dust interactions have been neglected. However the basic nonlinear wave propagation phenomena displayed by the present fluid model may not be significantly altered by these correlations in the framework of a hydrodynamic description.

3.7 Summary

One of the main result of this Chapter is a strong evidence of the existence of cusp solitons in a dusty plasma medium on the basis of 1-d numerical solutions using a

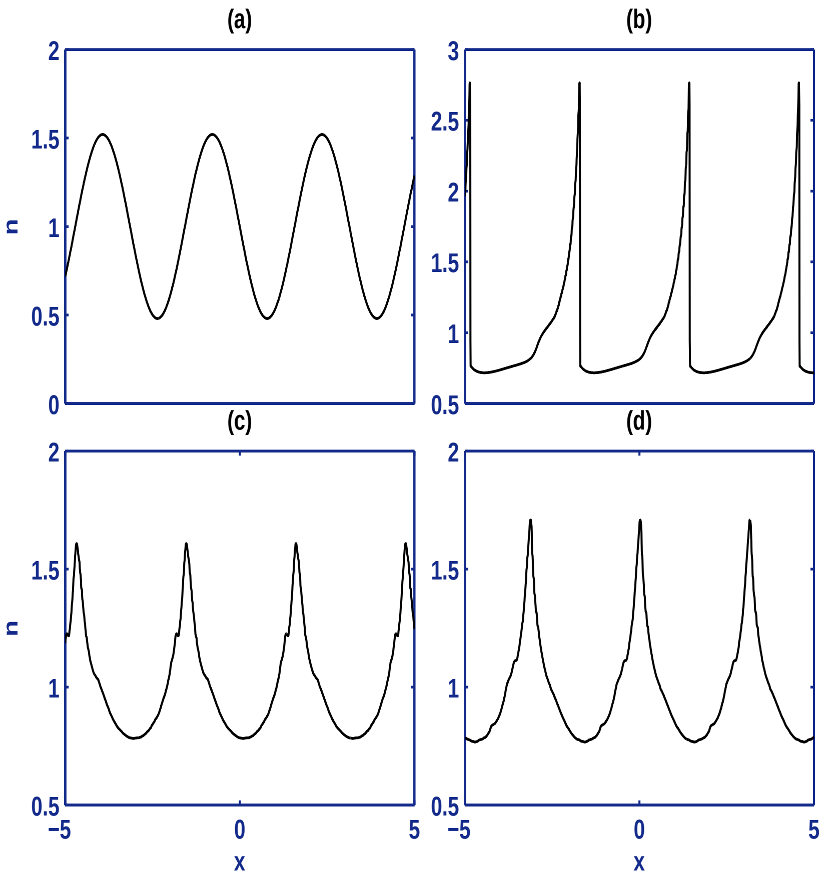

Figure 3.11: The evolution for sinusoidal perturbation for the case of finite temperature dusty plasma system $\alpha = 0.1$ has been shown. The various subplots (a), (b), (c) and (d) correspond to $t = 0$, $t = 1.227$, $t = 3.067$ and $t = 60.132$ respectively. The other parameters are same as that of Fig. 3.10. In this case also the development of shocks initially turning into cusp structure can be clearly observed.

fluid model. These nonlinear states of the dust acoustic wave are shown to be long lived structures and accessible from a variety of initial conditions. The conditions for their onset and existence are obtained by carrying out numerical simulation studies. Our results assume significance in the light of recent observation of similar structures in laboratory experiments and their potential role in influencing the micro-state of dusty plasmas.

4

Coherent solutions in strongly coupled dusty plasmas in 1-D

The behavior of strongly coupled dusty plasma medium in 1-D limit is the theme of this Chapter. Previous studies in the linear regime have shown marked characteristic differences with the weak coupling case. Some attempts have also been made earlier to study the weakly nonlinear response using the reductive perturbative approach for the strongly coupled dusty plasma medium. However, in those studies, use of an incorrect form (non - Galilean invariant form) of Generalized Hydrodynamic (GHD) description, led to the conclusion that it would support solitons of the KdV variety. In this Chapter we illustrate that for the correct set of equations no localized smooth solutions are permitted. It is shown that reductive perturbative analysis reduces the original GHD set of equations to Hunter Saxton nonlinear equation which permits a new variety of singular solutions. The Chapter also discusses the nonlinear evolution of different initial perturbations of arbitrary amplitude using the full set of equations.

4.1 Introduction

As mentioned in previous Chapters, the dust system can easily be driven in a strongly correlated regime. Thus, it is an ideal system for investigation of ideas related to phase transition and non - equilibrium thermodynamics [27]. The generalized hydrodynamic (GHD) fluid model provides the description of the dust fluid in both weak and strong coupling limits [46, 59, 99]. The strongly coupled dusty plasma has been investigated using this GHD model in some detail earlier specifically for the study of linear response of the medium in the small amplitude limit [59]. Such studies have revealed novel characteristic modification in the well known dispersion relation of the longitudinal dust acoustic mode. The group velocity of the mode shows reversal $\partial\omega/\partial k < 0$. It has also been shown that in the strongly correlated regime the viscosity no longer plays a dissipative role but is responsible for oscillatory characteristics. This results in the existence of transverse shear mode supported by the strongly correlated dust medium [23]. The longitudinal dust acoustic mode also gets modified. These studies were primarily confined to the linear regime of small amplitude.

In this Chapter, we investigate the high amplitude regime of the dusty plasma fluid depicted by the GHD model. We restrict to the study of the longitudinal response of the medium in present Chapter and provide comparison between the behavior of the dust fluid for weak and strong coupling regimes. We employ the reductive perturbative approach as well as studies through direct numerical evolution for our observations.

In section 4.2, the governing equations in 1-D limit for the GHD description of dusty plasma are written down. The linear dispersion characteristics of the longitudinal dust acoustic mode are obtained and compared with the observations of numerical evolution of small amplitude perturbations in section 4.3. This validates the numerical code developed by us for the GHD set of equations.

In section 4.4, we study the response of the medium at high amplitude where nonlinearity is of importance. For this purpose both reductive perturbative analytical scheme as well as the numerical simulation tools are employed. Our studies show that in the strong coupling regime of the dust fluid the GHD equations do not allow any localized smooth stationary solutions. The reductive perturbative approach does not lead to the simplified KdV form for the equations in the low amplitude limit. One also does not obtain smooth solutions through numerical eigenvalue search procedure. We show that in this case the reductive perturbation scheme leads instead to an altogether different equation, viz., the Hunter Saxton (HS) equation [8]. It is well known that the HS equation does not permit smooth localized solutions. The HS system admits singular solutions which have conservative as well as dissipative properties. The simplest variety of solutions of the HS equation can be cast in terms of a piecewise linear form. A physical understanding of the singular solutions of the HS equation has also been provided. In section 4.5, we summarize the work presented in this Chapter.

4.2 Governing equations

In 1-D (with variations only along x) the coupled GHD - Poisson set of equations (Eqs. 2.1,2.2,2.3) depicting a strongly coupled dust plasma can be written as :

$$\frac{\partial n_d}{\partial t} + \frac{\partial (n_d v_d)}{\partial x} = 0 \tag{4.1}$$

Here, v_d is the dust velocity along x. The evolution of v_d is obtained from the x component of the generalized momentum equation for the dust species.

$$\left[1 + \tau_m \left(\frac{\partial}{\partial t} + v_d \frac{\partial}{\partial x}\right)\right] \left[\left(\frac{\partial}{\partial t} + v_d \frac{\partial}{\partial x}\right) v_d + \frac{\alpha}{n_d}\frac{\partial n_d}{\partial x} - \frac{\partial \phi}{\partial x}\right] = \eta^* \frac{\partial^2 v_d}{\partial x^2} \tag{4.2}$$

Here ϕ is scalar potential and $\eta^* = (\frac{4}{3}\eta + \zeta)$, (where η and ζ are shear and bulk viscosity coefficients respectively). The equation reduces to conventional weakly coupled dust fluid for $\tau_m = 0$ as

$$\left(\frac{\partial}{\partial t} + v_d \frac{\partial}{\partial x}\right) v_d + \frac{\alpha}{n_d}\frac{\partial n_d}{\partial x} - \frac{\partial \phi}{\partial x} = \eta^* \frac{\partial^2 v_d}{\partial x^2} \tag{4.3}$$

The memory effects in this limit have no role. In the strongly coupled limit where the elastic behavior associated with solid like trait survives for times longer than the characteristic times of interest (*i.e.* $\omega\tau_m >> 1$) the Eq. (4.2) takes the form of

$$\left[\left(\frac{\partial}{\partial t} + v_d \frac{\partial}{\partial x}\right)\right] \left[\left(\frac{\partial}{\partial t} + v_d \frac{\partial}{\partial x}\right) v_d + \frac{\alpha}{n_d}\frac{\partial n_d}{\partial x} - \frac{\partial \phi}{\partial x}\right] = \frac{\eta^*}{\tau_m} \frac{\partial^2 v_d}{\partial x^2} \tag{4.4}$$

The behavior of the dust fluid in the three cases of $\tau_m = 0$, τ_m finite but small so as to have $\omega\tau_m \sim 1$ and $\omega\tau_m >> 1$ will be studied in detail. The scalar potential field ϕ is determined from the Poisson's equation

$$\frac{\partial^2 \phi}{\partial x^2} = [n_d + \mu_e exp(\sigma_i \phi) - \mu_i exp(-\phi)] \tag{4.5}$$

As explained in Chapter 2, time scales associated with the evolution of dust being long, the electrons and ions species are assumed to satisfy the Boltzmann distribution. The estimate of τ_m and its relationship with η are typically obtained through extensive molecular dynamic simulations and have been described in references [35, 62, 105, 106].

4.3 Validation of linear results

The numerical scheme for solving the complete set of coupled GHD - Poisson equation has already been discussed in Chapter 2. In brief, Equation (4.1) being a continuity equation has been solved by flux corrected scheme of Boris *et al.* [107]. The momentum Eq. (4.2) which has a second order time differentiation is split in terms of two first order convective differential equations and then the flux corrected scheme is applied to them for evolution.

$$\left(\frac{\partial}{\partial t} + v_d \frac{\partial}{\partial x}\right) v_d + \frac{\alpha}{n_d}\frac{\partial n_d}{\partial x} - \frac{\partial \phi}{\partial x} = \psi \tag{4.6}$$

$$\left(\frac{\partial}{\partial t} + v_d \frac{\partial}{\partial x}\right) \psi + \frac{\psi}{\tau_m} = \frac{\eta^*}{\tau_m}\frac{\partial^2 v_d}{\partial x^2} \tag{4.7}$$

At each time step the scalar potential ϕ is determined from the Poisson equation (4.5) which is a nonlinear equation for ϕ. A successive relaxation scheme [121] is employed for its solution. The pressure P has been determined from the equation of state. The numerical simulations for a small amplitude sinusoidal perturbation should be according to the linearized dispersion relation of for the medium.

The linearization of Eqs. (4.1,4.2,4.5) for an equilibrium homogeneous dust, ion and electron densities satisfying the charge neutrality condition, leading to the absence of any equilibrium electric field (thus $\phi_0 = 0$) yields the following dispersion relation:

$$-\omega^3\tau_m - i\omega^2 + \omega\left(\alpha\mu_d\tau_m k^2 + \frac{\tau_m k^2}{k^2 + \mu_e\sigma_i + \mu_i} + \eta^* k^2\right) + i\alpha k^2 + \frac{ik^2}{k^2 + \mu_e\sigma_i + \mu_i} = 0 \tag{4.8}$$

The dispersion relation of Eq. (4.8) reduces to Eq. (14) of Kaw *et al.* [59] in the limit of $\omega\tau_m << 1$ and when dust neutral collisions are absent. Also we recover the dust acoustic dispersion relation in the limit of $\eta^* = \tau_m = 0$

$$\omega^2 = \alpha k^2 + \frac{k^2}{k^2 + \mu_e \sigma_i + \mu_i} \tag{4.9}$$

We provide a comparison of the analytical dispersion relation with those obtained

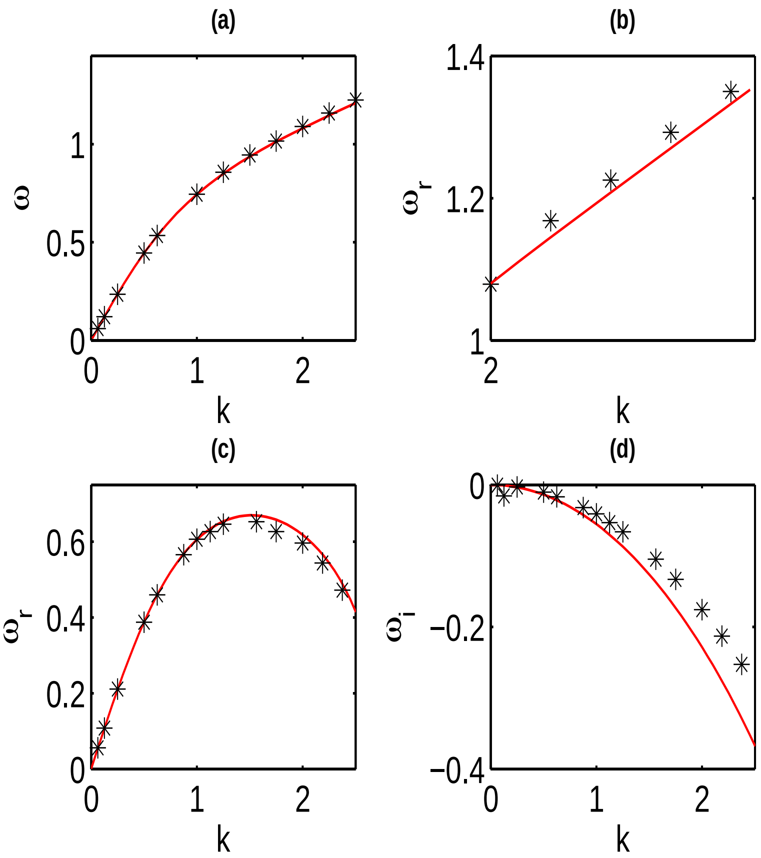

Figure 4.1: Linear Dispersion relation for the three cases of subplot (a) for $\tau_m = \eta^* = 0$, subplot(b) for $\omega\tau_m >> 1$, subplot(c) for $\omega\tau_m < 1$ (real part of frequency) and subplot(d) for $\omega\tau_m < 1$ (imaginary part of frequency). The solid line shows the analytical curve and the $*$ symbols have been obtained from the numerical simulation. The other parameters are $\alpha = 0.1, \mu_e = 0.1, \mu_i = 1 + \mu_e$ and $\sigma_i = 1.0$.

numerically in Fig. 4.1 The analytical dispersion relation of Eq. (4.9) has been shown in the subplot (a) of Fig. 4.1 as thick solid line. The frequency ω is real in this particular case. In subplot (b) of Fig. 4.1 we show the dispersion relation for the case when both τ_m and η^* are finite. This is the case for which $\omega\tau_m >> 1$. Clearly, the plot, therefore starts from a finite k and ω value. As expected the imaginary part of ω is very small and negligible for this case. Even though η^* is finite ω is real. Hence presence of viscosity causes no damping. In Fig. 4.1 A comparison of the subplot (a) and (c) shows that the dust acoustic dispersion relation shows a monotonic increase of frequency with the wave vector. The dispersion curve in the case of finite $\omega\tau_m < 1$ shows that the curve turns around with increasing value of the wave number. This implies a negative value of the group velocity ($\partial\omega/\partial k < 1$) talked about in some previous studies. This turning down of the dispersion curve depends primarily on value of compressibility factor μ_d, whose value turns negative as the value of coupling parameter Γ increases.

4.4 Nonlinear Studies for dust fluid in the strong coupling regime

Earlier studies in the nonlinear regime have primarily been based upon the reductive perturbative analytical scheme employed for the case of weak nonlinearity. However, the GHD equations employed in that case were not proper as they did not respect the Galilean invariance. The analysis done on such a incorrect equation led to the reduction of equations to the KdV form. However, when the correct equation are used which respect the criteria of Galilean invariance, the extra nonlinearity associated with the strong coupling parameter τ_m leads to an altogether different form of the reduced equation. It does not fall in the paradigm of the KdV set. The existence of smooth localized solutions are no longer permitted for strongly coupled dusty plasma medium. A detailed reductive perturbative calculation for the correct set of equation has been provided in the subsection below. We also show how the analysis leads to solutions with singular forms.

4.4.1 Reductive perturbation expression

We carry out the reductive perturbation analysis [122] retaining the additional convective term seeking analytical description in the weakly nonlinear regime for a strongly coupled dusty plasma. To keep track of the contribution due to the additional convective term in the reductive perturbation analysis, we attach an artificial coefficient ζ, i.e. the Eq. (4.4) is rewritten as:

$$\left[\left(\frac{\partial}{\partial t} + \zeta v_d \frac{\partial}{\partial x}\right)\right]\left[\left(\frac{\partial}{\partial t} + v_d \frac{\partial}{\partial x}\right) v_d + \frac{\alpha}{n_d}\frac{\partial n_d}{\partial x} - \frac{\partial \phi}{\partial x}\right] = \frac{\eta^*}{\tau_m}\frac{\partial^2 v_d}{\partial x^2} \tag{4.10}$$

We choose

$$\begin{aligned} n &= 1 + \epsilon n^{(1)} + \epsilon^2 n^{(2)} + \epsilon^3 n^{(3)} + \dots \\ v &= \epsilon v^{(1)} + \epsilon^2 v^{(2)} + \epsilon^3 v^{(3)} + \dots \\ \phi &= \epsilon \phi^{(1)} + \epsilon^2 \phi^{(2)} + \epsilon^3 \phi^{(3)} + \dots \end{aligned} \tag{4.11}$$

and stretched variables ξ and τ are such that, $\xi = \epsilon^{1/2}(x - \lambda t)$ and $\tau = \epsilon^{3/2} t$,so the new derivatives in form of old one are as follows

$$\frac{\partial}{\partial x} = \epsilon^{\frac{1}{2}}\frac{\partial}{\partial \xi} \quad ; \qquad \frac{\partial^2}{\partial x^2} = \epsilon \frac{\partial^2}{\partial \xi^2} \tag{4.12}$$

$$\frac{\partial}{\partial t} = -\lambda \epsilon^{\frac{1}{2}}\frac{\partial}{\partial \xi} + \epsilon^{\frac{3}{2}}\frac{\partial}{\partial \tau} \tag{4.13}$$

Collecting first two lowest order terms ϵ from the continuity equation yields

$$\frac{\partial}{\partial \xi}\left[v^{(1)} - \lambda n^{(1)}\right] = 0 \tag{4.14}$$

$$\frac{\partial n^{(1)}}{\partial \tau} + \frac{\partial}{\partial \xi}\left[v^{(2)} - \lambda n^{(2)}\right] + \frac{\partial}{\partial \xi}\left[n^{(1)} v^{(1)}\right] = 0 \tag{4.15}$$

From Poisson's equation we obtain

$$\left[\mu_e \sigma_i + \mu_i\right] \phi^{(1)} + n^{(1)} = 0 \tag{4.16}$$

$$\frac{\partial^2 \phi^{(1)}}{\partial \xi^2} = n^{(2)} + \left(\mu_e \sigma_i + \mu_i\right) \phi^{(2)} + \frac{1}{2}\left[\sigma_i^2 \mu_e - \mu_i\right]\left(\phi^{(1)}\right)^2 \tag{4.17}$$

and for Momentum equation we get

$$\lambda^2 \tau_m \frac{\partial^2 v_1}{\partial \xi^2} + \lambda \tau_m \frac{\partial^2 \phi_1}{\partial \xi^2} - \alpha \lambda \tau_m \frac{\partial^2 n_1}{\partial \xi^2} = \eta^* \frac{\partial^2 v_1}{\partial \xi^2} \tag{4.18}$$

$$\lambda^2\tau_m\frac{\partial^2 v^{(2)}}{\partial\xi^2}-\tau_m\lambda\frac{\partial}{\partial\tau}\frac{\partial v^{(1)}}{\partial\xi}-\zeta\tau_m\lambda v^{(1)}\frac{\partial^2 v^{(1)}}{\partial\xi^2}-\lambda\tau_m\frac{\partial}{\partial\xi}\frac{\partial v^{(1)}}{\partial\tau}-\frac{\lambda}{2}\tau_m\frac{\partial^2\left(v^{(1)}\right)^2}{\partial\xi^2}+$$
$$\tau_m\lambda\frac{\partial^2\phi^{(2)}}{\partial\xi^2}-\tau_m\frac{\partial}{\partial\tau}\frac{\partial\phi_{(1)}}{\partial\xi}-\zeta\tau_m v^{(1)}\frac{\partial^2\phi^{(1)}}{\partial\xi^2}-\alpha\lambda\tau_m\frac{\partial^2 n^{(2)}}{\partial\xi^2}+\tau_m\alpha\frac{\partial}{\partial\tau}\frac{\partial n^{(1)}}{\partial\xi}$$
$$-\frac{\alpha\lambda\tau_m}{2}\frac{\partial^2\left(n^{(1)}\right)^2}{\partial\xi^2}+\zeta\tau_m\alpha v^{(1)}\frac{\partial^2 n^{(1)}}{\partial\xi^2}=\eta^*\frac{\partial^2 v^{(2)}}{\partial\xi^2} \tag{4.19}$$

From first order terms of continuity, momentum and Poisson's equation the expression for phase velocity λ is,

$$\lambda^2=\frac{\eta^*}{\tau_m}+\alpha+\frac{1}{\mu_e\sigma_i+\mu_i} \tag{4.20}$$

Now replacing values for $\phi^{(2)}$ and $v^{(2)}$ from Eqs. (4.17 and 4.15) in equation (4.20) and writing the equation in terms of variable $n^{(1)}$, we get the simplified nonlinear equation as,

$$A\frac{\partial^4 n^{(1)}}{\partial\xi^4}+B\frac{\partial}{\partial\tau}\frac{\partial n^{(1)}}{\partial\xi}+C\frac{\partial^2}{\partial\xi^2}\left(n^{(1)}\right)^2+Dn^{(1)}\frac{\partial^2 n^{(1)}}{\partial\xi^2}=0 \tag{4.21}$$

Where the constants are,

$$\begin{aligned}
A&=\frac{\lambda}{\mu_e\sigma_i+\mu_i}\\
B&=\lambda^2\left(\mu_e\sigma_i+\mu_i\right)\\
C&=\lambda\left(\frac{\left(\mu_e\sigma_i^2-\mu_i\right)}{2\left(\mu_e\sigma_i+\mu_i\right)^2}-\frac{\lambda^2}{2}\left(\frac{\tau_m}{\eta^*-\lambda^2\tau_m}\right)+\left(\mu_e\sigma_i+\mu_i\right)\left(\frac{3\alpha}{2}+\frac{1}{\mu_e\sigma_i+\mu_i}\right)\right)\\
D&=\lambda\zeta\left(\left(\mu_e\sigma_i+\mu_i\right)\left(\frac{\eta^*}{\tau_m}+\frac{1}{\mu_e\sigma_i+\mu_i}\right)-1\right)
\end{aligned} \tag{4.22}$$

Thus the coefficient D arises due to the additional convective term that has now been retained in the momentum equation. It should also be noted that because of the term associated with the coefficient D the reduced Eq. (4.21) does not have the usual KdV form. Some of the coefficients of Eq. (4.21) can be absorbed in the length and time scales. We define the new length and time scales as $t_n=(A/B)t$ and $\xi_n=(\sqrt{2C/A})\xi$ and drop the suffix n to recast the equation as:

$$n_{t\xi}+n_{\xi\xi\xi\xi}+n_\xi^2+(\frac{D}{2C}+1)nn_{\xi\xi}=0 \tag{4.23}$$

Here for clear emphasis on form of Eq. (4.23), the first order density perturbation $n^{(1)}$ is replaced by n. It should be noticed that the coefficient of the last term cannot be absorbed and its difference from unity, viz., $D/2C$ is responsible for the equation not permitting a soliton solution. It can be seen that when $D = 0$ the equation can be integrated to yield KdV equation which permits soliton solutions. While on the other hand the integration of the complete equation yields

$$n_t + n_{\xi\xi\xi} + \frac{(n^2)_\xi}{2} + \frac{D}{2C}\int nn_{\xi\xi}d\xi = 0 \tag{4.24}$$

Using the assumption of periodicity and/or vanishing fields at $\xi = \pm\infty$ one can express the last term of the equation as

$$\int nn_{\xi\xi}d\xi = -\int (n_\xi^2)d\xi$$

However, the integrand being a positive definite quantity, in the presence of this term in the evolution equation (Eq. (4.23)) the value of the field n at both the boundary can not vanish and/or become identical. It is thus clear that the soliton condition can never be satisfied.

In the absence of dispersion and for the case when $D/C = 1$ Eq. (4.24) is the Hunter Saxton (HS) equation. Here we have performed a perturbative analysis in weak nonlinearity for complete GHD set of equations and then under simplified physical condition (i.e. ignoring dispersion), we obtained the HS form of equation. A HS equation could also be derived directly from initial generalized momentum equation neglecting the effect of dispersion.

In the strongly coupled limit $k\sqrt{\tau_m\eta^*} >> 1$, where k is the inverse scale length of the solution, $\eta^*/\tau_m >> C_{da}^2$ (C_{da} being the dust acoustic speed), i.e. when the elastic wave dominates the dust acoustic speed, one can ignore the contribution from the scalar potential ϕ and the thermal contribution due to P in the momentum equation. Physically, this is the regime when elastic coefficients due to correlations dominate over Boltzmann screening and thermal dispersion effects. The dusty plasma medium is, however, still in a fluid molten state with no lattice formation.

In this limit the dust fluid is governed by the following simplified equation:

$$\left[\frac{\partial}{\partial t} + v_d \frac{\partial}{\partial x}\right] \left[\frac{\partial v_d}{\partial t} + v_d \frac{\partial v_d}{\partial x}\right] = \frac{\eta^*}{\tau_m} \frac{\partial^2 v_d}{\partial x^2} \tag{4.25}$$

It should be emphasized that compressional velocity perturbations in the dust fluid will still produce density disturbances, which in turn will be shielded by electrons and ions producing potential perturbations. The inequality at the beginning of this paragraph ensures that the reaction back of these driven disturbances on the momentum equation is negligible. Physically Eq. (4.25) contains dispersion free linear elastic waves that are supported by the correlation driven elasticity coefficient and nonlinear contributions through inertial effects appear through the convective terms. In principle, linear wave dispersion may be introduced through a k dependent form of τ_m [62]; here we assume that this effect is small. Note that the second convective derivative which arose through constraints of Galilean invariance is playing a crucial role in the nonlinear dynamics. This equation can also model plastic flow deformation disturbances in solids undergoing failure through severe stresses. In the weakly nonlinear regime Eq. (4.25) can be subjected to a reductive perturbation analysis, by expanding,

$$v_d = \lambda + \epsilon v_d^{(1)} + \epsilon^2 v_d^{(2)} + \dots \tag{4.26}$$

$$w = \epsilon^{3/2}(w^{(1)} + \epsilon w^{(2)} + \dots) \tag{4.27}$$

where $w = (\partial/\partial t + v_d \partial/\partial x)v_d$. Further, using the stretched variables, $\xi = \epsilon^{1/2}(x - \lambda t)$, $\tau = \epsilon^{3/2} t$, taking $\lambda = \sqrt{\eta^*/\tau_m}$, and retaining terms up to second order for the v_d and w fields, we can obtain the following single equation in the variable $v_d^{(1)}$ (rewritten below without the superscript),

$$(v_{d\tau} + v_d v_{d\xi})_\xi = \frac{1}{2} v_{d\xi}^2 \tag{4.28}$$

The left hand side equated to zero is the nonlinear equation for dispersion less waves with the convective nonlinearity giving indefinite steepening of waves which can lead to wave breaking or form shocks, or solitons depending on whether nonlinearity, viscous dissipation (Burger's equation) or dispersion (Korteweg de Vries equation) dominates the physics of steepened waves. Here the extra convective derivative nonlinearity of the simplified generalized hydrodynamic model equation (4.25) is responsible for the nonlinear term on the right side of Eq. (4.28). This term dramatically changes the character of the equation and the nature of its solutions. Equation (4.28) is the so-called Hunter-Saxton equation, which has been derived earlier [8] for director fields [1] in liquid crystals, where the positional disorder of polymer molecules gives the medium fluid properties whereas the positional order due to correlations gives them crystal like properties. It is also the high frequency limit of the Cammasa- Holm equation [123] , which has been derived to describe the nonlinear dynamics and wave breaking of shallow water waves. These equations belong to a new class of equations which can be derived from variational principles in more than one non equivalent forms. They typically have an infinite number of conservation laws and possess singular solutions with infinite derivatives. If these solutions are propagating, they pass through each other undisturbed, except for a phase shift, somewhat like solitons.

We now recapitulate some properties [124] of the Hunter Saxton equation and its solution, which are of relevance to our problem, Firstly, integrating Eq. (4.28) over ξ we note that because of the positive definite value of the integral on the right side, if the solutions leave one boundary unperturbed, the other boundary is perturbed, thus showing the impossibility of smooth periodic or isolated solutions with undisturbed boundaries. Secondly, a Lagrange variable treatment for the derivative $v_{d\xi}$ shows that the velocity derivative blows up in a finite time. This indicates that the nonlinear disturbances will lead to a wave breaking like behavior in a finite time. However, since correlations lead to elasticity, we find wave breaking phenomenon with a difference. This is best illustrated by the exact solution [8] below. Hunter Saxton (HS) equation has step like piecewise continuous and non - smooth solutions. A single step solution may be written as

$$\begin{aligned} v_d(\xi,\tau;\alpha_a,\beta) &= U(\xi,\tau;\alpha_a) \quad if \quad \tau \leq 0 \\ &= U(\xi,\tau;\beta) \quad if \quad \tau \geq 0 \end{aligned} \tag{4.29}$$

[1] local orientation for long axes of liquid crystal molecules

where α_a and β are positive constants with condition $\beta \leq \alpha_a$ and,

$$\begin{aligned} U(\xi,\tau;\alpha_a) &= -\alpha_a\tau \qquad -\infty < \xi \leq -\frac{\alpha_a\tau^2}{2} \\ &= 2\frac{\xi}{\tau} \qquad -\frac{\alpha_a\tau^2}{2} < \xi < 0 \\ &= 0 \qquad 0 \leq \xi < \infty \end{aligned} \tag{4.30}$$

Also $U(\xi,0,;\alpha_a) = 0$ so that U is a continuous function of ξ and τ. Mathematically, the solution is a weak solution of the HS equation satisfying the condition

$$\int \left[\Phi_{\xi\tau}v_d + \frac{1}{2}\Phi_\xi v_d^2 - \frac{1}{2}\Phi v_{d\xi}^2\right] d\xi d\tau = 0 \tag{4.31}$$

for arbitrary test function Φ; this is weakly admissible if

$$(v_{d\xi}^2)_\tau + (v_d v_{d\xi}^2)_\xi = 2(\beta - \alpha_a)\delta(\tau)\delta(\xi) \tag{4.32}$$

From Eq. (4.32) we note that conservation of $\int v_{d\xi}^2 d\xi$ is strictly valid if $\beta = \alpha_a$. For any other value $\beta < \alpha$, the solution is dissipative but still weakly admissible. The solutions are non propagating in the wave frame traveling to the right with the linear phase velocity $\sqrt{(\eta^*/\tau_m)}$. Unlike the inviscid Burger equation, where the step becomes vertical (shock solution) and acquires a finite steady value consistent with conservation laws, the HS equation has a step solution with a slope and a step size that are time dependent. The remarkable feature of the solution is that as the left and right corners of the linear segment having negative slope collide for the creation of a 'shock wave' with infinite slope (which may lead to wave breaking) the spatial support in real space diminishes to a point and the step size vanishes simultaneously. Since the region of transition diminishes to zero size as the step approaches verticality, $\int v_{d\xi}^2 dx$ can remain conserved. In this case no norm is lost and 'energy' is conserved. This is unlike normal Burger's like shock wave where the step is constant and some energy is converted to heat. In fact at complete verticality, the HS solution has no step and that is why it is sometimes called a 'shock wave of zero strength'.

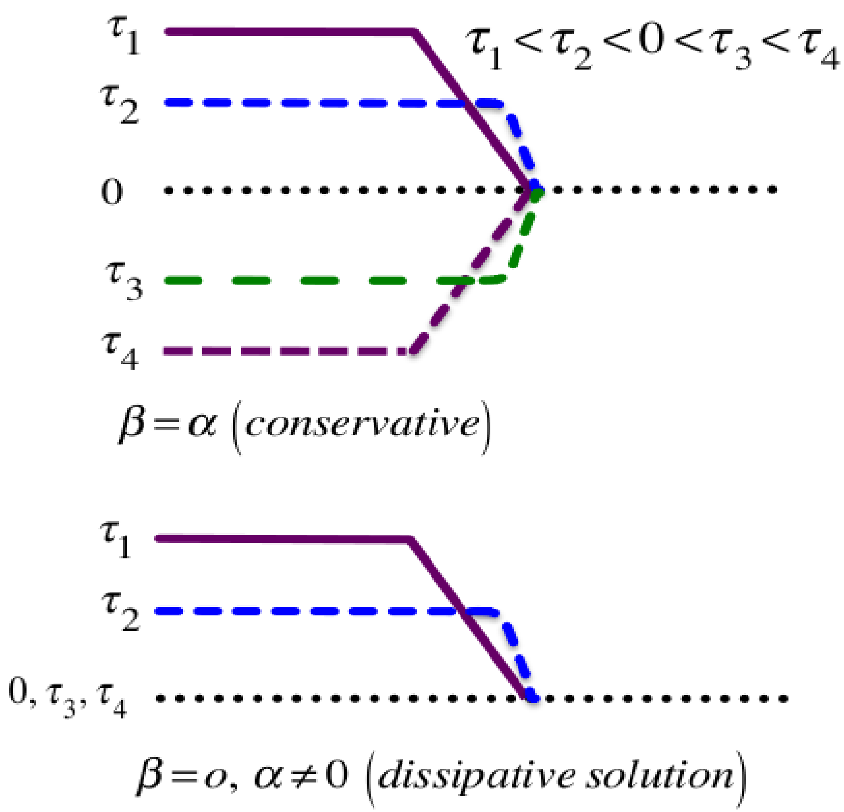

Figure 4.2: Schematic view of time evolution of solution (4.29) of the Hunter Saxton equation for the conservative and dissipative cases (redrawn from [8]).

However, we note that such shock waves of zero strength can form either conservative ($\beta = \alpha_a$) or dissipative ($\beta < \alpha_a$ including $\beta = 0$) global solutions. For example, for $\alpha_a \neq 0$, $\beta = 0$ the disturbance starts with a positive step of v_d on the left at $\tau < 0$ (see Fig. 4.2) and then this step goes to zero at $\tau = 0$ when the step becomes vertical. Thereafter ($\tau > 0$), the disturbance vanishes from everywhere. This is a dissipative global solution for which the entire energy in the initial disturbance damps away and disappears. This is akin to conventional wave breaking, where the infinite slope leads to toppling of the wave and conversion of coherent wave energy into chaotic multi stream motions. The conservative global solution, on the other hand, corresponds to $\beta = \alpha_a$ and results in a fresh disturbance with positive slope at $\tau > 0$, where the conserved $\int v_{d\xi}^2 dx$ energy results in a diminishing slope disturbance in a widening region (Fig. 4.2) as τ increases. This is a remarkable sequel to wave breaking with infinite slope at $\tau = 0$, a sequel in which the entire elastic energy of the infinite slope wave trapped in a region of zero size reappears as a coherent elastic disturbance. This is only possible due to the presence of the RHS of HS equation. The HS equation thus shows evidence for self consistent nonlinear elastic waves supported by correlations which steepen indefinitely but peter out in strength before they reach verticality; these are weakly nonlinear waves which steepen and want to break but cannot do so because of strong coupling and correlations. Physically, one may picture the global dissipa-

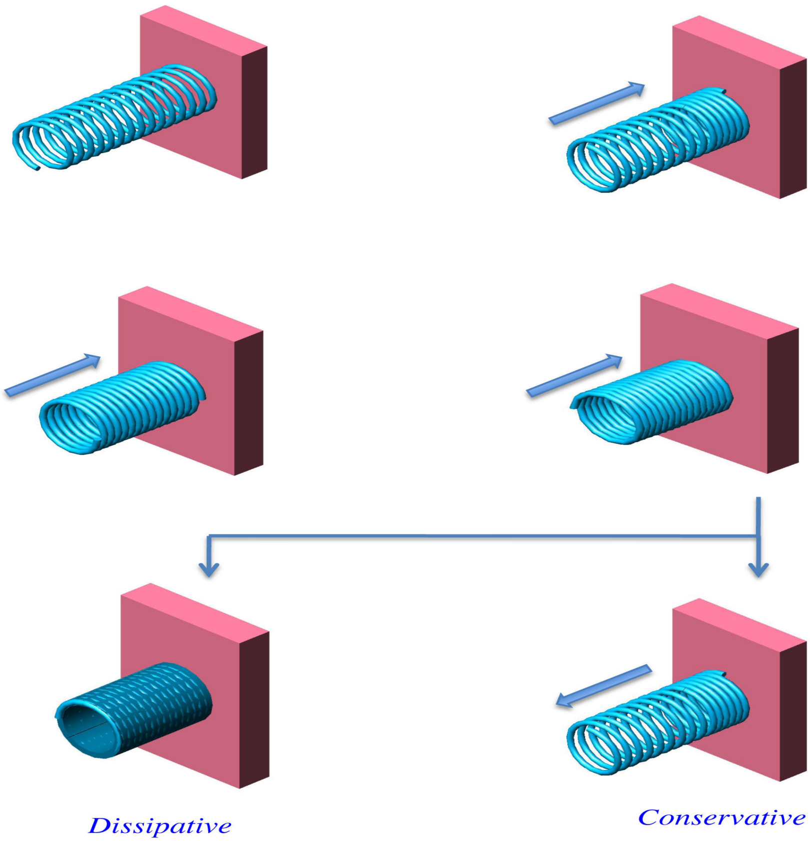

Figure 4.3: Cartoon picture showing energy conservation mechanism in Hunter-Saxton equation.

tive and conservative solutions described above as longitudinal disturbances along a spring attached to a wall (Fig. 4.3). Imagine a compressional disturbance coming towards the wall, steepening and becoming infinitely compressed at the wall. The subsequent behavior can be either inelastic (global dissipative solution) with the entire energy in the disturbance dissipated at the wall (say, because of plastic failure of the spring) and nothing returning back or elastic with a longitudinal disturbance of equal magnitude returning from the wall.

4.4.2 Singular solutions of the form of cusp

We demonstrate here the possibility of having singular cusp solutions for the HS equation, which can be obtained from Eq. (4.23) by ignoring the dispersive term. The field n is assumed to be a function of only one variable f which has a specific combination of time t and the spatial coordinate ξ. The function f is defined by an implicit relationship of the form

$$f = \kappa(\xi - Vt) + G(f) \tag{4.33}$$

It should be noted that the choice of $G = 0$ leads to the well known case wherein one seeks stationarity in a moving frame. This implicit function is a more generalized choice and has been made by several authors earlier [125]. Here G is another function of f. We have then

$$\frac{\partial}{\partial t} = \frac{\kappa V}{(1 - G_f)}\frac{d}{df}; \qquad \frac{\partial}{\partial \xi} = \frac{\kappa}{(1 - G_f)}\frac{d}{df} \tag{4.34}$$

Equation (4.23) can then be written as with $\hat{D} = D/2C$ and defining $s = (\hat{D} + 1)$

$$\frac{\kappa V}{(1 - G_f)}\frac{d}{df}\left\{\frac{\kappa}{(1 - G_f)}\frac{dn}{df}\right\} + s\frac{\kappa n}{(1 - G_f)}\frac{d}{df}\left\{\frac{\kappa}{(1 - G_f)}\frac{dn}{df}\right\} + \left(\frac{\kappa}{1 - G_f}\right)^2\left(\frac{dn}{df}\right)^2 = 0 \tag{4.35}$$

Equation can then further be simplified by canceling the common coefficient to obtain :

$$(sn - V)\frac{d}{df}\left\{\frac{1}{(1 - G_f)}\frac{dn}{df}\right\} + \frac{1}{(1 - G_f)}(\frac{dn}{df})^2 = 0 \tag{4.36}$$

We choose the function G such that $1 - G_f = n - V/s$ which then reduces the equation to

$$sn_{ff} = (s - 1)\frac{n_f^2}{(n - V/s)^2} \tag{4.37}$$

Defining $N = n - V/s$ we obtain

$$\frac{N_{ff}}{N_f} = \frac{s-1}{s}\frac{N_f}{N} \tag{4.38}$$

Integrating one obtains

$$N_f = \hat{K} N^{\frac{s-1}{s}} \tag{4.39}$$

For a negative value of $\hat{D}$ and an s which is less than unity it can be seen that $N_f \to \infty$ for $N \to 0$ or when $n = V/s$. Thus at a finite value of the field the derivative shows a tendency of blowing up which is one of the characteristic features of the cusp structures. In the next section we investigate the case of arbitrary amplitude, and show that the complete GHD set of equations also generate singular forms.

4.4.3 Cusp solutions for arbitrary amplitude

We now show that the full set of GHD equations in the strong coupling limit $\omega\tau_m >> 1$ can permit cusp solutions. Such a dynamical system is already explained with Eq. (4.25) with $\eta = \eta^*/\tau_m$. Here also like before we assume that the field depends on the space and time coordinate through a single variable f defined in Eq. (4.33) and using the corresponding transformations for the derivatives given in Eq. (4.34) we obtain

$$U\frac{d}{df}\left\{\frac{U}{1-G_f}\right\}\frac{dU}{df} = \frac{d}{df}\left\{\frac{1}{1-G_f}\frac{dU}{df}\right\} \tag{4.40}$$

Here, $\sqrt{\eta}U = v_d - V$. We choose the function G so as to have $1 - G_f = U$. This reduces the Eq. (4.40) to

$$U\frac{d^2U}{df^2} = \frac{d}{df}\left\{\frac{1}{U}\frac{dU}{df}\right\} = \left\{-\frac{U_f^2}{U^2} + \frac{U_{ff}}{U}\right\} \tag{4.41}$$

Here, the suffix f denotes differentiation with respect to f. Equation (4.41) can be rewritten as

$$\frac{U_{ff}}{U_f} = \frac{1}{(1-U^2)}\frac{U_f}{U} \tag{4.42}$$

The integration of Eq. (4.42) leads to the familiar equation, viz., known for permitting cusp solutions

$$\frac{dU}{df} = \frac{U}{\sqrt{1-U^2}} \tag{4.43}$$

Where the constant of integration has been absorbed in function f as a multiplication factor and sets the scale of the solution. Equation (4.43) is the equation of a zero total energy effective particle moving in a potential energy bowl with an inverse parabolic form near the origin that blows up at $U = \pm 1$. Thus if the effective particle starts from $U = 0$ with near zero velocity (U'), it falls towards $U = 1$ slowly at first and then rapidly, till it reaches the "wall" (singularity at $U = 1$) from where it is reflected back . It takes an infinite time to climb back to $U = 0$ again. The resulting solution is an isolated soliton like solution with a cusp at the maximum $U = 1$. The solution showing this property is

$$U \;\; = \;\; sech(f + \sqrt{1-U^2}) \tag{4.44}$$

This solution is illustrated in Fig 4.4 and shows infinite derivatives and a cusp singularity at $U = 1$ (that is, $v_d = \beta + \sqrt{(\eta^*/\tau_m})$. The phase speed and the scale size of these solutions are not directly determined by the maximum amplitude. The nature of singularity can be explored by expanding the solution around $U = 1$ and demonstrating that $U' \approx f^{-1/3}$. These cuspon like solutions are steady propagating solutions which are singular at a point and are dithering at the wave breaking amplitude. Physically, such solutions might arise when smooth nonlinear waves acquire amplitudes close to wave breaking, but because of conservation laws squeeze the infinite derivative region to a point with a finite elastic energy content. That this is indeed so, can be ascertained from the integral $\int U'^2 df = \int U' dU = \int U dU/\sqrt{1-U^2} = 1$ in normalized units. Such finite energy content singular solutions may have special stability properties.

4.4.4 Numerical evidence of formation of singular solution

There exist numerical evidence of spontaneous formation of singularities in derivatives in the strong coupling limit. In Fig. 4.5 we show the evolution of a localized Gaussian pulse through the GHD equations. The development of discontinuities are evident from the figure 4.5. Incidentally the evolution through the complete

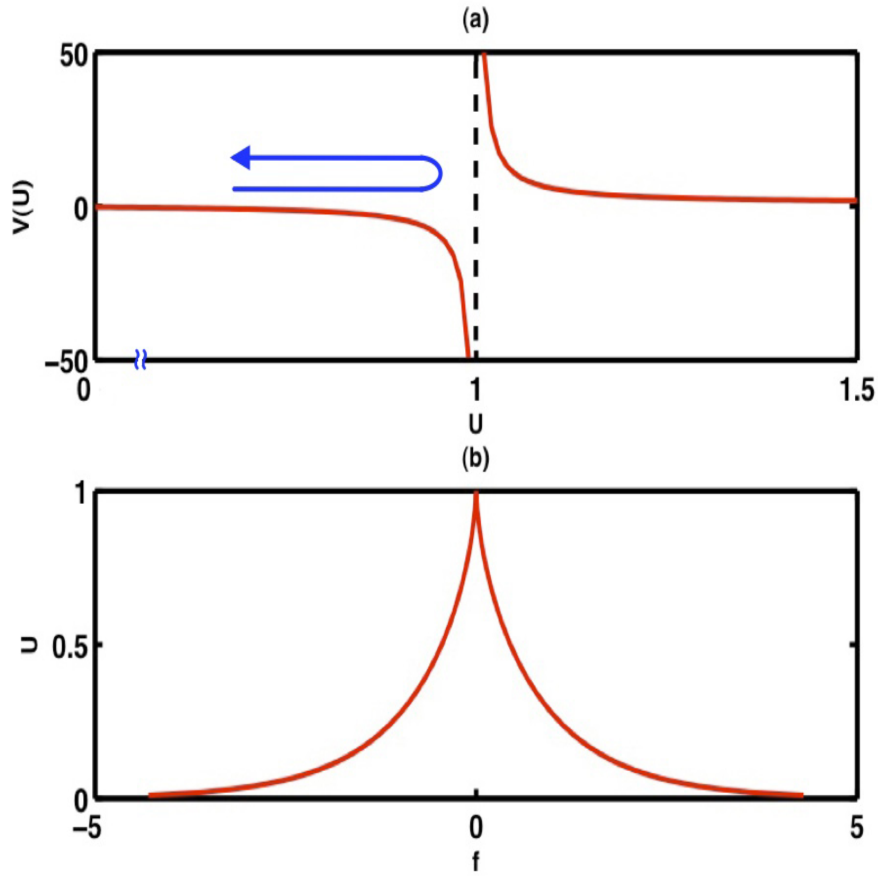

Figure 4.4: Form of potential energy "bowl" and zero energy "particle" orbit corresponding to a cuspon solution.

set shows the tendency of forming piecewise linear form, a characteristic trait of the HS solutions. A choice of high amplitude sinusoidal perturbation in this limit yields a train of singular cusp solutions.

4.5 Summary and conclusion

Physical phenomena typically involve observations of smooth analytic fields in space. However, there are instances when non - analyticity emerges in the observation associated with certain fields and/or their derivatives. One such example is the observation of cusp structures in variety of contexts. For instance, one observes cusp formation on the surface of any water body when waves originating

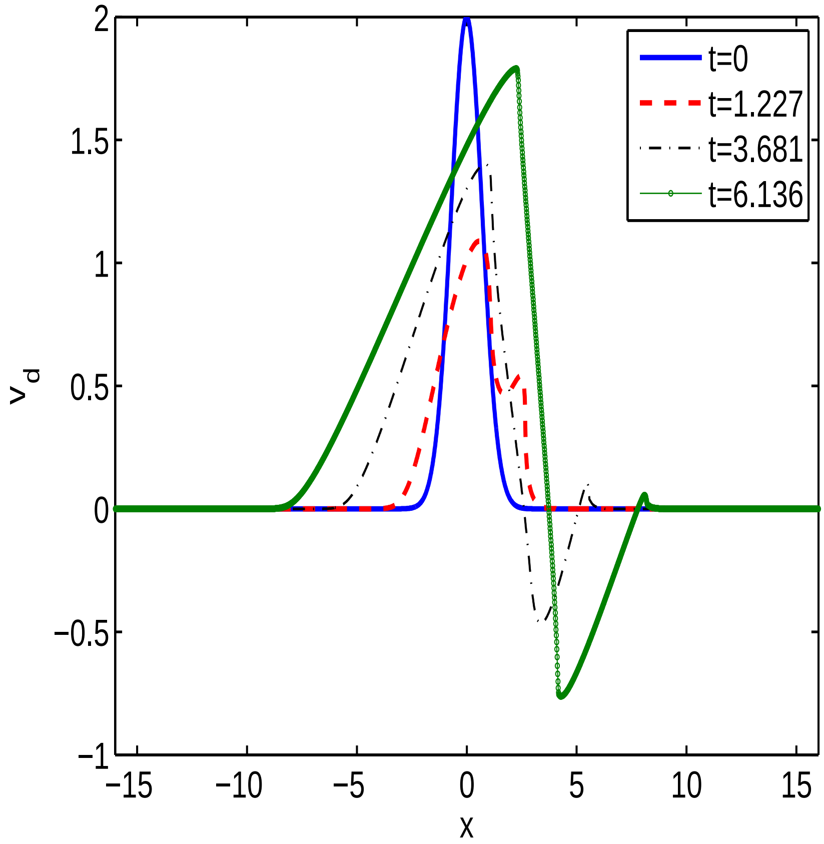

Figure 4.5: Evolution of localized (Gaussian) pulse with Eq. (4.25) valid for the strongly coupled dusty plasma. The parameter η^*/τ_m is chosen to be unity for simulation.

from opposite directions collide or when a high amplitude surface wave hovers around its wave breaking point. Recently, a number of experimental groups have reported the formation of cusp structures in the context of dusty plasmas. While Schwabe *et al.* [2] have observed such structures on the surface of voids formed in the dusty plasma system, the wave breaking experiments conducted by Teng *et al.* [1] are suggestive of cusp formation in the bulk. Against this backdrop we report the first observations of cusp formation in the 1-D numerical simulation of both weakly and strongly coupled dusty plasma medium. Large amplitude initial perturbations are shown to spontaneously develop propagating cusp structures in dust density and velocity. This shows that not only the cusp structures permitted by the governing equations but they are also stable and accessible in the context of dusty plasma. To illustrate this further we have also analytically shown that the equations describing these systems permit cusp solutions. Another noteworthy issue of our investigation are that while the weakly coupled dusty plasma medium follows the KdV paradigm and admits soliton solutions in the small amplitude limit, this is not possible for the strongly coupled plasma medium. An altogether different paradigm of Hunter - Saxton equations are relevant in the strong coupling regime. The HS equations were earlier invoked in the contexts of director fields of the liquid crystal and as the high frequency limit of the Camassa Holm equation employed for the description of the surface wave breaking in fluids. Here for the first time we have shown its applicability to a viscoelastic medium like a dusty plasma system.

They change, they deny, they contradict- and they call it growth.

Ayn Rand

5 Kelvin-Helmholtz instability in weakly coupled dusty plasmas: 2-D studies

In the previous Chapters (3,4), we have carried out 1-D studies of collective phenomena in weakly and strongly coupled dusty plasma medium where we discussed the existence, formation and evolution of coherent structures (e.g. solitons, shocks, cusps etc.) in such systems. The 1-D simulations presented in previous Chapters constrain the system wherein only longitudinal modes can be excited. In this Chapter and subsequent Chapters, we will study some nonlinear collective phenomena in 2-D. This adds another degree of freedom making way to study collective phenomena where variations along the transverse direction too are necessary. In this Chapter, we extensively explore the Kelvin-Helmholtz instability in the context of weakly coupled dusty plasmas. The linear and nonlinear (perturbative and exact nonlinear simulations) studies carrried out and a comparative study of growth rate and nonlinear evolution of this sheared flow instability has been made with hydrodynamic fluids.

5.1 Introduction

The classical Kelvin-Helmholtz (KH) instability has been extensively investigated in a variety of fluid systems and applied to many physical scenarios ever since the first enunciation of its physical mechanism by Helmholtz in 1868 [67] and its mathematical formulation by Kelvin in 1871 [66]. While much of the earliest work is devoted to the excitation of this instability in neutral hydrodynamic fluids [126, 127], the KH instability is also important in plasmas for understanding a variety of astrophysical phenomena involving sheared plasma flows [16, 128, 129]. In some of these applications the plasma can also have a significant dust component (e.g. in cometary tails, planetary ring systems, plasma torches in industrial applications etc.) [13, 15, 18–20] and it is important to study the characteristics of the KH instability in such a plasma.

Motivated by such considerations, in the present Chapter, we have carried out a basic investigation to look at the linear stability of the KH mode in a weakly coupled dusty plasma fluid. In particular, we have looked at the effect of compressibility and dispersion due to coupling with dust acoustic waves on the threshold and growth rate of the instability. While similar effects have been studied in the past in the context of neutral fluids [130] their manifestation in a dusty fluid can be quite distinct and different. In a dusty plasma compressibility arises through two mechanisms, namely, due to a finite dust temperature and also via the interaction energies of the dust fluid with the electron and ion species. In general the magnitude of compressibility depends on the temperature and density of these (electrons and ions) species. For this reason the variation of any of these parameters (ion density/dust charge, ion temperature/dust temperature, ion temperature/electron temperature, dust charge density, etc.) can cause large variations in the compressibility parameter. Thus, the dusty plasma can exhibit behaviour which can correspond to being totally in the incompressible regime to an extremely compressible one. This can be observed from Table - 5.1, where we show the typical range of the dust acoustic speed c_{DA} and the flow velocities and the resultant Mach number for various systems where dusty plasma is prevalent.

Table 5.1: Flow velocities in Dusty plasmas

Physical Systems	c_{DA} (mt/sec)	V_{d0} (mt/sec)	M_A
Lab. Dusty Plasmas ([4, 16, 71, 131, 132])	0.02 - 3.16	0.04 - 1	0.4 - 2
Comets and cometary tails ([14, 133])	0.02 - 10	$\sim 10 - 4000$	$\sim 1 - 400$
Saturn Rings([17, 19, 109])	3.1	0.5 - 100	0.15 - 32
Protoplanetary accretion disks([134])	~ 200	~ 10000	~ 5

Furthermore, the compressible dust perturbations can also be dispersive, which is quite unlike the sound waves in a neutral hydrodynamic fluid. For a detailed characterization of the influence of compressibility and dispersion on the KH mode we have carried out a non-local stability investigation for different shear flow profiles using both analytic and numerical approaches. Three distinct, simple and specific flow profiles, viz., step, piecewise linear and tangent hyperbolic profiles have been analysed. For the step/tangent hyperbolic profiles exact value of the growth rate have been obtained analytically/numerically respectively. A perturbative scheme for the evaluation of the growth rate and the threshold wave-number for the excitation of instability in terms of various orders of the compressibility parameter (Mach number) has been put forth. This scheme has been applied to the piecewise linear and the tangent hyperbolic cases. It has been shown that the analytic perturbative approximation is quite good when compressible effects are weak. We have also provided comparisons in suitable limits with the known results of neutral hydrodynamic fluid, all throughout our analysis, thereby putting our study in proper perspective. We find that the presence of a compressible mode reduces the growth rate and also diminishes the range of unstable wave-numbers. The threshold value of the wave-number beyond which the growth rate vanishes, is smaller in the presence of compressibility. We also find that when the dispersive effects are taken into account, the growth rate of the KH mode reduces further. The eigen functions of the unstable modes are broader in the presence of compressible effects and dispersion causes further broadening of its shape.

The nonlinear stage of the instability has also been investigated by numerically simulating the governing set of dusty plasma equations. The role of compressibility on saturation of the instability, formation of vortex structure in saturation state and process of mergers of vorticity patches have been illustrated by extensive simulations.

The Chapter is organized as follows. In section 5.2, we present the governing fluid equations for the weakly coupled dusty plasma system. Section 5.3 contains the linearized equations for the KH instability for a sheared equilibrium flow profile. In section 5.4 we provide a perturbative treatment to account for effects arising from weak compressibility, on the KH mode. The first order perturbative corrections are then compared with exact results obtained subsequently in section 5.5. In section 5.6, we provide a physical picture of the instability and discuss how compressibility causes the reduction of the KH growth rate. Section 5.7 contains a brief description of the numerical procedure adopted for the simulation of the fluid equations pertaining to the dusty plasma medium in 2-D. The section also contains the description of results obtained during the linear phase of the instability. These results essentially validate our code. In section 5.8 the salient observations from simulation in the nonlinear phase of the instability have been described and a physical interpretation of the results have been provided. Our results are briefly summarized and discussed in the concluding section 5.9.

5.2 Governing equations

The governing equations for a weakly coupled dusty plasma system comprises of continuity and momentum equations for the dust fluid along with Poisson's equation as described in Chapter 2. The momentum equation for weakly coupled dusty plasma system could be obtained from Eq. (2.1) in the limit of $\tau_m d/dt << 1$. The normalized form of the momentum equation for this dust fluid system can be written as:

$$\left(\frac{\partial}{\partial t} + \vec{v_d} \cdot \nabla\right) \vec{v_d} + \frac{\alpha}{n_d} \nabla n_d - \nabla \phi = 0 \tag{5.1}$$

Here, we have considered inviscid dust fluid. The continuity and Poisson's equations are referred from Eqs. (2.2, 2.3). We do not consider the effect of the evolution of energy and/or temperature in the present work. It should be noted from Eq. (5.1) that the compressible perturbations can arise both from the ∇n_d as well as $\nabla \phi$ terms in the equation.

5.3 Equations for linear instability analysis

We linearize the Eqs. (2.2,2.3,5.1) around the equilibrium dust density n_{d0} and a sheared dust flow velocity $\vec{v}_0 = \hat{y} v_0(x)$ along $\hat{y}$ which varies with x. Various specific forms of the flow velocity will be chosen for the analysis later. For the sake of tractability and simplicity we consider here only 2-D perturbations lying in the $x - y$ plane (of flow and the shear direction) for our analysis. The linearized equations after Fourier analyzing in y and time coordinates can be written as

$$-i\Omega n_1 + n_{d0}(ik_y v_{1y} + v'_{1x}) = 0, \tag{5.2}$$

$$-i\Omega v_{1x} + \alpha n_1' - \phi_1' = 0, \tag{5.3}$$

$$-i\Omega v_{1y} + ik_y(\alpha n_1 - \phi_1) + v_{1x}v_0' = 0, \tag{5.4}$$

$$\phi_1'' - k_y^2\phi_1 = n_1 + (\mu_e\sigma_e + \mu_i)\phi_1 \tag{5.5}$$

Here prime ($\prime$) as a superscript denotes a derivative with respect to x (the coordinate along which the equilibrium velocity is sheared). The subscripts 0 and 1 denote the equilibrium and the perturbed quantities respectively and $\Omega = (\omega - k_y v_0)$. Eliminating all fields in terms of ϕ_1 from the set of Eqs. (5.2,5.3,5.4,5.5) we obtain

$$\left\{\frac{d^2}{dx^2} - k_y^2\right\}\left\{\phi_1 - \alpha\left(\frac{d^2}{dx^2} - k_y^2 - \mu_e\sigma_e - \mu_i\right)\phi_1\right\} = \Omega^2\left(\frac{d^2}{dx^2} - k_y^2 - \mu_e\sigma_e - \mu_i\right)\phi_1$$
$$- \frac{2k_y v_0'}{\Omega}\frac{d}{dx}\left\{\phi_1 - \alpha\left(\frac{d^2}{dx^2} - k_y^2 - \mu_e\sigma_e - \mu_i\right)\phi_1\right\}, \tag{5.6}$$

which represents the linearized final equation for our instability analysis.

A simplified limiting case is when the perturbations are quasineutral. The quasineutral perturbations essentially stand for those perturbations for which the left hand side of the Poisson's equation [Eq. (5.5)] can be ignored, *i.e.* $\nabla^2\phi_1 \approx 0$. Thus, for this case there exist a simple relationship

$$\phi_1 = -n_1/(\mu_e\sigma_e + \mu_i) \tag{5.7}$$

in the linear regime between the scalar potential and the density perturbation. In the quasineutral limit when we ignore $\nabla^2\phi_1$ it can be shown that the Eq. (5.6) gets simplified to

$$n_1'' - k_y^2 n_1 + \frac{2k_y n_1' v_0'}{\Omega} + \frac{\Omega^2}{\alpha_1}n_1 = 0 \tag{5.8}$$

Here, $\alpha_1 = \alpha + 1/(\mu_e\sigma_e + \mu_i)$ and we have used Eq. (5.7) to express ϕ_1 in terms of n_1. Thus, α_1 represents the total effect of compressibility arising from finite dust temperature as well as interactions due to ion and electron species of the plasma. It is interesting to note that Eq. (5.8) has two more representations as written below.

$$\psi'' + \left\{\frac{\Omega^2}{\alpha_1} - k_y^2 - \frac{k_y v_0''}{\Omega} - \frac{2k_y^2 v_0'^2}{\Omega^2}\right\}\psi = 0 \tag{5.9}$$

This arises when first derivative of n_1 in Eq. (5.8) is eliminated by using the transformation $\psi = n_1/\Omega$. The other form of the equation is in terms of the perturbed velocity field v_{1x}

$$k_y \Omega v_{1x} - \left\{ \frac{k_y v_0' v_{1x} + \Omega v_{1x}'}{k_y - \Omega^2/\alpha_1 k_y} \right\}' = 0 \tag{5.10}$$

In fact Eq. (5.10) is the familiar linearized Kelvin - Helmholtz (KH) instability equation for a neutral compressible fluid [130]. This is expected as in the quasineutral limit the equations for dust fluid should reduce to those of the neutral compressible fluid. The perturbed velocity v_{1x} is related to n_1 with the relationship $v_{1x} = -in_1'/\Omega$. Any of these Eqs. (5.8,5.9,5.10) can be used for the purpose of evaluating the growth rate and the unstable eigenfunction for a compressible fluid without dispersive effects. The choice of a particular form out of these three equations is often guided by whichever simplifies the analysis of any given problem at hand.

For an incompressible fluid we have $1/M_A = \sqrt{\alpha_1}/V_0 = \infty$. Here M_A is the Mach number. In this case there exist no density perturbations in the fluid. The variable n_1 of Equation (5.8) in this limit essentially represents the pressure perturbations of the fluid. All these three forms, viz., Eq. (5.8), Eq. (5.9) and Eq. (5.10) in the limit of $\alpha_1 \to \infty$ (for finite non zero V_0) reduce to the familiar incompressible limit of the linearized KH equation, *viz.,*

$$\left(\frac{d^2}{dx^2} - k_y^2 \right) v_{1x} + \frac{k_y v_0''}{\Omega} v_{1x} = 0 \tag{5.11}$$

5.4 Perturbative treatment for compressibility

The value of the KH growth rate and the threshold wave vector for instability along the periodic flow direction for the incompressible case (with $\alpha_1 = \infty$) are well known. The growth rate has a typical bell shaped form as a function of $k_y \epsilon$, where k_y is the wavenumber along the flow direction and ϵ is the shear width of the equilibrium flow. The growth rate is zero at $k_y = 0$, maximizes and then again falls back to zero at a threshold value of wavenumber $k_y = k_{yth}$. It is observed that k_{yth} is typically of the order of $1/\epsilon$ and is exactly $= 1/\epsilon$ for a tangent hyperbolic form of the shear velocity.

It would be interesting to see how the compressibility alters the growth rate and the unstable range of wave numbers. To understand this analytically we employ a perturbative treatment for weakly compressible cases in this section. We consider here the case of large α_1 and evaluate the role of compressibility by considering a perturbative expansion in $\mathcal{O}(1/\alpha_1)$ around the zeroth order known incompressible result. The problem is thus cast in various orders of $\nu = 1/\alpha_1$. We assume that the eigenvalue and the eigenfunction can be expanded as $\omega = \omega^{(0)} + \omega^{(1)} + ...$, and $v_{1x} = v = v^{(0)} + v^{(1)} + ...$ respectively. The superscripts index inside the brackets represent the various orders of ν the function is dependent upon. We have dropped the suffix $1x$ from v_{1x} (representing perturbation from equilibrium shear flow). The zeroth order of Eq. (5.10) is

$$v^{(0)\prime\prime} + \left(-k_y^2 + \frac{k_y v_0''}{\Omega^{(0)}}\right) v^{(0)} = 0 \tag{5.12}$$

The first order expansion of Eq. (5.10) in $1/\alpha_1$ is given by the following equation :

$$\begin{aligned} &v^{(1)\prime\prime} + \left(-k_y^2 + \frac{k_y v_0''}{\Omega^{(0)}}\right) v^{(1)} - \frac{k_y v_0''}{\Omega^{(0)2}} \omega^{(1)} v^{(0)} \\ &+ \frac{1}{\alpha_1 k_y^2 \Omega^{(0)}} \left\{\Omega^{(0)2}(k_y v^{(0)} v_0' + v^{(0)\prime}\Omega^{(0)})\right\}' = 0 \end{aligned} \tag{5.13}$$

We multiply Eq. (5.13) by $v^{(0)}$ and integrate over x. For the first term the x differentiations are transferred to $v^{(0)}$ from $v^{(1)}$. Using Eq.(5.12) the first two terms then vanish. The remaining equation can then be cast as

$$\omega^{(1)} \int \frac{v_0'' v^{(0)2}}{\Omega^{(0)2}} dx = \frac{1}{\alpha_1 k_y^3} \int \frac{1}{\Omega^{(0)}} \left[\Omega^{(0)2}(k_y v_0' v^{(0)} + \Omega^{(0)} v^{(0)\prime})\right]' v^{(0)} dx \tag{5.14}$$

By evaluating the two integrals for the zeroth order wavefunction for specific shear flow profiles one can get the value for $\omega^{(1)}$. For the step function profile the effect of compressibility can be evaluated exactly analytically (this is shown in the next section). It shows that the growth rate reduces due to compressibility. For other profiles the exact result is obtained numerically which also show that the growth rate reduces due to compressibility. We will show in the section IV when we consider specific profiles that perturbative expression for $\omega^{(1)}$ from Eq. (5.14) also shows it to be negative. Furthermore, for weak compressibility the perturbative expressions are in good agreement with the exact results obtained numerically.

We now obtain the expression for the altered threshold wavenumber k_y for growth, by the first order perturbative treatment. To evaluate the threshold we put $\omega = 0$ and look for the change in the value of k_y from its original incompressible value of $k_y^{(0)}$ Thus, expanding $k_y = k_y^{(0)} + k_y^{(1)} + ...$ in this case we have the zeroth order equation as

$$v^{(0)\prime\prime} - \left(k_y^{(0)2} + \frac{v_0''}{v_0}\right) v^{(0)} = 0 \tag{5.15}$$

The first order equation is

$$\begin{aligned} & v^{(1)\prime\prime} - \left(k_y^{(0)2} + \frac{v_0''}{v_0}\right) v^{(1)} - 2k_y^{(0)} k_y^{(1)} \\ & - \frac{v_0}{\alpha_1}\left(v^{(0)} v_0'' - v^{(0)\prime\prime}\right) - \frac{2v_0'}{\alpha_1}\left(v^{(0)} v_0' - v^{(0)\prime} v_0\right) = 0 \end{aligned} \tag{5.16}$$

We again apply the same technique of multiplying Eq. (5.16) by $v^{(0)}$ and integrating over x. We transfer the two spatial derivatives from $v^{(1)}$ in the first term of Eq. (5.16) to $v^{(0)}$ and use Eq. (5.15). The contribution from the first two terms of Eq.(5.16) therefore vanishes from the integration. Again the first order correction for k_y can be obtained from the following expression :

$$2k_y^{(0)} k_y^{(1)} \alpha_1 \int v^{(0)2} dx = -\int \left[v_0 v_0'' v^{(0)2} + 2v_0'^2 v^{(0)2} - v_0^2 v^{(0)} v^{(0)\prime\prime} - 2v_0 v^{(0)} v_0' v^{(0)\prime}\right] dx \tag{5.17}$$

Simplifying Eqn.(5.17) we get a final expression as follows

$$k^{(1)} = -\frac{1}{2k^{(0)}\alpha_1} \frac{\int_{-\infty}^{\infty} \left(v_0' v^{(0)} - v_0 v^{(0)\prime}\right)^2 dx}{\int_{-\infty}^{\infty} v^{(0)2} dx} \tag{5.18}$$

Both the integrands of the numerator as well as that of the denominator of Eq. (5.18) being positive definite, it shows that $k^{(1)}$ would be negative. The shows clearly that the threshold value of the wavenumber decreases in the presence of compressibility. The integrals in Eq. (5.18) has been evaluated numerically for obtaining the value of $k^{(1)}$ for specific flow profiles. This is discussed in section V.

5.5 Instability analysis for specific flows

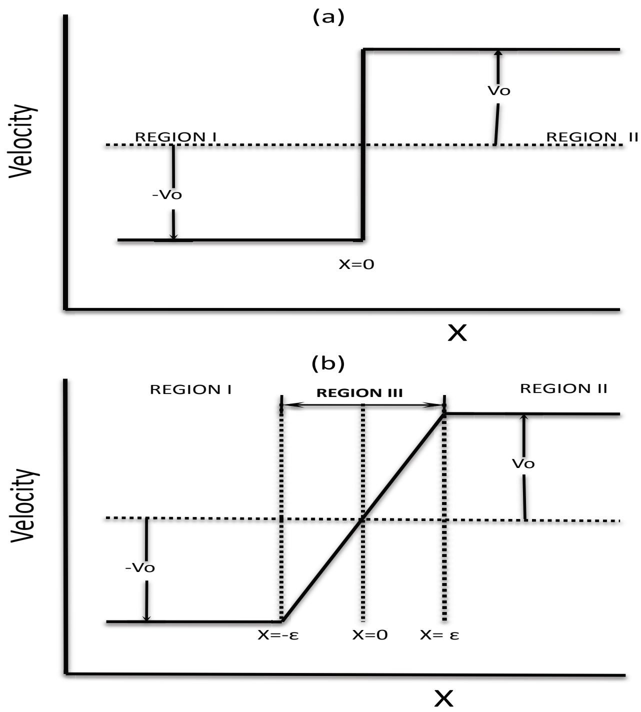

Figure 5.1: The equilibrium dust shear velocity profiles have been shown in the figure. The subplot (a) shows the step function shear flow velocity and (b) represents a piecewise linear flow profile.

We now try solving the linearized equations Eqs. (5.8,5.9,5.10) for specific given profiles of the sheared flow velocity exactly. Often for analytical tractability one considers simple forms of the equilibrium velocity flow profiles. For complicated shear flow structure numerical solutions are obtained. Typically, the simplest case that has often been considered is the case when the flow velocity has a step function form about a point say at $x = 0$. In this case, the velocity is uniform on both sides of $x = 0$ but the values differ by a finite amount. The form of such a flow profile has been illustrated in Fig. 5.1(a). In this case the eigenvalue equation turns out to be homogeneous in the two regions and can be expressed in terms of exponential functions. However, to obtain the final solution the eigenfunctions in the two separate regions have to be matched at the location of discontinuity. There are two matching conditions (the differential equation [Eq. (5.8)] being of second order under the quasineutral assumption) for the fields. The Eq. (5.8) can be expressed in three equivalent forms of differential equations in terms of variables v_{1x}, n_1 and ψ. The form of two matching conditions in terms of each variables can be written down as follows:

$$\begin{aligned} f_1(v_{1x}) &= \Omega v'_{1x} + k_y v'_0 v_{1x}; \qquad f_2(v_{1x}) = \frac{v_{1x}}{\Omega} \\ f_1(n_1) &= \frac{n'_1}{\Omega^2}; \qquad f_2(n_1) = n_1 \\ f_1(\psi) &= \frac{\psi'}{\Omega} - \frac{k_y v'_0 \psi}{\Omega^2}; \qquad f_2(\psi) = \Omega\psi \end{aligned} \tag{5.19}$$

These need to be satisfied at the location of the discontinuity of the equilibrium flow. For the full fourth order differential equation [Eq. (5.6)] for which dispersive effects from Poisson's equation have been incorporated four matching conditions are required. These matching conditions are as follows :

$$\begin{aligned} f_1(\phi_1) &= \frac{-\alpha\phi_1^{'''}}{\Omega^2} + \frac{(1+\alpha R)\phi_1^{'}}{\Omega^2}; \qquad f_2(\phi_1) = -\alpha\phi_1^{''} + (1+\alpha R)\phi_1 \\ f_3(\phi_1) &= \alpha\phi_1^{'}; \qquad f_4(\phi_1) = \alpha\phi_1 \end{aligned} \tag{5.20}$$

where $R = k_y^2 + \mu_e\sigma_e + \mu_i$.

The step velocity profile is an extreme case of any flow profile with zero shear width. In a realistic situation the flow shear would always have a finite shear width. A piecewise linear velocity flow profile as shown in Fig. 5.1(b) takes account of a finite shear width through a middle region where the equilibrium flow varies linearly with x, thereby connecting the two layers with disparate flows. The matching conditions of Eq. (5.19) being valid for the abrupt step function discontinuity, clearly, also holds for any smoother profile, the piecewise linear case being one.

5.5.1 Step profile

The equilibrium velocity profile is chosen to have a step function form as shown in Fig. 5.1(a). For this profile $v_0 = -V_0$ for $-\infty < x < 0$ (we denote this by Region I) and $v_0 = V_0$ for $0 < x < \infty$ (Region II). Thus, there is an abrupt jump in the flow at $x = 0$. The simplicity of the profile renders the possibility of exact analytical evaluation of the growth rate as we would now observe. The linearized equation takes a simple homogeneous form in the two regions. We employ Eq. (5.8) for n_1 for the purpose of analysis here. Denoting the fields in the two regions by suffix I and II we have

$$n''_{1,I,II} - k_y^2 n_{1,I,II} + \frac{\Omega^2_{I,II}}{\alpha_1} n_{1,I,II} = 0 \tag{5.21}$$

The solutions for $n_{1,I,II}$ in the two regions can now be obtained easily and have the following form:

$$n_{1,I} = B \exp\left\{\sqrt{k_y^2 - \Omega_I^2/\alpha_1 x}\right\}; \quad n_{1,II} = A \exp\left\{-\sqrt{k_y^2 - \Omega_{II}^2/\alpha_1 x}\right\}$$

The boundary condition for the solution to vanish at $\pm\infty$ has been used. Now, by employing the matching conditions we seek to obtain the eigenvalue ω. This is provided by

$$\omega^2 + (k_y V_0)^2 = \frac{(\omega^2 - (k_y V_0)^2)^2}{2k_y^2 \alpha_1} \tag{5.22}$$

The above equation in the limit of $\alpha_1 \to \infty$ gives the correct growth rate $\gamma = i\omega = k_y V_0$ for the incompressible step function profile of the flow. The growth rate for the compressible case can be obtained by choosing α_1 finite. Solving the biquadratic equation for ω, we obtain

$$\omega^2 = k_y^2 \left[V_0^2 + \alpha_1 \pm \sqrt{\alpha_1^2 + 4\alpha_1 V_0^2}\right] \tag{5.23}$$

Expanding the expression for growth rate in powers of $1/\alpha_1$ we have

$$\omega^2 = k_y^2 \left[-V_0^2 + \frac{2V_0^4}{\alpha_1}\right]$$

showing clearly that compressibility reduces the KH growth rate. There exists a lower threshold on α_1, which is the square of dust acoustic speed c_s^2 beyond which the instability cannot be excited. This threshold condition can be obtained by demanding that ω^2 remain negative for instability, which yields

$$| V_0 | < \sqrt{2\alpha_1}$$

This shows that for instability, the dust acoustic speed in the medium has to be faster than the flow velocity. In other words the instability is possible only when the flow velocity is subsonic.

In the above derivation we had used quasineutral assumption for simplification. We now consider the full equation including the effect of dispersion arising from the Poisson's equation. For step flow profile the form of Eq. (5.6) in both regions can be expressed in terms of field variable ϕ_1 with suffix I and II denoting the respective regions.

$$-\alpha\Phi''''_{I,II} + \left(1 + \alpha R + \alpha k_y^2 - \Omega^2_{I,II}/n_0\right)\Phi''_{I,II} + \left(-k_y^2 + \alpha R k_y^2 + R\Omega^2_{I,II}/n_0\right)\Phi_{I,II} = 0 \tag{5.24}$$

In the above the perturbed field ϕ_1 has been represented by Φ to simplify the notation as the suffix due to region I and II are also to be incorporated. Now,

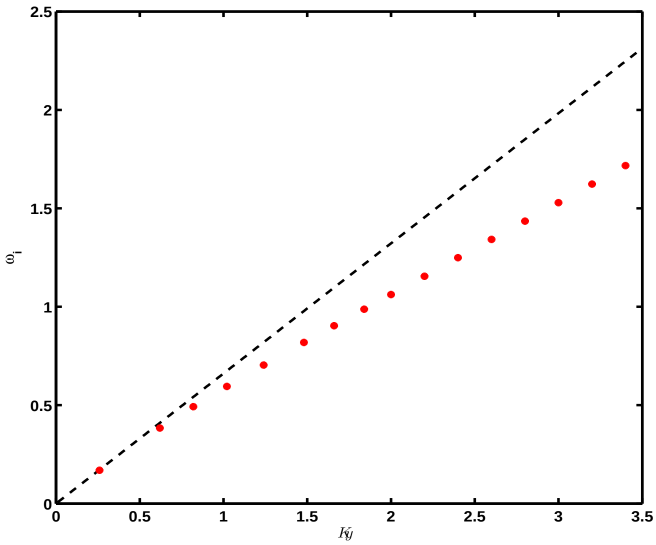

Figure 5.2: Figure shows linear growth for $\alpha = 1$ for the quasineutral case (dashed line) and with dispersive correction due to $\nabla^2\phi_1$ (shown by circles). The other parameters are $V_0 = 1, \mu_e = 0.1, \mu_i = 1 + \mu_e$ with step shear flow profile.

choosing appropriate form of exponential solution for Eq. (5.24) so that they vanish at $\pm\infty$ and utilizing the four matching conditions provided by Eq. (5.20) we obtain a set of four coupled equations relating the coefficients of the four exponential functions. For non - trivial solutions, the determinant of the coefficient matrix viz., $det \parallel M \parallel = 0$ should vanish. This condition gives the eigenvalue ω. The matrix M has the following form:

$$M = \begin{vmatrix} 1 & -1 & 1 & -1 \\ p & -q & r & -s \\ (-\alpha p^2 + 1 + \alpha R) & (\alpha q^2 - 1 - \alpha R) & (-\alpha r^2 + 1 + \alpha R) & (\alpha s^2 - 1 - \alpha R) \\ \begin{array}{c}(-\alpha p^3/\Omega_+^2 \\ +(1+\alpha R)p/\Omega_+^2)\end{array} & \begin{array}{c}(\alpha q^3/\Omega_-^2 \\ -(1+\alpha R)q/\Omega_-^2)\end{array} & \begin{array}{c}(-\alpha r^3/\Omega_+^2 \\ +(1+\alpha R)r/\Omega_+^2)\end{array} & \begin{array}{c}(\alpha s^3/\Omega_-^2 \\ -(1+\alpha R)s/\Omega_-^2)\end{array} \end{vmatrix}$$

Here, the following notations have been used:

$$\Omega_\pm = \omega \pm k_y V_0$$

$$p = \left(-a_+/2 + \surd(a_+^2 - 4b_+)/2\right)^{1/2}$$

$$q = -\left(-a_-/2 + \surd(a_-^2 - 4b_-)/2\right)^{1/2}$$

$$r = \left(-a_+/2 - \surd(a_+^2 - 4b_+)/2\right)^{1/2}$$

$$s = -\left(-a_-/2 - \surd(a_-^2 - 4b_-)/2\right)^{1/2}$$

Also the coefficients $a_\pm$ and $b_\pm$ are

$$a_\pm = -(1/\alpha)(1 + \alpha R + \alpha k_y^2 - \Omega_\pm^2)$$

$$b_\pm = -(1/\alpha)(R\Omega_\pm^2 - k_y^2 - \alpha R k_y^2)$$

The roots ω, for above determinant has been calculated numerically. We shown in Fig. 5.2 the growth rate obtained as a function of k_y and for $\alpha = 1$. A comparison with the non - dispersive compressible growth rate shown in the same figure 5.2 for this range of parameter shows that the dispersive effect reduces the growth rate.

The step profile, however, is too simplistic and somewhat unrealistic. It shows that the growth rate increases indefinitely with increasing value of k_y. A realistic flow in general will change over some finite width say ϵ. When k_y^{-1} becomes comparable to ϵ the effects due to finite width may become important. In fact for the case of incompressible fluid, it has already been shown that the growth rate vanishes when $k_y\epsilon \geq 0.639$ for a piecewise linear profile and for $k_y\epsilon \geq 1$ for a tangent hyperbolic form of the velocity profile [135]. To discern the effect of compressibility on such a limit, as well as to identify any other role that the compressibility of the fluid may have on the mode, we next carry out analysis for the two cases of piecewise linear and the smooth tangent hyperbolic profiles of the velocity. For these cases it is not possible to obtain the growth rate analytically, we employ the perturbative scheme and numerical eigen value search for our studies.

5.5.2 Piecewise linear profile

The form of the piecewise linear profile is shown in Fig. 5.1(b). We have now Region I and II for $-\infty < x < -\epsilon$ (where $v_0 = -V_0$) and $\epsilon < x < \infty$ (where $v_0 = V_0$). The middle region $-\epsilon < x < \epsilon$ is termed as region III for which $v_0 = V_0 x/\epsilon$. The eigenvalue for this system in the incompressible limit which is the zeroth order expansion result in the compressibility parameter of $1/\alpha_1$, can be evaluated easily and is given by the following expression:

$$\omega^{(0)2} = \frac{1}{4}\left[\left(\frac{V_0}{\epsilon} - 2k_y V_0\right)^2 - \frac{V_0^2}{\epsilon^2}\exp(-4k_y\epsilon)\right] \tag{5.25}$$

This expression (Eq. (5.25)) is same as that obtained by Drazin [126] for $V_0 = \epsilon = 1$. It should be noted that the above expression easily reduces to the result of the step velocity flow profile in the limit of $\epsilon \to 0$. The zeroth order eigenfunctions corresponding to Eq. (5.25) are as follows :

$$\begin{aligned} v_I^{(0)} &= B\exp(k_y x) \\ v_{II}^{(0)} &= A\exp(-k_y x) \\ v_{III}^{(0)} &= A_0\exp(-k_y x) + B_0\exp(k_y x) \end{aligned} \tag{5.26}$$

The relationship between the coefficients A, B, A_0 and B_0 are obtained from matching conditions and they are given by :

$$B = A_0 f_B = A_0\left[1 + \frac{\epsilon}{V_0}\left(2\Omega_+ - \frac{V_0}{\epsilon}\right)\right]\exp\left(2k_y\epsilon\right)$$

$$B_0 = A_0 f_{B0} = \frac{\epsilon A_0}{V_0}\left[2\Omega_+ - \frac{V_0}{\epsilon}\right]\exp\left(2k_y\epsilon\right)$$

$$A = A_0 f_A = A_0\left[1 + \frac{\epsilon}{V_0}\left(2\Omega_+ - \frac{V_0}{\epsilon}\right)\exp\left(2k_y\epsilon\right)\right]$$

This completely determines the eigenfunction in the zeroth order.

To evaluate the correction in the threshold value of the wavevector due to compressibility we substitute $\omega = 0$ in the above expressions. The coefficients of the zeroth order wavefunction f_B, f_{A0} and f_{B0} in the limit of $\omega = 0$ are then related as:

$$\tilde{f_B} = [1 + (2k_0\epsilon - 1)]\exp\left(2k_0\epsilon\right)$$

$$\tilde{f_{B0}} = (2k_0\epsilon - 1)\exp\left(2k_0\epsilon\right)$$

$$\tilde{f_B} = 1 + (2k_0\epsilon - 1)\exp\left(4k_0\epsilon\right)$$

Using these relationships the numerical value for k_1 from Eq. (5.18) for $\alpha_1 = 50$ and $\epsilon = 0.5$, turns out to be $k^{(1)} = -0.5976$ and $k^{(1)}\epsilon = -0.2988$. Thus, the new threshold on the wavenumber for these compressibility parameters is $k_{yth} = (0.639 - 0.2988)/\epsilon = 0.3402/0.5 = 0.6804$. It should be noted that for this value of $\alpha_1 = 50$, the second order corrections are of order $\mathcal{O}(k^{(1)}/k^{(0)})^2 \sim 0.2$ which is quite high. Since the exact value can not be evaluated for the piecewise linear profile we are in no position to judge the accuracy of the perturbative treatment and to ascertain upto what α_1 the perturbative treatment would work fine. In the next section we carry out the analysis for a smooth tangent hyperbolic profile. For this particular profile the role of compressibility can be exactly determined by evaluating the eigenvalue and the eigenfunction for the Eqs. (5.2,5.3,5.4,5.5) numerically. We then compare these results with our perturbative analysis.

5.5.3 Tangent hyperbolic profile

We now choose a smoothly varying equilibrium profile of the form of a tangent hyperbolic function $v_0(x) = V_0\tanh(x/\epsilon)$ and study the linear problem defined by the complete set of Eqs. (5.2,5.3,5.4,5.5) by solving it numerically. This has two objectives, we are able to consider the effects of compressibility non perturbatively, thereby checking the conclusions of a perturbative treatment presented earlier. The second objective is to understand the role of $\nabla^2\phi_1$ on the instability. In the presence

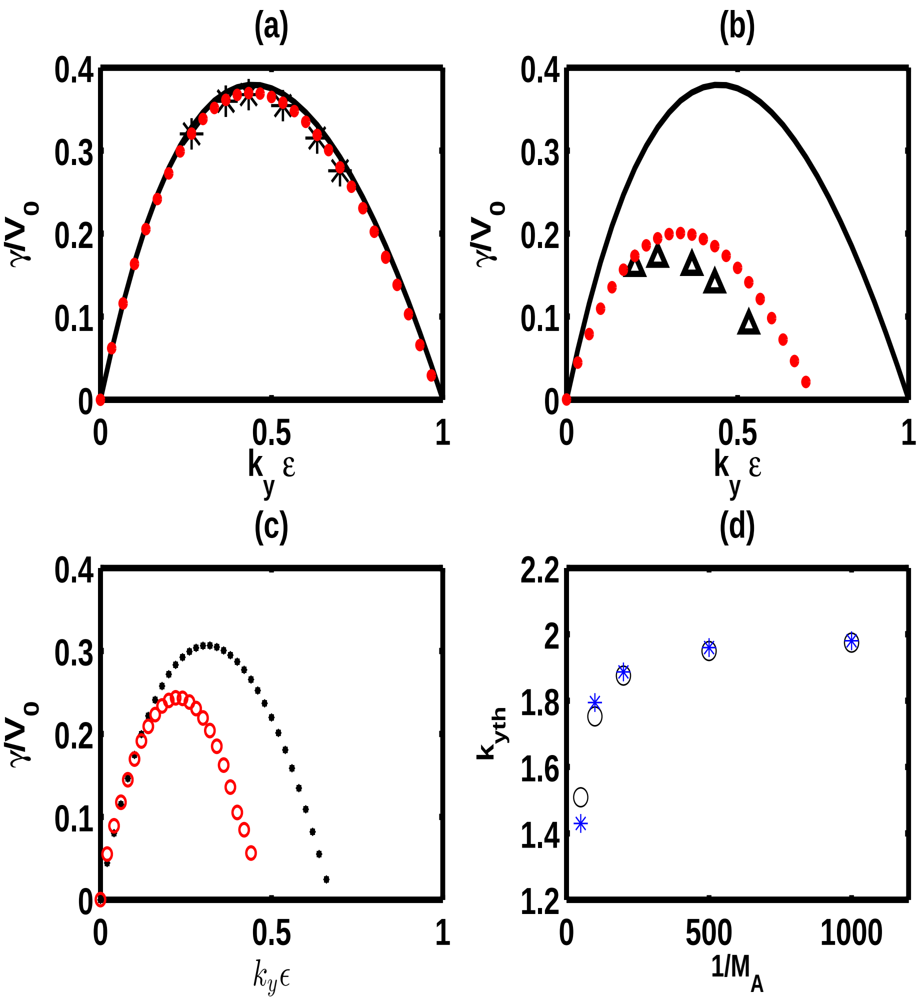

Figure 5.3: The plot of γ/V_0 (where γ is the linear growth rate) as a function of $k_y\epsilon$ has been shown for a tangent hyperbolic shear flow profile. In subplot (a) the solid line corresponds to the incompressible case $M_A = 0$ ($\alpha = \infty$), the small dots and the stars represent the exact and the perturbative values respectively for $M_A = 0.158$. Subplot (b) solid line again shows the incompressible case and the dots and triangles are the exact and perturbative values for $M_A = 0.7$. Subplot (c) is for $M_A = 0.5$ for which the solid circles and the hollow circles correspond to quasineutral and the dispersive cases. Subplot (d) shows a comparison of the threshold wavenumber evaluated exactly ($*$) and by perturbative scheme ($\circ$) as a function of $1/M_A$.

of this term the equations are fairly cumbersome to make any analytical progress, hence this effect is investigated numerically with the help of a smooth flow profile. For the numerical scheme, we use the linearized Poisson's equation Eq. (5.5) to express n_1 in terms of ϕ_1 and its derivatives. The set of Eqs. (5.2,5.3,5.4) are then discretized in x space. Eigenvalue is then obtained by the standard routines of Matrix eigenvalue evaluation.

In Fig. 5.3(a), we show a comparison between the growth rate as a function of $k_y\epsilon$ for the incompressible $\alpha = \infty$ and the compressible $\alpha = 1000$ cases (solid lines and solid circles respectively). Clearly, the growth rate diminishes in the presence of compressible perturbations. We have also shown the estimates obtained from the first order perturbation treatment by stars for some particular values of the wavenumber in the figure. This has been shown for points around the maximum growth rate where $\omega^{(0)}$ being large the perturbative treatment would hold. For one typical value of $k_y\epsilon$ (say $= 0.4333$) the incompressible growth rate is $\omega^{(0)} = i1.896$, the exact compressible growth rate $\omega = i1.847$, thereby implying that $\omega^{(1)} = i(1.896 - 1.847) = i0.05$. The ratio, $\omega^{(1)}/\omega^{(0)} \approx 0.02$ is small and the second order corrections are of the order of 10^{-4} which can be ignored. Thus, the first order corrections work fine for this high value of α. This is the reason that the perturbative treatment provides a very good agreement for this particular case as the figure shows.

In Fig. 5.3(b) we have shown a plot for the case when the value of $\alpha = 50$. In this case the effect of compressibility is not weak to warrant a perturbative analysis. This can be observed by comparing the two exact results obtained numerically, viz., the incompressible (solid line) and the compressible (circles) cases. They differ significantly. Clearly, the second order terms, e.g. $\mathcal{O}(\omega_1/\omega_0)^2$ would be significant for this case, which has been ignored in our perturbative treatment. As expected, the estimates obtained from our first order perturbative analysis shown by triangles in the Fig. 5.3(b) are also not close to the exact numerically obtained values for the compressible case denoted by circles. For this case we had also evaluated the exact growth rate with the dispersive corrections through $\nabla^2\phi$. The dispersion, however, does not seem to play any significant role for this particular value of α. The growth rate was found to exactly overlap with the quasineutral plots denoted by circles in Fig. 5.3(b).

At higher compressibility, viz., $\alpha = 1$ the differences between the dispersive and non - dispersive cases start showing up. In Fig. 5.3(c) the plots show a comparison of growth rates for a quasineutral non dispersive case (solid circles) with that obtained by incorporating dispersive effects for $\alpha = 1$. In this strongly compressible case, the effect of dispersion is clearly evident. The growth rate shows reduction due to dispersion at higher wavenumbers. This effects the threshold wavenumber of the instability which gets considerably reduced in the presence of dispersion. The

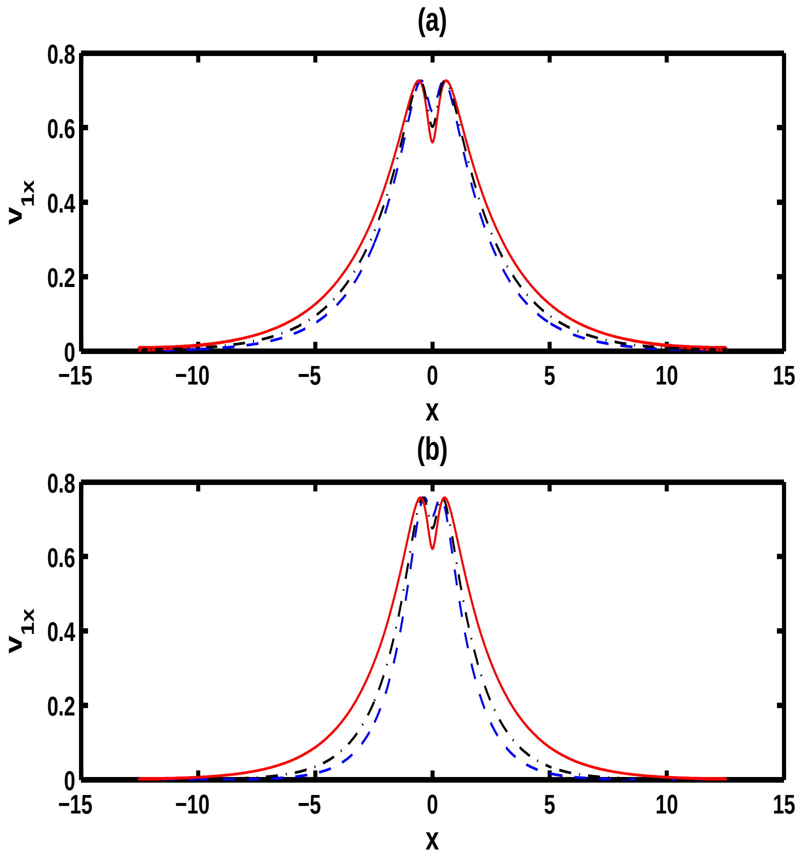

Figure 5.4: Plot of the eigenvector v_{1x} as a function of x has been shown. The subplot (a) is for $k_y = 0.5334$. the solid, dot-dashed and dashed lines represent $\alpha = 50$, $\alpha = 100$ and $\alpha = \infty$ respectively. Subplot (b) shows the eigenfunctions for the maximally growing mode for $\alpha = 50$, $\alpha = 100$ and $\alpha = \infty$ by solid, dot- dash and dahsed lines respectively.

exact results clearly show that compressibility reduces the threshold wavenumber for instability and dispersion at higher compressibility further limits the unstable domain. We now provide a comparison with the exact threshold wavenumber with that evaluated from our perturbative analysis presented in section IV. This has been shown in the plot of Fig. 5.3(d). The symbol asterix($*$) and circles($\circ$) denote the exact and perturbative evaluation of k_{yth}. The perturbative result improves with increasing value of α. These results are for $\epsilon = 0.5$ and it should be observed that for higher α values the k_{yth} slowly asymptotes towards the incompressible limit of $1/\epsilon$.

We now study the properties of the eigenfunctions of the unstable KH mode for the various cases. The solid, dot dashed and dashed lines are the unstable eigen modes for $\alpha = 50$, $\alpha = 100$ and the $\alpha = \infty$ (incompressible) respectively in Fig. 5.4. While the plots in Fig. 5.4(a) correspond for a specific wavenumber value of $k_y = 0.5333$, in Fig. 5.4(b) the maximally unstable eigen mode has been plotted. It should be noted that the eigenfunctions have a double humped form. The KH mode is essentially driven by the second derivative of the equilibrium shear flow profile. The second derivative maximizes at two locations in the tangent hyperbolic shear flow. It is at these locations that the unstable KH eigen mode also maximizes. The comparison of various α values clearly illustrates that compressibility broadens the eigen mode form. This behaviour of the eigenfunction can be readily understood from the analytic expression of the eigenfunction that has been obtained for the step velocity profile in Eq. (5.21). The slow decay of the exponential along the shear direction x in the presence of finite α_1 testifies to the broader wave functions for compressible cases.

In Fig. 5.5, we provide a comparison of the eigenfunction for the compressible quasineutral case with the one having contribution from $\nabla^2\phi_1$ and thereby having dispersive contributions. We observe that the eigenfunctions get even more broader when dispersion is taken into account.

5.6 Physical interpretation

The process of KH instability can be understood from the schematic cartoon presented in Fig. 5.6. The equilibrium dust flow velocity $\vec{v}_0$ has a step profile and is depicted by the arrows pointing along $\pm V_0$ in the three subplots. This flow corresponds to a vortex sheet denoted by the thin solid (black) line in the figure. The equilibrium vorticity $\vec{\Omega}_0 = \nabla \times \vec{v}_0$ points inside the plane of the paper.

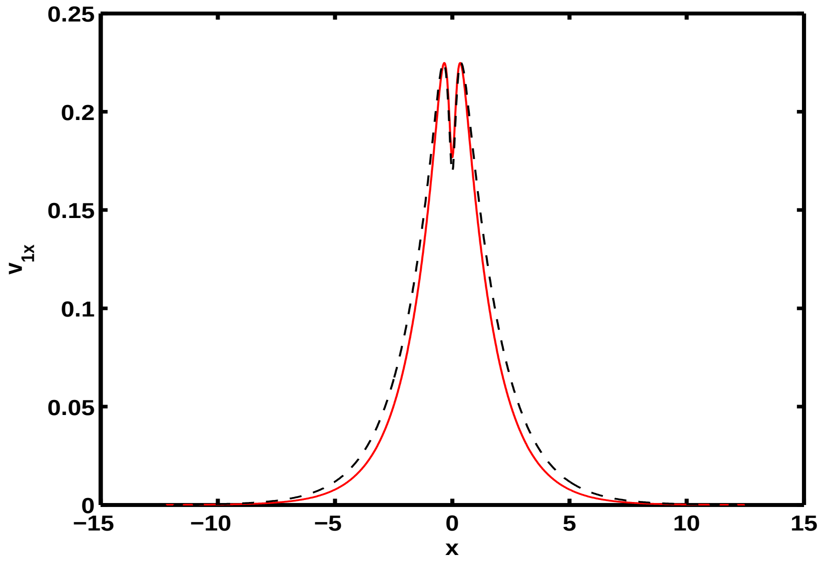

Figure 5.5: Plot of eigenfunction v_{1x} as a function of x for the quasineutral case (solid line) and the one with dispersive corrections arising from $\nabla^2\phi_1$ (dashed lines) for $\alpha = 1$ and $k_y = 1$.

The curl of the inviscid dust momentum equation (Eq. 5.1) yields the following evolution equation for the vorticity $\vec{\Omega} = \nabla \times \vec{v}$

$$\frac{\partial}{\partial t}\vec{\Omega} + \vec{v}\cdot\nabla\vec{\Omega} - \vec{\Omega}\cdot\nabla\vec{v} = 0. \tag{5.27}$$

Similarly, taking the divergence one obtains

$$\frac{\partial}{\partial t}\nabla\cdot\vec{v} = \vec{\Omega}\cdot\vec{\Omega} - \vec{v}\cdot\nabla\times\vec{\Omega} + \nabla^2\left(\phi - \frac{v^2}{2}\right) - \nabla\cdot\bar{\alpha}\nabla n. \tag{5.28}$$

Here, $\bar{\alpha} = (\alpha/n)$. For the 2-D case considered by us one would have $\vec{\Omega}\cdot\nabla\vec{v} = 0$. In addition if the system is incompressible we have $\nabla\cdot\vec{v} = 0$ for all times. Thus, for such a case the right hand side of Eq. (5.28) is balanced for all times. It is clear from Eq. (5.27) that for the 2-D incompressible case the vorticity gets convected by the flow velocity.

The perturbed vortex sheet has been shown by the curve depicted in the form of a ribbon with segments $A-B-C-D-E$ identified in the figure 5.6. The perturbed velocity disturbance shown in the subplot(a) of Fig. 5.6 has an associated perturbed vorticity which enhances and diminishes the equilibrium vorticity at locations B and D respectively. The equilibrium flow velocity has a configuration such that it brings the vorticity along A to C nearer and extends it from C to E as illustrated in the subplot(b) of the Fig. 5.6. When the vorticity patch between A and C are brought closer it further enhances the vorticity around B, thereby setting up an instability process. This is the basis of the conventional KH mode instability process. For the compressible case due to the additional $\nabla \cdot \vec{v}$ dependent term the vorticity is not tied to the fluid flow. As the flow tries to bring the vorticity patches along the segment $A - B - C$ nearer, the compressibility effects come into play. The divergence in the flow acquires a finite value in this case (even if it were zero to begin with) and acoustic perturbations get excited as has been schematically shown in subplot(c) of the Figure. This essentially inhibits the process of bringing the segment $A - B - C$ closer, thereby reducing the growth rate of the KH mode. It should also be noted that if the time scale of the acoustic perturbation is similar and/or faster than the growth period the flow would never be able to bring the segments $A - B - C$ closer and/or move the segments $C - D - E$ farther away. In this case then the instability would get totally suppressed. The mathematical analysis essentially conveys this physical mechanism for the stabilization of the KH mode in the presence of compressible perturbations.

We also wish to point out that the KH instability is related to the convection of the vorticity by the fluid flow velocity. Thus, the vorticity merely re-arranges spatially in the 2-D incompressible case. In the presence of compressibility and/or three dimensional perturbations, the vorticity is not carried by the fluid flow but evolves due to additional terms as well. The presence of compressible acoustic perturbations causes the the growth rate to get reduced, as some energy is spent on its excitation. Any 3-D perturbation would have to bend the equilibrium vorticity lines in the third dimension instead of merely convecting the vorticity lines in the 2-D plane. Since the bending of vorticity lines would require additional straining, this would reduce the growth rate of the KH mode. We, therefore, feel that the maximum growth rate is for those modes which have variations only in the 2-D plane of shear and flow. Next, we investigate the process of nonlinear saturation of the KH mode by carrying out nonlinear simulations. The details of the numerical studies are presented in the subsequent sections.

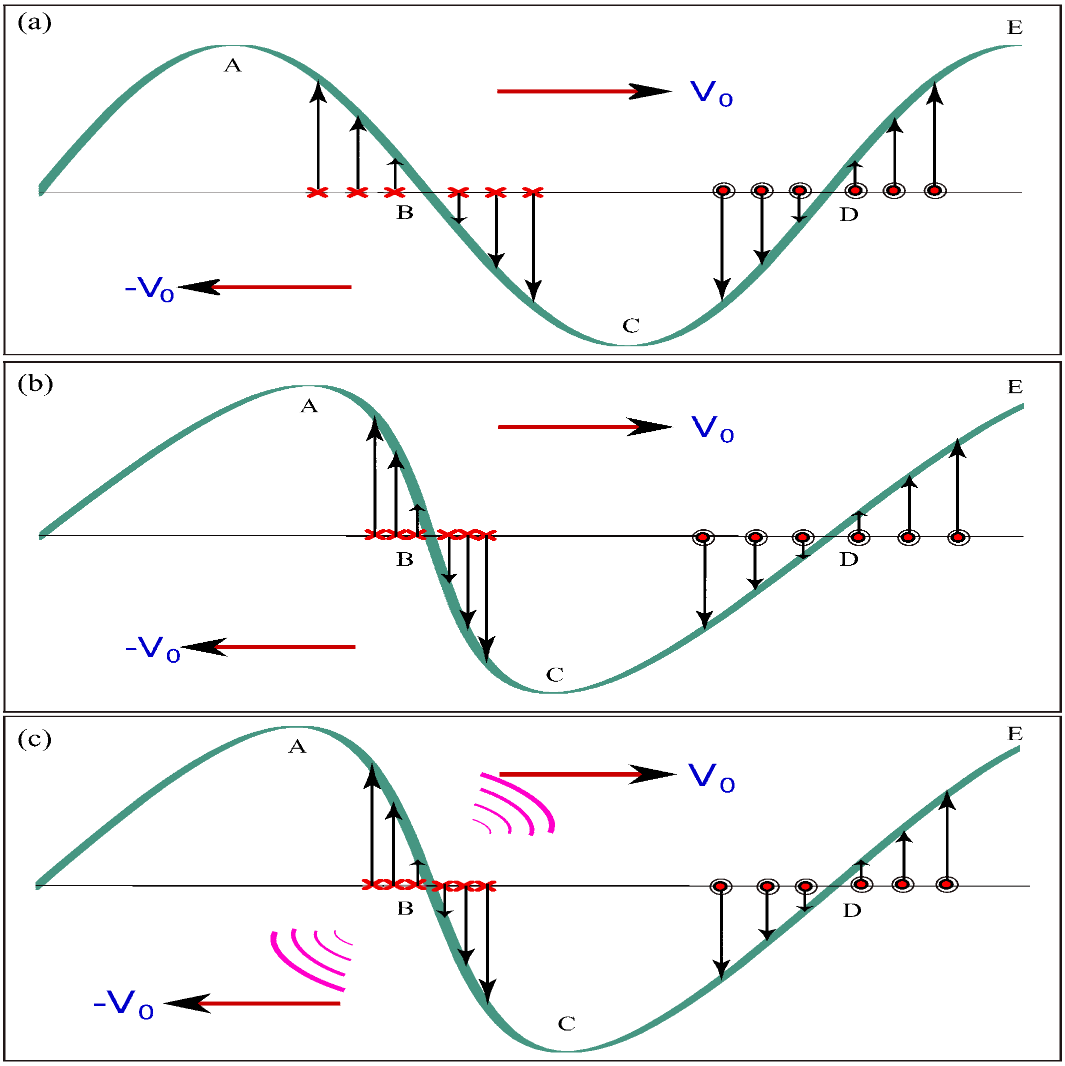

Figure 5.6: A schematic cartoon illustrating the physical mechanism of the KH instability. The equilibrium flow has a step profile and is represented by the arrows pointing at $\pm V_0$. The associated vortcity sheet is shown by the horizontal solid line. This equilibrium vorticity is directed into the plane of paper. The cross and dot indicate the perturbed vorticity directed into and out of plane of paper respectively. Subplot (a) shows the initial sinusoidal perturbation in the flow due to which the equilibrium vorticity gets enhanced over locations B and reduced over locations D. Subplot(b) and (c) show the development of the KH instability schematically for the incompressible and compressible cases. The physical distinction between the two have been described in section VI in detail.

5.7 Numerical scheme and validation of the code

The governing equations for the dust fluid are simulated numerically in two dimensional $x - y$ plane for the purpose of nonlinear studies. The continuity and the momentum equations (2.2,5.1) have been solved with the help of flux corrected scheme of Boris *et. al.* [107]. A time splitting method is adopted to integrate along the two directions. At each time step the scalar potential ϕ is determined from the Poisson equation (2.3). It should be noted that the Poisson equation is a nonlinear equation in ϕ here, as the right hand side has an explicit dependence on ϕ. To obtain ϕ from Eq. (2.3) we therefore employ a successive relaxation scheme at each time step. A converged solution is fed at each time step in Eq. (5.1) for the purpose of evolution.

We choose an equilibrium sheared flow configuration for the dust fluid defined by a flow of the form

$$\vec{v}_0 = V_0 \tanh(x/\epsilon)\hat{y} \tag{5.29}$$

along the $\hat{y}$ direction. The equilibrium velocity profile thus has a tangent hyperbolic form and its shear width is defined by the value of ϵ. At any time the flow velocity of the dust fluid in 2-D is then given by

$$\vec{v}(x, y, t) = \vec{v}_0 + \vec{v}_1(x, y, t) = V_0 \tanh(\frac{x}{\epsilon})\hat{y} + \vec{v}_1(x, y, t) \tag{5.30}$$

which is the sum of the equilibrium flow velocity $\vec{v}_0$ and the perturbed flow velocity $\vec{v}_1(x, y, t)$.

In the numerical simulation the instability will manifest as the growth of the deviation of the velocity field $\vec{v}_1$ from the equilibrium flow profile. In general, for an unstable system $\vec{v}_1$ would automatically emerge in simulation from numerical noise. However, such a process would take a long time. To hasten the development of the fluctuations to a level where the perturbation could be easily distinguished from the equilibrium, we choose an initial finite but small amplitude (compared to the equilibrium amplitude) of $\vec{v}_1$. The two components of $\vec{v}_1$ have been chosen in our simulations here to have the following form at $t = 0$

$$
\begin{aligned}
v_{x1} &= V_1 k_y \cos(k_{yp} y) \exp\left(-x^2/\sigma^2\right) \\
v_{y1} &= V_1 \left(\frac{2x}{\sigma^2}\right) \sin(k_{yp} y) \exp\left(-x^2/\sigma^2\right)
\end{aligned}
\tag{5.31}
$$

Here, $1/k_{yp}$ and σ define the length scales of the chosen initial velocity perturbation. It should be noted that with this choice, the initial velocity profile satisfies the incompressible condition, viz., $\nabla.\vec{v} = 0$. For compressible dusty plasma medium, imposing such an initial condition is, however, not essential. We have, however, chosen such initial condition to have it identical to the case of neutral hydrodynamic case with which comparisons would be made in the present Chapter. Here, V_1 is the amplitude of initial perturbation and σ is a parameter which defines the extent of initial perturbation around the shear width of the equilibrium flow. To confine it within a shear width one makes a choice of $\sigma \leq \epsilon$.

As time progresses, the perturbed velocity grows exponentially. The perturbed kinetic energy associated with the perturbed velocity field is given by the expression

$$
\tilde{E} = \frac{\int \left(v_{x1}^2 + v_{y1}^2\right) dxdy}{\int dxdy} \tag{5.32}
$$

The tracking of this quantity as a function of time provides a good measure of the growth of the instability and its saturation in the nonlinear regime. We show the evolution of $\tilde{E}$ as a function of time in the semilog plot in Fig. 5.7 for four different cases.

In subplot(a) and (b) we have shown the result of the studies for the case $\alpha = \infty$ and $\alpha = 50$ respectively, $V_0 = 5$ for both the cases. All the other parameters in this case are identical and have been provided in the figure caption (Fig. 5.7). In both cases the perturbed energy initially grows exponentially as illustrated by the linear behaviour of the energy evolution in the semilog plots of the Fig. 5.7. The slope of the curve in this regime (for example, Fig. 5.7 (a)) $= 3.45$ matches closely with twice the value of the growth rate $= 1.896$ corresponding to the maximally growing mode of the KH instability. The dotted line drawn alongside represents the curve with slope twice the analytical growth rate of the fastest growing KH mode for the system Subplot (c) and (d) we have chosen $\alpha = 1$ where effects of dispersion start playing role for the shorter scales permitted by the simulation box size. The results in subplot (c) show the case for which the effect of dispersion was deliberately dropped. Instead of using Poisson's equation one assumed quasineutrality here. The subplot(d) on the other hand retains the effect of dispersion as the Poisson equation is used. For (c) and (d) we had also chosen the value of $V_0 = 1$. It should be noted that while the linear growth rate scales with V_0, the perturbed energy for the smaller choice of V_0 saturates at a smaller value. This is reasonable as the nonlinear effects sets in when the perturbed velocity starts becoming comparable to the value of the equilibrium flow velocity.

5.8 Nonlinear phase of the KH instability

After the initial exponential rise, the perturbed energy ultimately saturates. This happens typically when the perturbed velocity fields achieve amplitudes which are comparable to equilibrium values. We now present our observations pertaining to this nonlinear phase of the instability.

The evolution of power in perturbed velocity field for various cases have been shown in Fig. 5.7. The description has been provided in the figure caption. In all these cases a distinct oscillation are observed in the nonlinear phase of the evolution. Furthermore, a comparison of subplot(a) and (b) shows that the amplitudes of the oscillations are more pronounced in the compressible case than that of the incompressible case. Similarly, a comparison of subplot(c) and (d) shows that dispersive effects have more pronounced amplitude of oscillations. In addition to these reversible oscillations, the plots also show that at a later stage an irreversible increase in the power of perturbed velocity occurs. This has been shown by encircling the region in all the subplots of Fig. 5.7. Thus, the salient features during the nonlinear phase are (i) the reversible oscillations in the power of perturbed velocity, the amplitude of which gets pronounced for the compressible and dispersive cases and (iii) the irreversible increase of the saturation level resulting in an observation of second saturation regime at a later time in all these plots. We will provide an interpretation for these observations shortly. The snapshots of vorticity contours have been shown in Fig. 5.8 and Fig. 5.9 for the incompressible

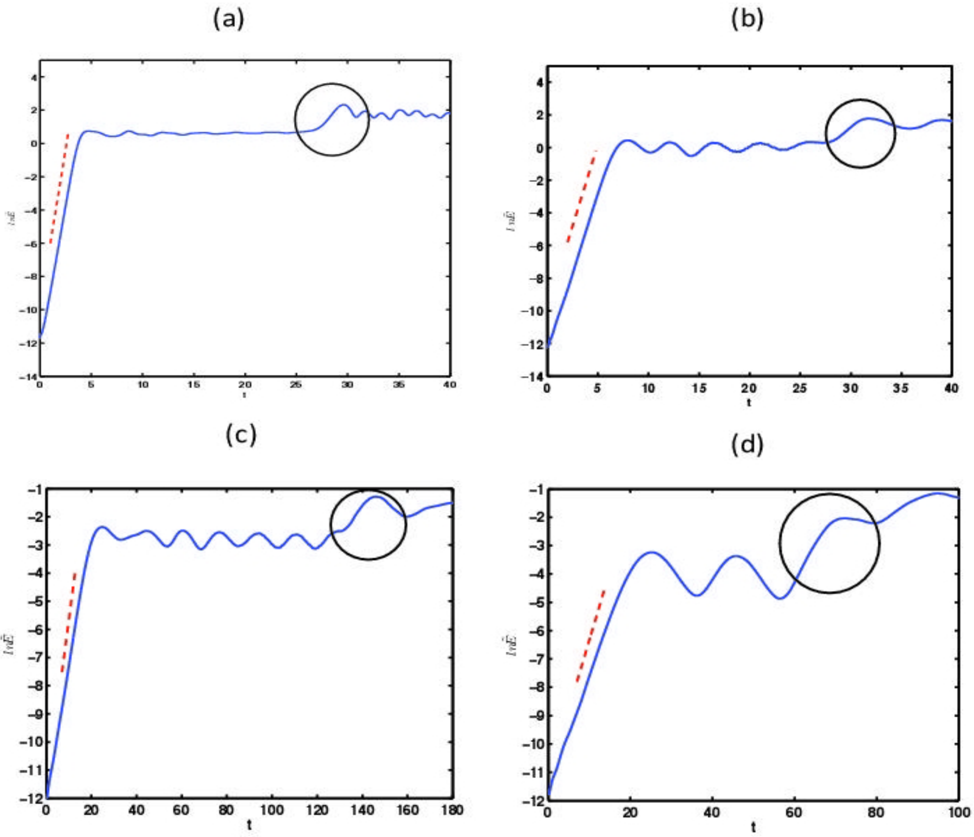

Figure 5.7: The evolution of $\log(E)$ (Eq. (5.32)) with time has been shown. The straight segment represents the linear growth of the instability. The dashed line alongside has been plotted for comparison and has twice the slope of the exact analytical value of maximally growing mode mentioned for each cases below. The curve in all the subplots later saturate corresponding to the nonlinear regime of the instability. In addition reversible oscillations and a second phase of growth and subsequent saturation of E at a higher level (Shown by the encircled region) at later time is also observed in all the cases. Subplot (a) shows the evolution for incompressible case with $M_A = 0.0, (\alpha = \infty), V_0 = 5$, the analytical growth rate for this case is $= 1.896$ and the growth rate evaluated from the simulation is $= 3.45$. Subplot (b) shows the evolution for compressible case with $M_A = 0.7, (\alpha = 50), V_0 = 5$, the analytical growth rate for this case is $= 1.05$ and the growth rate evaluated from the simulation is $= 1.9477$. Subplot (c) and (d) compare the quasineutral and dispersive cases respectively for evolution of $\log(E)$ for which $(\alpha = 1), V_0 = 1$. For quasineutral case (c), the analytical growth rate for this case is $= 0.3063$ and the growth rate evaluated from the simulation is $= 0.5043$. While for dispersive case (d), the analytical growth rate for this case is $= 0.2432$ and the growth rate evaluated from the simulation is $= 0.4165$.

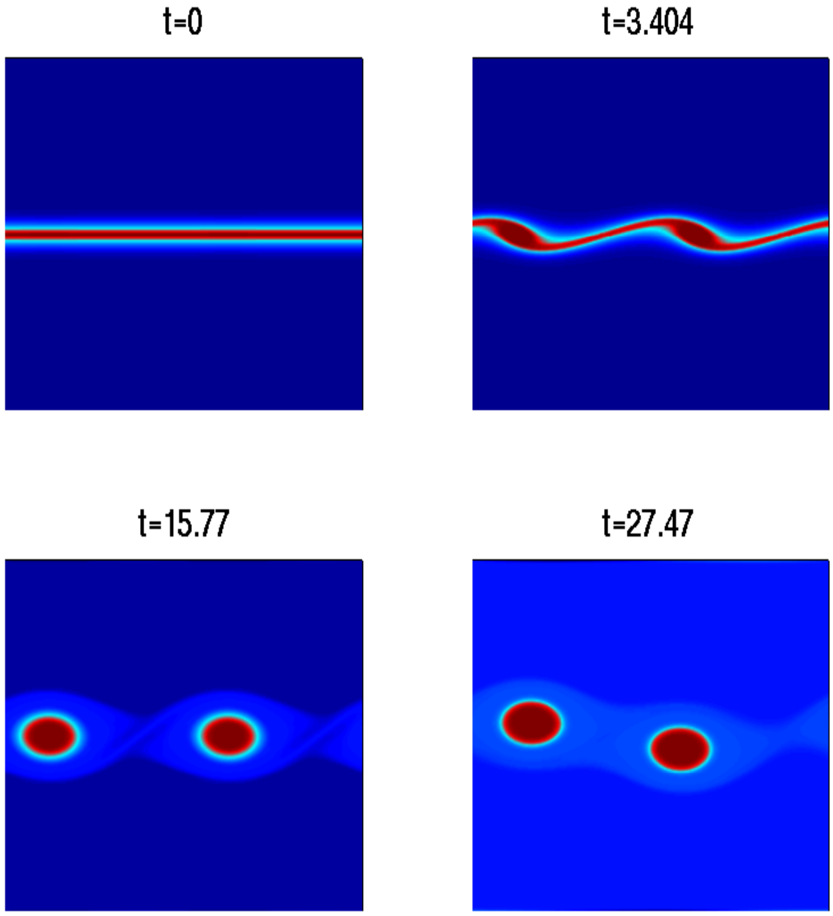

Figure 5.8: The various subplots show the vorticity contours at various times obtained from numerical simulation of the incompressible fluid system. At $t = 3.404$ the flow is in the linear growth regime of the KH instability, at $t = 15.77$ the system is in the first saturated nonlinear regime, at $t = 27.47$ the vortices have just started to merge.

case. While in Fig. 5.8, we have shown the snapshots pertaining to the period of linear growth regime and when the power in perturbed flow saturates at the first lower level, the plots in Fig. 5.9 on the other hand correspond to the time when the power in perturbed flow velocity shows irreversible rise and leading subsequently to the second level of saturation. In Fig. 5.10 and Fig. 5.11, the snapshots similarly correspond to the compressible, dispersive case. From these snapshots it is clear that the KH mode initially develops as a perturbation around the shear flow re-

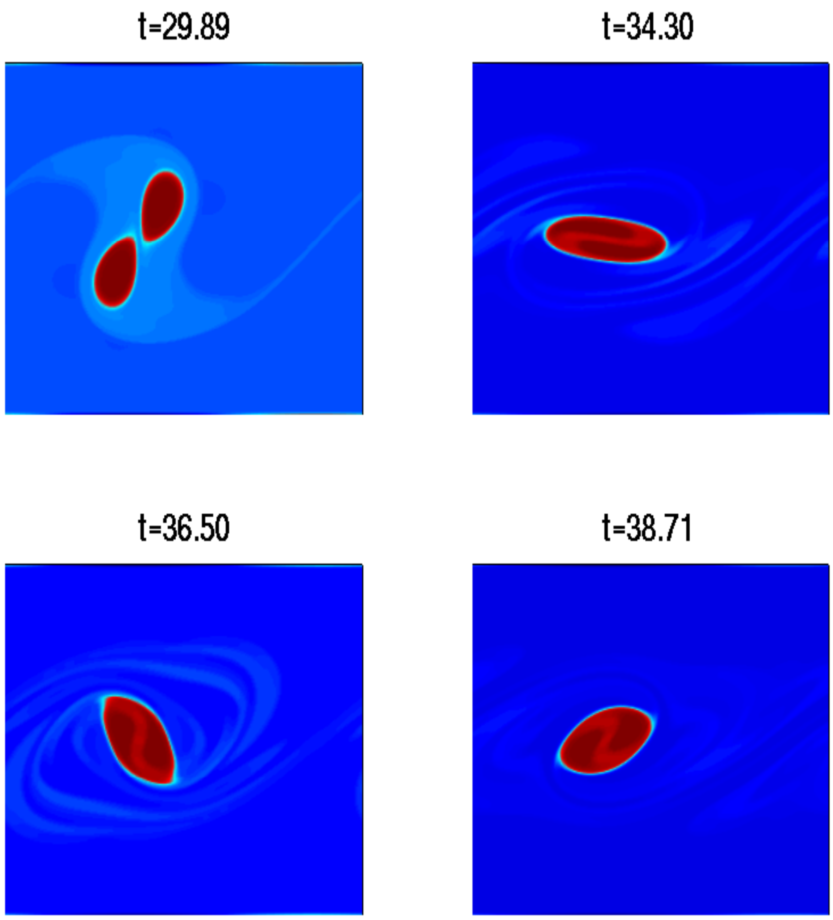

Figure 5.9: The evolution of vorticity contours for the incompressible case for times when the two distinct vorticity patches are about to merge $t = 29.89$, and at other times $t = 34.30, 36.50, 38.71$ the vortex has already merged and the various stages of its rotation has been depicted.

gion. The maximally growing mode permissible by the system is observed during the linear phase. For instance in the second subplot of Fig. 5.8 the maximally growing mode permissible for a box size of $L_y = 20$ corresponds to $k_y = 0.63$. This is what develops initially as can be seen from the subplot at $t = 3.404$ of Fig. 5.8. This time corresponds to the linear growth period of the instability as can be observed from the energy evolution shown in Fig.5.7 for this case. Two modes of this wavenumber get accommodated in the box size, hence two structures develop later (subplot at time $t = 15.77$, when the energy shows first saturation regime). We note that for this incompressible case the structure during the saturation regime (e.g. from time $t = 6$ to $t = 26$, the first saturation regime of the nonlinear phase) is essentially isotropic.

In Fig. 5.9, we have plotted the stages where the two isotropic structures begin to coalesce and ultimately merge with each other. The time corresponding to the merging process matches with the irreversible increase of perturbed energy (see Fig. 5.7). The process of merging for the incompressible case can be understood by invoking the existence of the second enstrophy (mean square vorticity) invariant in addition to the energy invariant for the system, which promotes the inverse cascade of flow structures. After the merging process the structure remains somewhat anisotropic. The subplot (a) of Fig. 5.7 for this time regime shows somewhat pronounced oscillations. We have observed that at a later stage as the structure isotropizes the amplitude of the oscillations also become weak. For the compressible dispersive case, the vorticity contours have been shown in the plot of Fig. 5.10 and Fig. 5.11. Here, again in the linear regime the most unstable mode permissible with the simulation box size, namely $k_y = 0.94$ appears. For this case $L_y = 20$, same as before. Thus, three modes develop and ultimately form three distinct vortex structures. In this case, we note, however, that the three vorticity patches that develop are *anisotropic*. Thus, as they rotate they generate reversible oscillations in the perturbed velocity power. These structures (even though they correspond to compressible dispersive simulations for which the second enstrophy invariant does not exist) also coalesce and show mergers. The merging process in this case also leads to an irreversible increase in E. The reversible oscillations of E correspond to the rotation of vorticity patches. The rotation of the asymmetrical vortex patches generates the reversible oscillations in E, with minima coinciding with the instant when the longer axis of the patch is aligned along the flow direction and the maxima when it is aligned orthogonal to flow, along the shear direction. Thus, higher the anisotropy of the vortex patch, higher is the amplitude of oscillation. From the snapshots of vorticity contours it is clear that the vorticity patches get distinctly anisotropic as compressibility and/or dispersive effects increase. We would delve into the reason behind this shortly.

We now reflect upon the mechanism of the nonlinear saturation of the KH instability. Once the perturbed velocity reaches a level in which it becomes com-

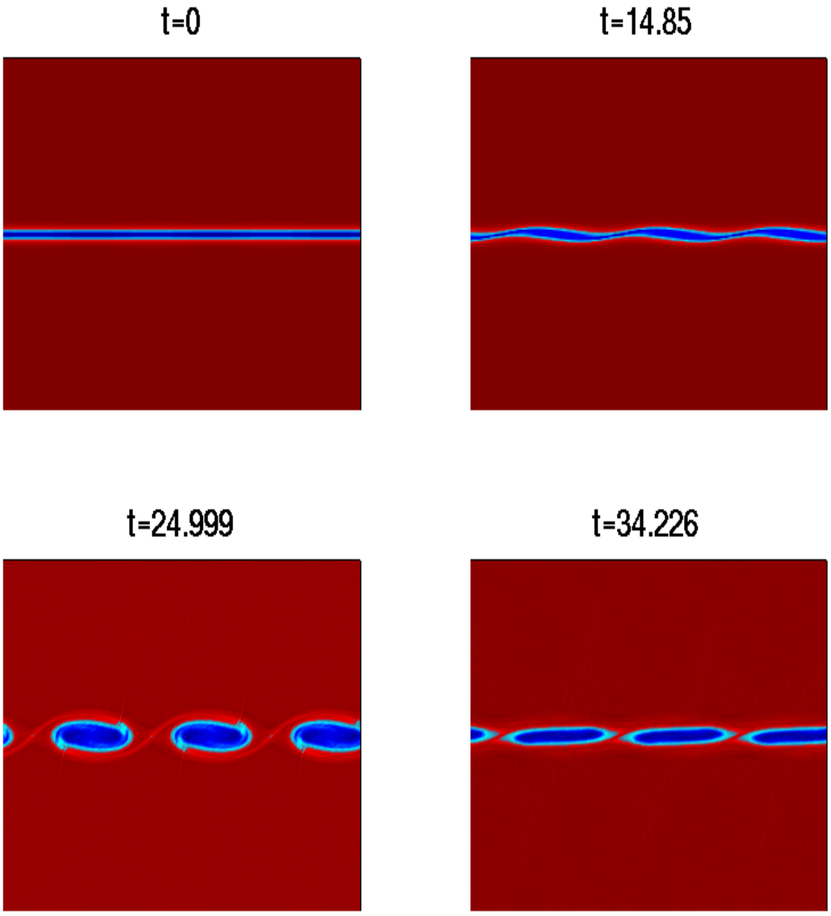

Figure 5.10: The various subplots show the vorticity contours at different times obtained from numerical simulation of compressible dust fluid. The subplot at $t = 14.85$ shows the linear regime of evolution, while the anisotropy of vortex structures in flow direction (y-axis) and direction of flow discontinuity is shown at times $t = 24.999$ and 34.226.

parable to the order of the original equilibrium flow, it alters the equilibrium shear configuration itself. The new sheared flow profile can be observed by averaging the $\hat{y}$ component of the velocity over y coordinate. Thus, the altered sheared profile is $\bar{v}_y = \int v_y dy/L_y$. The effective shear width of this average flow, viz., ϵ_{eff} is observed to get broader with time in comparison to ϵ, the shear width of the original flow profile at $t = 0$. When the instability saturates (as evidenced from the evolution of E) the effective shear width ϵ_{eff} also stabilizes at a particular value

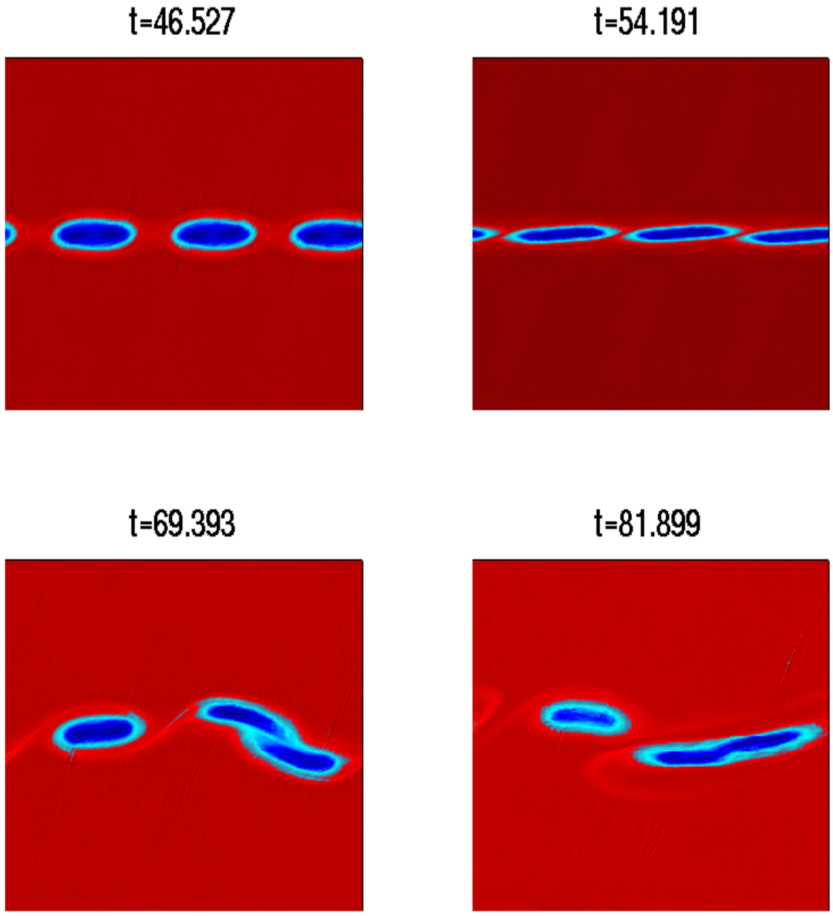

Figure 5.11: The subplots show the evolution of vorticity contours for compressible and dispersive dust fluid with parameters same as in Fig. 5.10. The subplot at $t = 54.191$ shows the start of merger of vortices while the vortex coalescing is observed at advance times $t = 69.393$ and 81.899.

(broader than ϵ). In the nonlinear phase the ϵ_{eff}, acts as the shear width of the modified profile and decides the further course of evolution. In Fig. 5.12 (a) and (b) we have shown the modified average profile of $\bar{v}_y$ for the cases corresponding to those depicted for E evolution in subplots (a) and (b) of Fig. 5.7 respectively. These velocity profiles have been shown in Figs. 5.12(a,b) for three different times (i) $t = 0$ (original profile depicted by solid lines), (ii) $t = 9.626$ (corresponding to first saturated regime of perturbed energy shown by dash lines) and (ii) $t = 34.303$

(the profile in the second saturated regime shown by dash dot lines). An effective shear width was obtained by fitting these profiles to a tangent hyperbolic form. At $t = 9.626$, the shear width are $\epsilon_{eff} = \epsilon_{i1} = 1.2$ and $\epsilon_{eff} = \epsilon_{c1} = 0.9$, here the suffix i and c correspond to incompressible and compressible cases respectively. Similarly, the width at $t = 34.303$ are $\epsilon_{eff} = \epsilon_{i2} = 2.4$ and $\epsilon_{eff} = \epsilon_{c2} = 1.8$ for the two cases.

Now, as mentioned before the broadend shear profile decides the future course of action. This profile can be unstable only if there exists a $k < A/\epsilon_{eff}$ permitted by the simulation box. This relation with $A = 1$ for the incompressible flow and $A < 1$ (for $\alpha = 50$, it can be seen from Fig. 5.3 that $A = 0.72$) for the compressible case decides the threshold wave number for the instability (as the linear growth rate plots of Fig. 5.3(b) for the two cases shows). Clearly, then for similar simulation box sizes and hence similar permissible range of k the ϵ_{eff} for the compressible case at saturation would be less compared to the effective shear width for the incompressible simulations. This is indeed what the plots of Fig. 5.12 illustrates. At $t = 9.626$ the perturbation has maximum power in a mode number of 2, i.e. $k_2 = 2 \times 2\pi/L_y = 0.63$ (two wavelengths in the simulation box). This mode is stable according to the threshold criteria for both the incompressible and compressible cases for their respective shear widths of ϵ_{i1} and ϵ_{c1}. The perturbed energy, therefore, remains at a stationary level at k_2 in the first saturation regime. However, there is another scale $k_1 = 2\pi/L_y = 0.314$ (longest scale) which is also permitted by the simulation box and is unstable for the shear width $\epsilon_{i,c1}$ of the altered profile of the first stage. For this scale, the calculation shows that $k_1\epsilon_{i1} = 0.3768 < 1$ for the incompressible case and $k_1\epsilon_{c1} = 0.2826 < A$ for the compressible case. This longest scale mode which is susceptible to instability then develops from the background and is ultimately responsible for causing the merger of the two vorticities producing an irreversible jump in the energy. After this merger the respective ϵ_{eff} increases further as we have already noted and acquires a value such that even the k_1 is beyond the threshold of the unstable wavelength domain. Since, no permissible modes of the system are unstable anymore the system relaxes to a final saturated state.

The above description also provides an explanation for the underlying reason for observing more prominent reversible oscillations in energy when compressibility and dispersive effects are added. The vorticity patches, (essentially representing the perturbation scales) typically have the scale of k_y^{-1} along the flow direction and ϵ_{eff} in the shear direction in the nonlinear saturated state. For the incompressible hydrodynamic case the two scales are related by the condition of $k_y\epsilon_{eff} = 1$, implying that the vortex pattern is symmetrical in this case. For the compressible and dispersive cases, however, the two dimensions of the vortex patch at a saturated state are related by the condition of $k_y\epsilon_{eff} = A < 1$ and are hence asymmetric. The numerical simulation yields the dimension of the vorticity patches which are very closely related by this theoretical condition. This explains why the reversible oscillations get pronounced with increasing compressibility and dispersion.

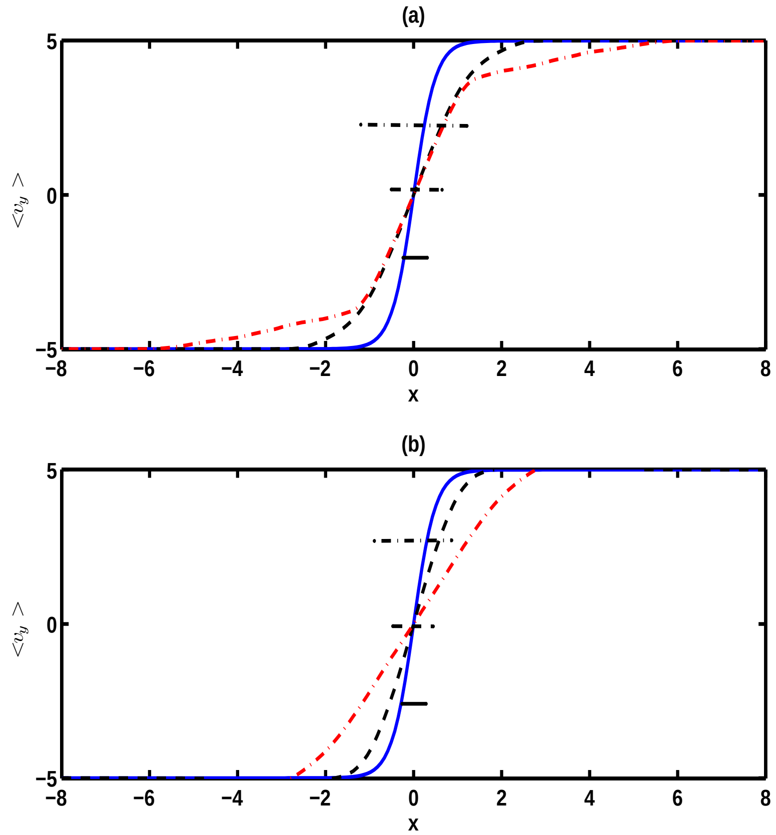

Figure 5.12: The subplots (a) and (b) show the evolution of the average profile $\bar{v}_y = \int v_y dy/L_y$ for the incompressible and the compressible cases respectively. The solid, dashed and the dash dot plots show the profile at $t = 0$ (original), $t = 9.626$ (first saturation regime) and $t = 34.303$ (second saturated regime).Their respective fitted shear width also shown by horizontal lines with respective line styles(i.e. solid, dashed and the dash dot lines for $t = 0$, $t = 9.626$ and $t = 34.303$ respectively).

5.9 Summary and conclusion

A weakly coupled dusty plasma system behaves like a fluid which differs from the neutral hydrodynamic fluid in certain ways. The dust fluid can have a very strong compressible nature. The compressibility arises in this case not merely from thermal effects but also due to its interaction with electron and ion charged species. Furthermore, unlike the neutral fluid it can support dispersive compressible perturbations. Keeping these features in view, a prominent fluid instability, namely the Kelvin - Helmholtz mode has been studied for the weakly coupled dusty plasma system in both linear and nonlinear regimes.

A detailed characterization of the instability in the presence of weak and strong compressibility as well as dispersion has been carried out in this Chapter. The behaviour of the KH mode has been investigated both analytically and by the help of numerics for exact eigenvalue evaluation for various shear flow profiles. The studies point out that compressibility has a stabilizing role on the KH mode. The dispersion effect becomes significant only when the fluid is highly compressible. Furthermore, the dispersion is observed to further stabilize the unstable modes, typically at higher wavenumber domain. We have also provided a first order perturbative calculation for weakly compressible cases. The perturbative evaluation of the change in growth rate and the altered threshold wavenumber matches very well with the exact results obtained numerically.

The nonlinear studies have also been carried out by simulating the governing equations numerically. Various distinctive characteristic features in the nonlinear regime associated with compressible and dispersive perturbations have been observed and identified. A physical interpretation of the results have also been provided for its understanding. In short the simulations confirm the characteristics analytical linear growth rate features of the instability. The reduction in growth rate in the presence of compressible and dispersive perturbations have been confirmed through numerical simulations results as well. The presence of compressibility and dispersion also reduces the range of the unstable wave numbers. We have shown that this introduces interesting characteristic features during the nonlinear phase. The effective shear profile in the saturated state of the KH instability shows a weaker broadening for the compressible and dispersive cases as compared to the incompressible fluid. Furthermore, our simulations show that the vortex merging process, reminiscent of 2-D inverse cascade of energy spectrum for systems preserving energy and enstrophy invariants, is preserved even for the compressible dusty plasma medium. This leads to a coherent nonlinear saturated state in 2-D.

6

Kelvin-Helmholtz instability in strongly coupled dusty plasmas: 2-D studies

In the previous Chapter 5, we have provided a detailed description about the linear and nonlinear aspects of KH instability in weakly coupled dusty plasma medium. But, as we have mentioned earlier that due to high charge of the dust species, it can be easily found in the strongly coupled regime. Here, in this Chapter, we have employed the generalized hydrodynamic description of dusty plasmas to include the the effect of strong coupling on the sheared flows in such systems. In the presence of strong coupling, we report the existence of a local instability along with KH instability in strongly coupled dusty plasma medium. We have also observed the phenomenon of recurrence of instability due to competition of strong coupling and compressibility of medium. Apart from this, we have provided a criteria for growth of KH instability in such system.

6.1 Introduction

Plasma can often be found in strongly coupled regime, which is defined by the condition of having the inter particle potential energy being comparable or exceeding the thermal kinetic energy of the particles. This condition can be expressed in terms of coupling parameter Γ for strongly coupled plasmas [28]. The strongly coupled plasma medium have invoked considerable research interest due to the novel features associated with this state [9,11] and its occurrence in a variety of realistic situations. The normal electron - ion plasma can be in a strong coupling regime when cooled by laser radiation in electrostatic traps and cyclotrons [136, 137]. They tend to crystallize and form "Coulomb crystals as well as liquids" [138]. Furthermore, the crystallization of electrons at 2-D Helium and Hydrogen surfaces are other examples of such a state [139]. While these experiments require fairly complicated apparatus, it is rather easy to produce a dusty plasma medium in strongly coupled state in laboratory. This is so as the inter particle separation is small and each of the dust particles can acquire a large number of electrons to be in a highly charged state, e.g. ($10^4 - 10^6$) electronic charges. A number of microgravity and gravity experiments show dust crystallizations in the strongly coupled limit [26, 27, 81].

Normally, the coupling parameter Γ remains well below unity for most of high temperature plasmas. For instance, for $Z \sim 1$, a plasma at a temperature of $10^6 K$ can even at a high density of the order of $10^{26} cm^{-3}$ would be in a weakly coupled regime with the coupling parameter below unity. This is why only either high density cold plasmas or dusty plasmas with very high charge on dust particles can fulfill the condition of $\Gamma \geq 1$ [28]. As dusty plasmas can be found in the strong coupling regime even at low densities, it provides one with a unique opportunity to investigate the behavior of a strongly coupled plasma medium over the phase domains right from gaseous to liquid to that of solid.

The weakly coupled dusty plasmas ($\Gamma < 1$) can be easily treated like a fluid. However, in the very strong coupling limit where crystallization occurs, the fluid model is clearly not an adequate description. There is, however, an intermediate regime of the coulomb coupling parameter in which the the dusty plasma exhibits properties which are intermediate to fluid and solid like behavior. This is a rather interesting phase, as in this case the medium behaves like a visco-elastic system [99]. The particles are not rigidly fixed at any locations like in a solid medium. They can wander around, but retain a certain memory of their dynamics. The visco - elastic medium is often depicted in terms of a Generalized Hydrodynamic (GHD) model [59]. In the context of dusty plasma it was adopted by Kaw *et al.* and was found to provide a good description for the transverse shear waves supported by the strongly coupled dusty plasma medium [23, 77].

The dusty plasma medium is often observed with significant amount of sheared flows, for instance in cometary tails, protoplanetary disks, etc. In some of these cases the medium can be in a strongly coupled state. It is well known that shear flows are susceptible to the well known fluid Kelvin - Helmholtz (KH) instability [126, 127]. We had in our recent studies shown the effect of compressibility and dispersion on the KH mode for the dusty plasma medium in the weak coupling regime [97]. In this Chapter our aim is to study KH instability in context to strongly coupled dusty plasma fluid and in particular seek the influence of the transverse shear waves (which are the normal modes of the medium) on the KH instability.

The Chapter has been organized as follows. Section 6.2 provides the details of the governing equations for the visco-elastic dust fluid. In section 6.3 we study the linear regime of the KH instability for such a visco-elastic fluid. We choose a specific tangent hyperbolic form of sheared flow profile for this purpose. The effect and role of strong coupling on the growth rate are discussed and comparison with the weak coupling limit is provided in this section. We also show the existence of local instability in the strong coupling limit, this is not possible for the normal hydrodynamic fluids. In section 6.4 we describe the numerical results obtained from the numerical simulation of the Generalized Hydrodynamic (GHD) model. We show that the growth of perturbed energy agrees with the prediction of the linear studies presented in section 6.3. In the nonlinear regime the simulations show fascinating characteristics. A phenomena of the recurrence of the KH instability is seen due to the repeated sharpening of the shear flow. In addition these cyclic events are associated with a bursts of activity in terms of the emission of transverse and compressional waves.

The emission and propagation of transverse shear wave from the sheared flow equilibrium is a natural outcome. The sheared equilibrium configuration chosen initially for these studies can in general be viewed as the superposition of the eigen state of the transverse shear waves. At low amplitudes (when each of the constitutive transverse shear normal mode is in linear domain) such an initial configuration would lead to independent propagation of all the modes. However, a sheared flow configuration being unstable to the KH destabilization, the sheared configuration of each of the mode by itself would be susceptible to the excitation of KH instability. We seek the possible excitation of KH instability in the sheared configuration of one single mode of the propagating transverse shear wave in section 6.5. In section 6.6 we summarize our observations.

6.2 Governing equations

The dynamics of strongly coupled dusty plasma medium has been described using GHD set of Eqs. (2.1,2.2,2.3). The description of model and its parameters have been provided in Chapter 2. We have chosen a simplified system geometry for our studies, where variations are confined in 2-D $x-y$ plane and the third dimension of z is the axis of symmetry. The equilibrium flow is assumed to be directed along y and assumed to be sheared along x. Thus the flow direction (i.e. y) is assumed periodic at boundary while the shear direction (i.e. x) is considered to be non periodic at boundary.

For the purpose of our investigation we take the basic equilibrium flow to have the following form:

$$\vec{v_0} = v_{y0}(x)\hat{y} \tag{6.1}$$

In the next section we study the stability of this flow in the 2-D $x-y$ plane, wherein the role of strong coupling effects would be investigated.

6.3 Linear studies

We linearize the Eqs. (2.1,2.2,2.3) in the presence of the equilibrium flow defined by Eq. (6.1). The field variables are perturbed such that,

$$\vec{v} = v_{1x}\hat{x} + [v_{y0}(x) + v_{1y}]\,\hat{y}; \qquad n = n_0 + n_1; \qquad \phi = \phi_1 \tag{6.2}$$

Here, the fields with subscript $'1'$ denote the perturbed fields and those with subscript $'0'$ represent the equilibrium. The linearized equations upon Fourier analyzing in time and the y coordinate yields the following:

$$\begin{aligned}
&-i\Omega n_1 + n_0 v_{1x}^{'} + ik_y n_0 v_{1y} = 0\\
&(1 - i\tau_m\Omega)\left(-i\Omega v_{1x} + \alpha n_1^{'} - \phi^{'}\right) = \eta\left(v_{1x}^{''} - k_y^2 v_{1x}\right)\\
&(1 - i\tau_m\Omega)\left(-i\Omega v_{1y} + v_{1x}v_0^{'} + ik_y\alpha n_1 - ik_y\phi_1\right) = \eta\left(v_{1y}^{''} - k_y^2 v_{1y}\right)\\
&\phi_1^{''} - k_y^2\phi_1 = n_1 + (\mu_e\sigma_i + \mu_i)\,\phi_1
\end{aligned} \tag{6.3}$$

Here, $\Omega = \omega - k_y v_{y0}$, the superscript $'$ shows the derivative with respect to x and $\alpha = \mu_d \gamma_d T_d / T_i Z_d$.

The parameter $\sqrt{\alpha}/V_0$ in such a case represents the ratio of sound speed with dust flow velocity and hence is effectively the typical inverse Mach number of the dusty plasma flow under consideration. Here V_0 is the amplitude of initial sheared flow velocity. Thus by choosing the value of α ranging from $0 - \infty$ one can carry out investigation for an incompressible dusty plasma medium to a compressible case.

The assumption of incompressibility simplifies the system of equations, as one can then explicitly choose $\nabla \cdot \vec{v} = 0$. Also the continuity equations can then be dropped. A further simplification is possible by concentrating only on long wavelength quasi neutral responses. For this case the left hand side of the Poisson's equation can also be ignored. We discuss this particular simplified incompressible limit in the next sub-section 6.3.1. The general case is then discussed in the subsequent sub-section.

6.3.1 Incompressible dust fluid

The incompressibility assumption simplifies the set of linearized equations (6.3) wherein they can be represented in terms of v_{1x} alone

$$
\begin{aligned}
& k_y \Omega \left(1 - i\tau_m \Omega\right)^2 v_{1x} - \left(v_{1x} v_{y0}^{''} + \frac{\Omega v_{1x}^{''}}{k_y} \right) \left(1 - i\tau_m \Omega\right)^2 + \frac{i\eta}{k_y} \left(v_{1x}^{''''} - k_y^2 v_{1x}^{''} \right) \left(1 - i\tau_m \Omega\right) \\
+ \;& \eta \tau_m v_{y0}^{'} \left(v_{1x}^{'''} - k_y^2 v_{1x}^{'} \right) = i\eta k_y \left(v_{1x}^{''} - k_y^2 v_{1x} \right) \left(1 - i\tau_m \Omega\right) \qquad (6.4)
\end{aligned}
$$

Rearranging the above equation we can write Eq. (6.4) alternatively as

$$
\begin{aligned}
& v_{1x}^{''''} - \frac{i k_y \tau_m v_{y0}^{'}}{(1 - i\tau_m \Omega)} v_{1x}^{'''} - 2k_y^2 v_{1x}^{''} + \frac{i k_y^3 \tau_m v_{y0}^{'}}{(1 - i\tau_m \Omega)} v_{1x}^{'} + k_y^4 v_{1x} \\
- \;& \frac{i k_y^2 \Omega \left(1 - i\tau_m \Omega\right)}{\eta} v_{1x} + \frac{i k_y \left(1 - i\tau_m \Omega\right)}{\eta} \left(v_{1x} v_{y0}^{''} + \frac{\Omega v_{1x}^{''}}{k_y} \right) = 0 \qquad (6.5)
\end{aligned}
$$

In the incompressible case, the fluid velocity can be expressed in terms of a stream function so as to have $v_{1x} = \partial \Psi / \partial y$ and $v_{1y} = -\partial \Psi / \partial x$, the Eq. (6.5) then can be written in terms of stream function Ψ as

$$\left[\frac{d^2}{dx^2} - k_y^2\right]^2 \Psi = \frac{ik_y\left(1 - i\tau_m\Omega\right)}{\eta}\left[\frac{-\Omega}{k_y}\left(\frac{d^2}{dx^2} - k_y^2\right) - \frac{d^2 v_{y0}}{dx^2}\right]\Psi$$
$$+ \frac{ik_y\tau_m dv_{y0}/dx}{(1 - i\tau_m\Omega)}\left[\frac{d^3}{dx^3} - k_y^2\frac{d}{dx}\right]\Psi \tag{6.6}$$

It can be easily seen that Eq. (6.6), in the limit of $\tau_m = 0$, reduces to the linearized equations discussed by Drazin for the KH mode in viscous fluids [126]. In the absence of equilibrium flow, one obtains dispersion relation for transverse shear wave from Eq. (6.5) as

$$\omega = \frac{-i}{2\tau_m} \pm 0.5\sqrt{\frac{-1}{\tau_m^2} + \frac{4\eta k^2}{\tau_m}} \tag{6.7}$$

In the limit of strong coupling (i.e. $\omega\tau_m >> 1$), the dispersion relation for the pure transverse shear could be written as

$$\frac{\omega^2}{k^2} = \frac{\eta}{\tau_m} \tag{6.8}$$

We next consider the local limit, wherein the equilibrium velocity flow is assumed to vary rather slowly in comparison to the perturbation scales. In this limit v_{y0} and its derivative can be treated as parameters in a local sense. The system can then be Fourier analyzed in the x coordinate as well. This yields

$$\mid k \mid^4 - \frac{k_x k_y \tau_m v_0^{'} \mid k \mid^2}{(1 - i\tau_m\Omega)} - \frac{i\Omega}{\eta}(1 - i\tau_m\Omega) \mid k \mid^2 + \frac{ik_y}{\eta}(1 - i\tau_m\Omega)v_0^{''} = 0 \tag{6.9}$$

Fig. 6.1 shows a two dimensional growth rate plot for existing local instability. It could be seen clearly that the local instability growth is symmetric for both k_x and k_y directions. Equation (6.9) is a cubic equation in Ω and reduces to a quadratic form for the case when $\omega\tau_m >> 1$ and $v_{y0}' = 0$, but the second derivative term v_{y0}'' is taken as finite. In can be shown that in this case we get a stable system as

$$\Omega = \left(\frac{1}{2}\right)\left[\frac{k_y v_{y0}^{''}}{\mid k \mid^2} \pm \sqrt{\left(\frac{k_y^2 v_{y0}^{''2}}{\mid k \mid^4} + \frac{4\eta \mid k \mid^2}{\tau_m}\right)}\right]$$

However, we observe that the presence of finite v'_{y0} can result in producing a

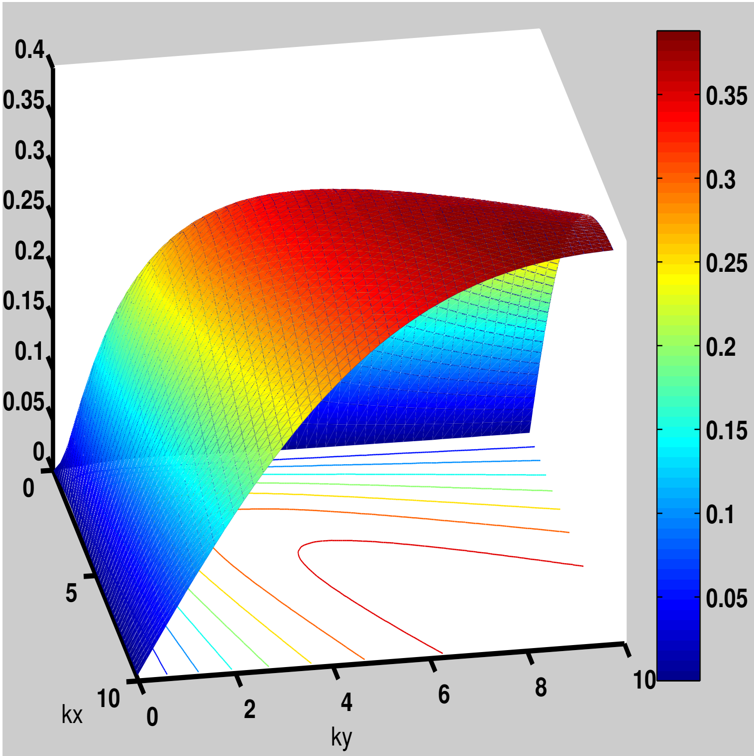

Figure 6.1: Growth rate of local instability for visco-elastic fluids. The equilibrium flow parameters are $v_0 = 0.5, v_0^{'} = 0.8$ and $v_0^{''} = 0.8$. The strong coupling parameters are chosen as $\tau_m = 10$ and $\eta = 0.5$.

local instability for the system. This has been illustrated by the plots of the Fig. (6.2), which shows a finite imaginary positive value of ω for various set of parameters. Such a local instability is altogether absent in the case of sheared flows in neutral hydrodynamic fluids. Thus, this is one of the new features associated with strong coupling properties of the system. Furthermore, it can also be seen that the transverse shear waves acquires a weak dispersion in the presence of v'_{y0}.

6.3.2 The general case

The eigen values of the complete general set of linearized Eq. (6.3) can be obtained numerically for specific choices of the flow profile. The set of equations involves four fields and takes considerable time to seek the eigen spectrum and the parameter scan for the study of the influence of strong coupling effects. As an alternative one

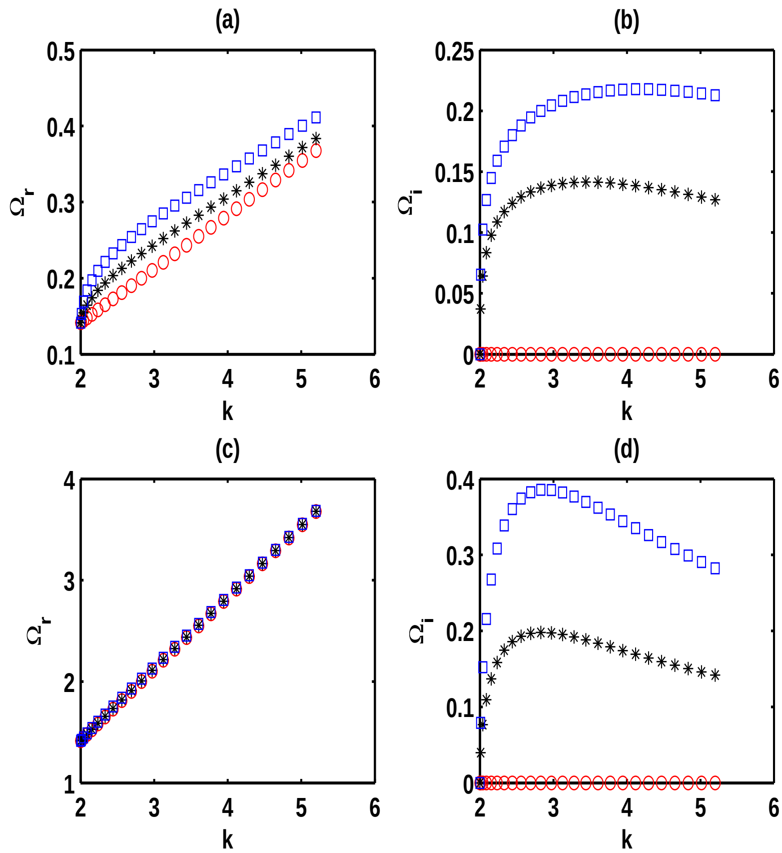

Figure 6.2: Dispersion relation for Eq. (6.9) with finite $v_{y0}^{'}$ parameter while other parameters are $\eta = 0.1, \tau_m = 20$ for subplot (a) and (b) while $\eta = 10, \tau_m = 20$ for subplot (c) and (d). $v_{y0}^{''}$ is taken to be zero. For all subplots, $v_{y0}^{'}$ is $0, 0.4$ and 0.8 represented by circle, star and square respectively.

can also employ a simplified case of quasi neutral response for which the dispersive effects appearing in Poisson equation can be ignored and one has instead a simple algebraic relationship between the potential and the density perturbations.

$$\phi_1 = -n_1/\left(\mu_e \sigma_i + \mu_i\right) \tag{6.10}$$

This assumption has been invoked for simplicity and leads to a more simplified set. We have shown in our earlier work on weakly coupled dusty plasma system studies that dispersive effects reduce the growth rate, however, the reduction is insignificant at high values of the α parameter. We have in our linear studies, therefore, often chosen to consider the quasi neutral case, defined by the following simplified equation

$$\begin{aligned}
&-i\Omega n_1 + n_0 v_{1x}^{'} + ik_y n_0 v_{y1} = 0 \\
&(1 - i\tau_m\Omega)\left(-i\Omega v_{1x} + \alpha_1 n_1^{'}\right) = \eta\left(v_{1x}^{''} - k_y^2 v_{1x}\right) \\
&(1 - i\tau_m\Omega)\left(-i\Omega v_{1y} + v_{1x}v_0^{'} + ik_y\alpha_1 n_1\right) = \eta\left(v_{1y}^{''} - k_y^2 v_{1y}\right),
\end{aligned} \quad (6.11)$$

to study the effects of strong coupling. Here $\alpha_1 = \alpha/n_0 + 1/(\mu_e\sigma_i + \mu_i)$. Choosing Tangent Hyperbolic equilibrium sheared flow profile with ϵ as the shear width as shown in the following equation

$$\vec{v}_0 = V_0 \tanh(\frac{x}{\epsilon})\hat{y} \quad (6.12)$$

We discretized the set of Eqs. (6.11) on a spatial grid of x coordinate and obtain the eigenvalues ω numerically by standard procedures. The positive imaginary part of which provides for the growth rate γ.

We show in Fig. (6.3) and Fig. (6.4) the role of varying the two parameters associated with strong coupling η and τ_m respectively, on the growth rate of the KH mode. We have the plot of γ/V_0 vs. $k_y\epsilon$ for various cases in the two figures. In Fig. (6.3), the incompressible weakly coupled dusty plasma system (the hydrodynamics case) for reference, has been shown by a black thick line. For the rest of the plots the value of Mach number has been chosen to be 0.707, and hence they all have effects due to compressibility. The plot with circles (red in color online) is again for a weakly coupled dust fluid obeying hydrodynamical equations. For such a Mach number when the value of η parameter is increased keeping τ_m fixed, the growth rate is found to decrease and the threshold wavenumber for instability also reduces. The variation in growth rate with respect to τ_m has another interesting aspect. We observe that for flows with any given specific Mach number and a specific value of $\eta = \eta_s$ say, the two curves for $\eta = 0$, $\tau_m = 0$ (weakly coupled inviscid dust shown by red circles in Fig. (6.4)) and $\eta = \eta_s$, $\tau_m = 0$ (weakly coupled viscous dust system, shown by diamonds in Fig. (6.4)) define the upper and lower limit of the growth rate respectively for any value of τ_m. As τ_m is increased for all cases of $\eta = \eta_s$ the growth rate increases from the lower curve and merges with the upper curve at very high values of τ_m. It has been observed by us earlier in the

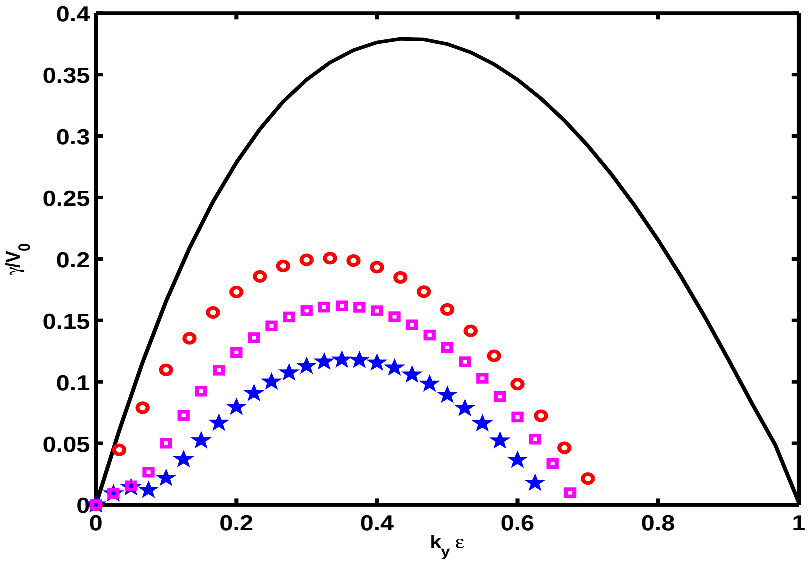

Figure 6.3: The scaled growth rate γ/V_0 Vs $k_y\epsilon$. The smooth line (black) represents the scaled growth rate of incompressible dust fluid and rest are all compressible cases with Mach no of 0.707 with circles(red) for weakly coupled dust fluid while square(magenta) and stars(blue) represents case of $\eta = 2$ and $\eta = 5$ respectively for strongly coupled dust fluid. The value of τ_m is kept fix at 20 for these strong coupling cases. The other parameters are $V_0 = 5$ and $\epsilon = 0.5$ (shear width as defined in Eq. (6.12)) .

context of 1-D simulations as well [96] that the strongly coupled dust behaviour described by the GHD set of equations, at very high values of τ_m behaves similar to an inviscid weakly coupled hydrodynamic dust fluid.

It appears that in the limit of $\tau_m \to \infty$ the unity from the operator $1 + \tau_m d/dt$ (Eq. (2.1)) can be ignored. Dividing the equation by τ_m, one can then ignore $\eta/\tau_m \nabla^2 \vec{v}$ from right hand side. Thus one is left with an equation which has the form of the weakly coupled fluid system with an additional time derivative acting on all the terms.

6.4 Nonlinear studies

We have also investigated the nonlinear regime of the instability numerically. For this purpose the complete set of equations defined by Eq. (2.1,2.2,2.3) have been utilized. The quasineutral assumption is considered for these numerical studies. The assumption of incompressibility have not been invoked a - priori for any of

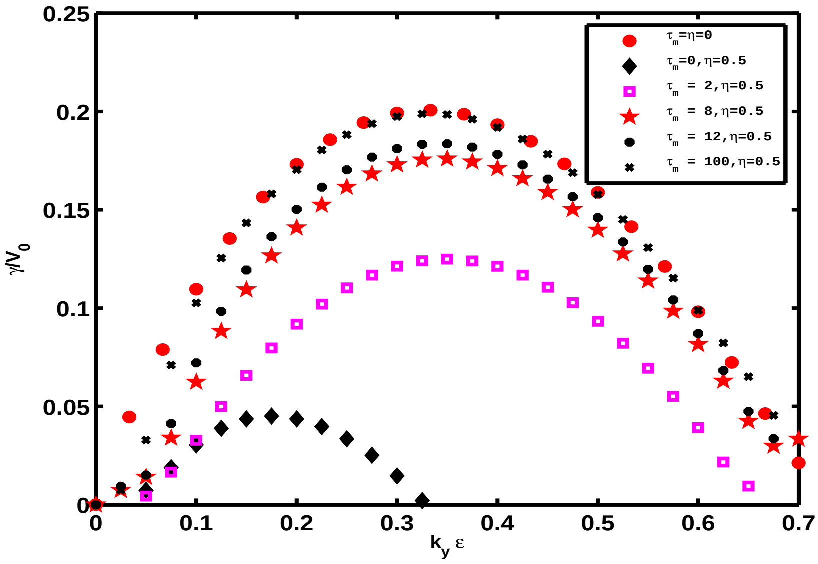

Figure 6.4: The scaled growth rate γ/V_0 Vs $k_y\epsilon$ for fixed value of $\eta = 0.5$ and various values of $\tau_m = 0$ (diamond), $\tau_m = 2$ (square), $\tau_m = 8$ (star), $\tau_m = 12$ (dot) and $\tau_m = 100$ (x mark). The red circles show the case of weakly coupled dust fluid. The other common parameters are $V_0 = 5$, $\epsilon = 0.5$ and mach no 0.707.

the cases studied by simulations. A flux corrected scheme proposed by Boris et al. [107], have been adopted for the purpose of evolving the set of equations (2.1,2.2) in the 2-D $x - y$ plane. As the scheme numerically solves the continuity form of equations with possibility of inclusion of various source terms, we split Eq. (2.1) as two separate equations of the following form

$$\left[1 + \tau_m \left(\frac{\partial}{\partial t} + \vec{v} \cdot \nabla\right)\right] \vec{\psi} = \eta \nabla^2 \vec{v}$$
$$\left(\frac{\partial}{\partial t} + \vec{v} \cdot \nabla\right) \vec{v} + \alpha \frac{\nabla n}{n} - \nabla \phi = \vec{\psi} \tag{6.13}$$

The initial condition is chosen as

$$v_x = v_{1x} = V_1 k_{yp} \cos(k_{yp} y) \exp(-x^2/\sigma^2)$$
$$v_y = v_{1y} = V_0 \tanh(\frac{x}{\epsilon}) + V_1 \left(\frac{2x}{\sigma^2}\right) \sin(k_{yp} y) \exp(-x^2/\sigma^2) \tag{6.14}$$

The first term in the expression for v_y defines the equilibrium flow of Tangent hyperbolic profile defined in Eq. (6.12). Here k_{yp} is a mode over which the perturbation has been excited to facilitate the growth of instability. The perturbation is taken such thats its effects die out in nonperiodic direction before it reaches to boundary. The value of parameters chosen in typical run are $V_0 = 5.0, V_1 = 10^{-2}, \sigma = 0.8$ and $\epsilon = 0.5$. The evolution is tracked by studying the evolution of the total perturbed

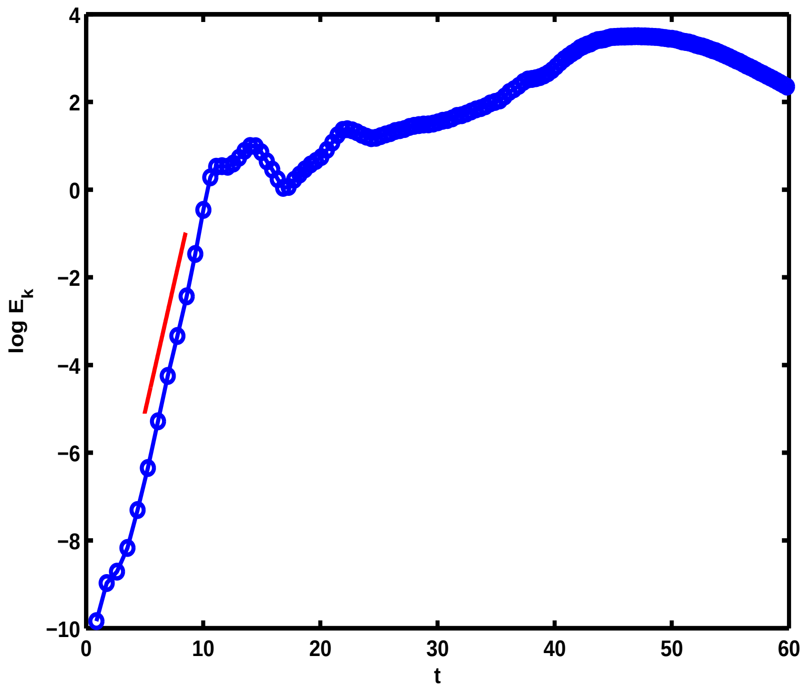

Figure 6.5: The Perturbed kinetic energy(log scale) Vs. time for the strong coupling dust fluid. $\eta = 5$ and $\tau_m = 20$ has been choosen for this case. Other parameters in simulation are same as Fig. (6.3).

kinetic energy, $E_{PKE} = \int\int \mid (\vec{v} - \vec{v}_0) \mid^2 dxdy$. The spatial profiles of velocity, density and potential obtained from simulation is also preserved at regular intervals. The evolution of the E_{PKE} for one typical simulation case has been shown in the plot of Fig. (6.5). It clearly shows that during the initial phase the linear instability mechanism is operative. The growth rate obtained from simulations are observed to match well with the predictions of the linear analysis. In the nonlinear regime the behaviour of the E_{PKE} evolution is somewhat distinct in the strongly coupled case than what is seen in the other weakly coupled fluid cases. For instance the simulations of incompressible fluid shows saturation and a constancy of E_{PKE} and the compressible and the dispersive cases show periodic oscillations in E_{PKE} [97] in the nonlinear regime. These periodic oscillations were attributed to the rotation of the vortex structure that ultimately forms as an aftermath of the KH instability in these cases. While for the incompressible fluid case the final saturated structure typically has a circular form, its rotation does not cause any periodic change in E_{PKE}. For the compressible and dispersive cases the vortices that finally form have an elliptical shape. Their rotation then shows up as periodic oscillations in the E_{PKE}. The rotation frequency of the vortex was shown to match with the observed oscillation in E_{PKE} in these cases. It was also observed that when the vortices merge an irreversible sudden increase in the value of E_{PKE} is observed. In the strong coupling case, though the E_{PKE} in the nonlinear regime exhibits non-stationarity it does not show any periodic characteristics. We would see subsequently that this is associated with the elasticity of the medium causing the sharpening of the shear layer and recurrence of the KH excitation phenomena for a couple of times.

We show in Fig. (6.6) and Fig. (6.7) the snapshots of the $2-D$ spatial profile of the curl and the divergence of the velocity field respectively for the simulation run corresponding to plot of E_{PKE} evolution shown in Fig. (6.5). The initial state as chosen is clearly divergenceless ($\nabla \cdot \vec{v} = 0$) and constitutes uniform strip of vorticity. During the linear phase $t = 10.01$ (comparison of timing can be seen from Fig. (6.5)) the usual bending of the vorticity strip due to the KH instability can be seen. At later stage it breaks up in anisotropic vorticity patches. Apart from the vorticity patches at the main central region, the emission of transverse waves separating from the central region and moving towards the boundaries can also be discerned clearly from the snapshots. These emissions are caused by the local instability which is possible in the case of the strongly coupled medium and about which we discussed in section 6.3 earlier. The spatial profile of divergence shown in Fig. (6.7) illustrates the compressional nature of these emissions.

These vorticity patches, however, are observed to change their shape as they rotate. This is quite unlike the other cases (e.g. incompressible and compressible weaky coupled fluids). Here the vorticity patches get stretched against the background flow, as they rotate. The elastic nature of the medium in this case lets the vorticity patch get extended. The extended structures then coalesce again to form

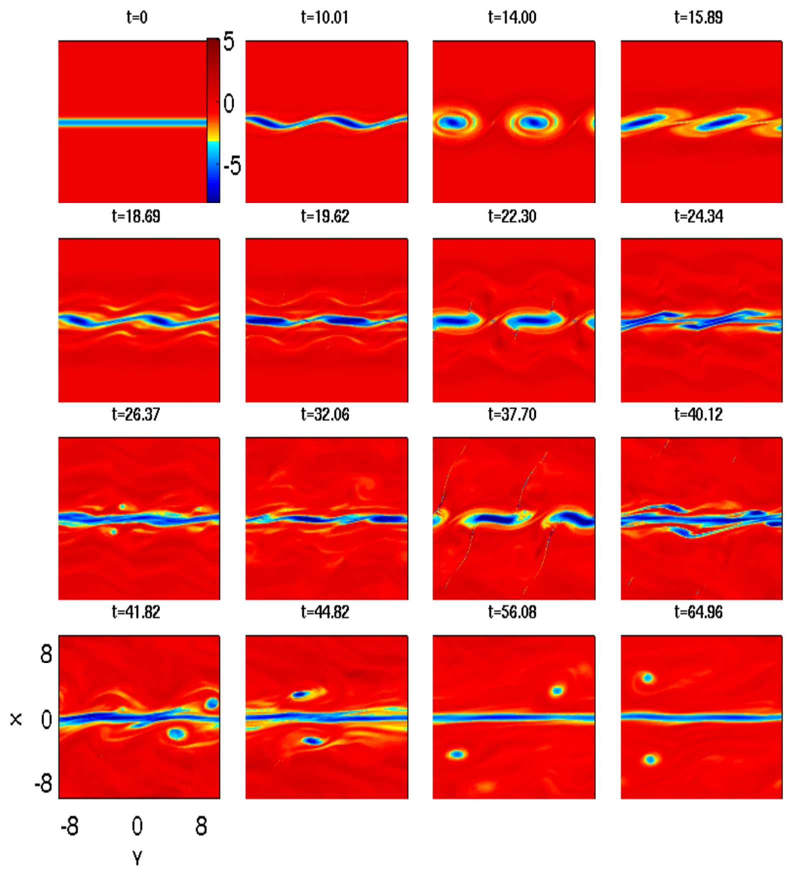

Figure 6.6: Nonlinear evolution of vorticity contours at different times for parameter values $\eta = 5, \tau_m = 20$ and mach no 0.707 for this case. Other simluation parameters are $V_0 = 5$ and $\epsilon = 0.5$. Quasineutrality has been taken under consideration.

a very thin vorticity strip (see blue colored patches) as shown in the snapshots of Fig. (6.6) at $t = 18.69$ and $t = 19.62$). During this extension and coalescence phase there is an intense activity in terms of the emission of shear waves. This is reminiscent of the process when an elastic medium as it snaps back produces intense oscillations.

It is interesting to observe that the thin central vorticity strip developed after the coalescence is now again sharp enough to suffer KH destabilization. This again results in the formation of rotating vortices ($t = 22.30$). The same process then repeats itself. At a later stage one also observed that smaller lumps of vorticity gets separated from the central region. This is when the medium yields and breaks apart as it is no longer possible for it to sustain the strain. Some of these smaller

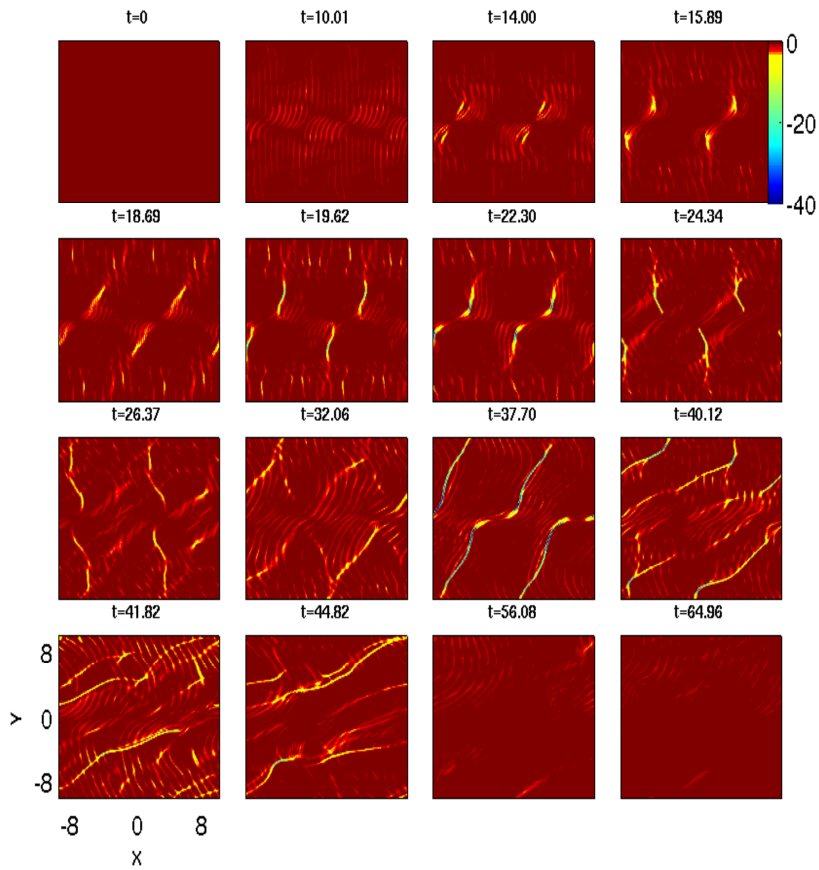

Figure 6.7: Nonlinear evolution of divergence of velocity field contours at different times for parameter values $\eta = 5, \tau_m = 20$ and mach no. 0.707 for this case. Other parameters in simulation are $V_0 = 5$ and $\epsilon = 0.5$. Quasineutrality has been taken under consideration.

structures upon reaching the region of uniform background flow form circular patterns and are seen to be well preserved for quite a long duration. This entire repetitive nature of the process can be summarized as follows:

- ⋆ **Initial Configuration:** Initially, the shear scale $\epsilon = \epsilon_{init}$ is sharp enough to cause destabilization of shear flow (Fig. 6.6, subplot at $t = 0$ and $t = 10.01$).

- ⋆ **Nonlinear regime:** In this regime, the effective shear width ($\epsilon = \epsilon_{eff}$) is broader and the growth of KH mode is no longer sustained. The saturated KH mode forms elliptical vortices (Fig. 6.6, subplots at $t = 14.00$, $t = 22.30$, and 37.70).

- ⋆ **Elliptical vortices:** The elliptical vortices formed in nonlinear regime rotate and get stretched by the background flow. Basically, the elastic nature of the medium stretches the elliptical vortices further to form sharp shear flow structures (Fig. 6.6, subplots at $t = 15.89$, $t = 24.34$, and $t = 40.12$).

- ⋆ **Coalescence of sharper elliptical vortices:** Elongation of elliptical vortices leads to formation of a sharper shear width and hence this configuration is once again susceptible to KH destabilization (Fig. 6.6, subplots at $t = 18.69$ and $t = 26.37$).

- ⋆ **Recurrence:** Thus the phenomena of KH destabilization recurs in this case of strong coupling. (Fig. 6.6, subplots at $t = 19.62$ and $t = 32.06$).

6.5 KH destabilization of transverse shear wave propagation

The sheared velocity flow is susceptible to KH destabilization process. Clearly, the sheared configuration of flow in the transverse shear wave mode also ought to be susceptible to this instability. However, as shown in Fig. 6.8 when we choose an intial configuration with a sinusoidal perturbation of the form

$$\vec{v_0} = V_0 * \sin K_y y\hat{x} \tag{6.15}$$

with $V_0 = 1e - 3$ and $K_y = 0.6382$ the wave propagates smoothly without any distortion. For this particular case we had chosen $\eta = 5$ and $\tau_m = 100$. The analytical phase velocity in this case being $v_{ph} \sim \sqrt{\eta/\tau_m} = 0.05$ also gets verified by the numerical evolution of the profile. Fig. 6.9 shows the comparison of the dispersion relation between the analytical and the simulation results. We also observe from our simulations (Fig. 6.8) that the amplitude diminishes due to the dissipative effect of η. However, even though the flow had a sheared configuration in this mode there is no trace of the KH instability.

We have carried out simulations for the magnitude of V_0 to 0.1 and 2.0 shown in Figs. 6.10 and 6.11 respectively. For $V_0 = 1e{-}3$ again there is no trace of instability. However, for $V_0 = 2.0$ the distortions confirming the presence of KH instability can be easily seen. From these simulations it appears that the KH destabilization is

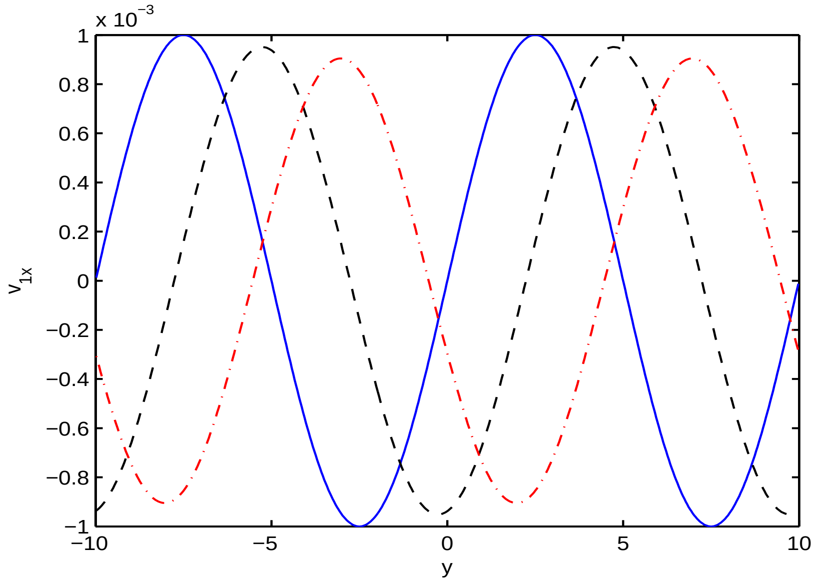

Figure 6.8: Transverse wave propagation of $k_y = 0.6382$ mode for the initial flow profile Eq. (6.15). The other parameters of simulation are $V_0 = 1e-3, \eta = 5$ and $\tau_m = 100$.

preferred when the amplitude of the shear flow is high. a simple interpretation for these observations can be provided by considering the comparison of the growth period of the KH instability and the time period of the transverse mode. When the growth rate of the KH mode is slower that the transverse shear wave frequency, the wave propagation does not get hinderd by the instability process. On the other hand when the reverse is true the instability manifests itself. A comparison of the growth rate further testifies to this. The typical growth rate of the KH mode can be approximated as $\gamma_{kh} \sim K_y V_0$ (the step velocity case). For the two cases of Fig. 6.10 and Fig. 6.11 the transverse shear wave frequency is from Eq. 6.7 is $\omega_T \sim 0.2236$. For the case (Fig. 6.10) in which the KH is suppressed we have $\omega_T > \gamma_{kh}$ and for the other case (Fig. 6.11) we have $\omega_T < \gamma_{kh}$.

6.6 Summary

The fluid Kelvin-Helmholtz instability in the context of a strongly coupled dusty plasma medium has been investigated in detail. In particular it is of interest to understand the role of visco-elasticity and the existence of transverse shear waves in a strongly coupled medium on the fluid KH instability. A generalized fluid

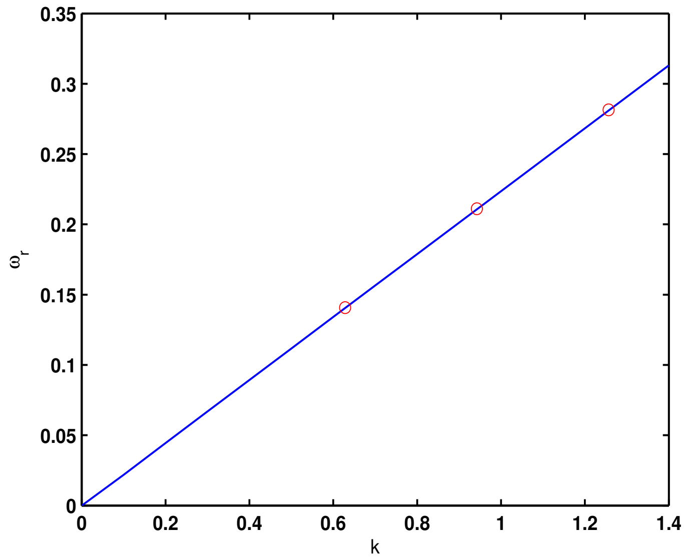

Figure 6.9: The analytical dispersion relation (blue line) Eq. (6.7) with numerical dispersion relation (red circle) for transverse shear waves in viscoelastic fluids with large solid like properties.

hydrodynamic model (GHD), which captures these aspects of the strong coupling state, has been used to represent the behaviour of dusty plasma medium in this regime.

A complete parametrization of the KH growth rate, in terms of the memory relaxation parameter employed in the GHD model to depict strong coupling effect, have been carried out. It is observed that the growth rate of KH mode reduces in a strongly coupled medium. Furthermore, in addition to the KH mode a local instability driven by the shear flow is also found to exist in the strongly coupled medium. The existence of this local mode causes emission of transverse shear modes. These linear results were verified in the nonlinear simulations conducted by us.

The simulations showed interesting phenomena of recurrence of the KH mode in the nonlinear regime. The KH mode typically saturates by generating vorticity structures which typically have much broader width for sustaining the KH mode. The 2-D constraints of the normal fluid on enstrophy can only make the scale lengths associated with the shear scale get further broadened due to coalescence in the case of normal fluids. However, the GHD fluid has no such constraint in

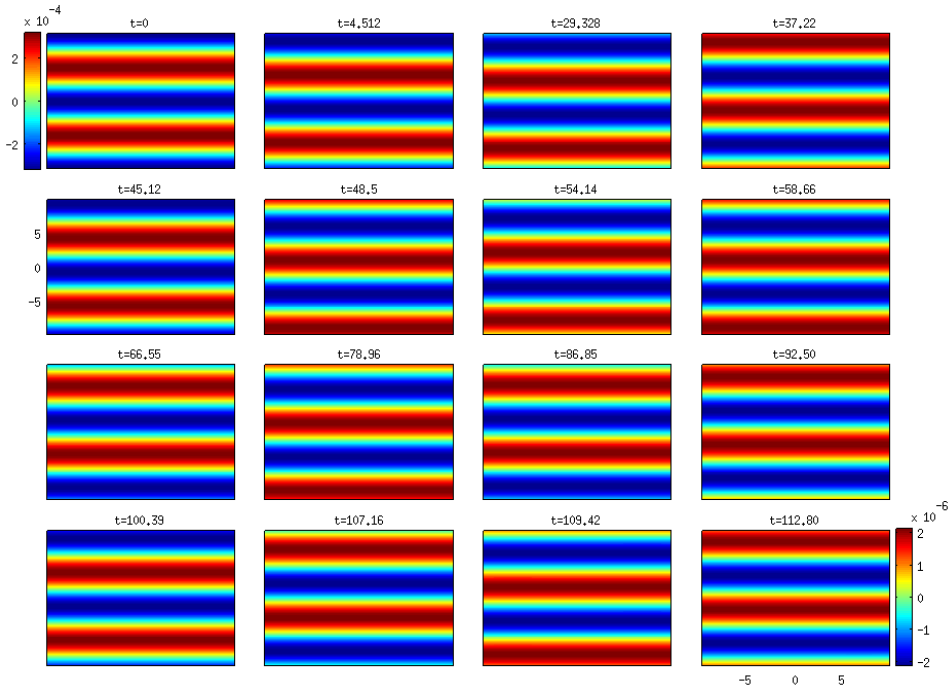

Figure 6.10: Vorticity of a initial flow as a transverse perturbation in velocity as given by Eq. (6.15). The parameters are $V_1 = 1e-3, \eta = 5$ and $\tau_m = 100$ and the perturbation wave number correspond to two mode numbers ($K_y = 0.6382$) in the system.

2-D. In fact the elastic nature of the strongly coupled fluid causes the individual vortices as they rotate to get stretched and form sharper flow structures. Thus unlike a 2-D normal fluid in a 2-D visco-elastic fluid one observes formation of short scale structures. These sharp structures are then again susceptible to the KH instability. This cycle was observed to get repeated several times in some of our simulations. It ultimately stops as a result of system exhausting up its free energy associated with the shear flows. An additional channel of free energy exhaustion is associated with shear flow is the local instability supported by the medium due to which strong emission of transverse as well as compressional wave are observed. We have demonstrated a rich variety of response in a 2-D strongly coupled visco-elastic dusty plasma medium by our simulations conducted here for an equilibrium shear flow configuration. Further studies to understand the competition between the local instability and the KH mode in getting rid of the free energy associated with the shear flow in a visco-elastic medium is necessary. It is also clear from

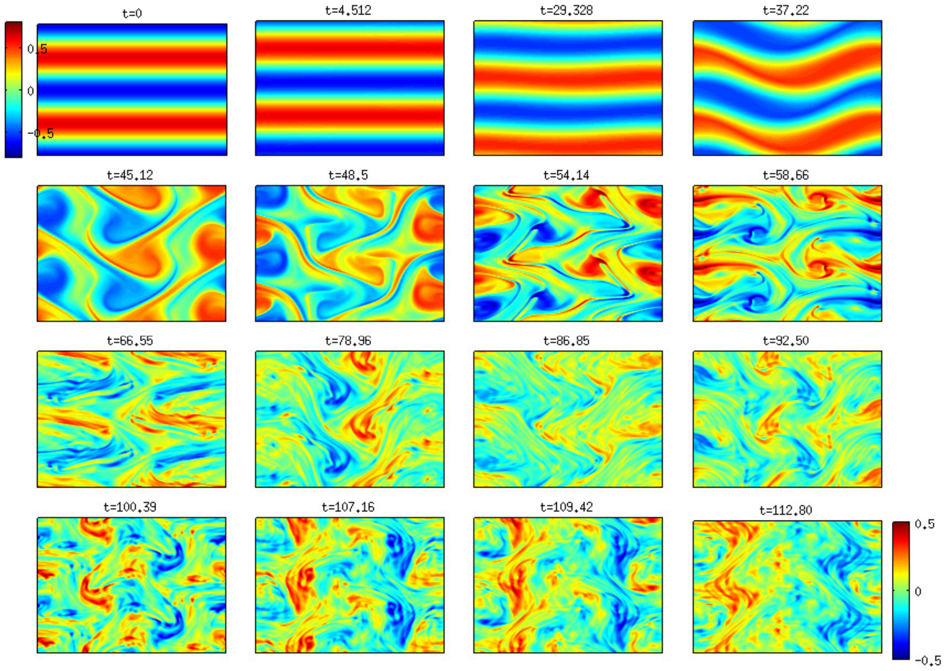

Figure 6.11: Vorticity of a initial flow as a transverse perturbation in velocity as given by Eq. (6.15). The parameters are $V_1 = 2.0, \eta = 5$ and $\tau_m = 100$ and the perturbation wave number correspond to two mode numbers ($K_y = 0.6382$) in the system.

our simulations that in a 2-D visco-elastic medium the possibility of formation of short scales does exist. Thus unlike the hydrodynamic fluid the cascade behaviour of the energy spectrum is quite distinct and should be investigated in detail.

Big whirls have little whirls That feed on their velocity, And little whirls have littler whirls And so on to viscosity.

L.F. Richardson

7 Visco - Elastic Turbulence

In Chapter 6, we have made observations of small scale structure formation during evolution of 2-D K-H instability for strongly coupled dusty plasma medium. Thus, the Generalized Hydrodynamic description of visco - elastic fluids suggests that the inverse cascade is not the only preferred mechanism for energy transfer in such systems. To look in to nature of power spectra for flows in these fluids, we have carried out the simulations for the evolution of initial random fluctuation with spectra in a prescribed band of wave numbers. It is observed that the power spectra for visco-elastic fluids is distinct from that of hydrodynamic fluids and displays clear scale separation.

7.1 Introduction

The characterization of fluid flows has been of great interest in past and a significant amount of research have been dedicated to this particular area [140,141]. The interest ranges from laminar to turbulent flows, viscous to inviscid flows, variety of unsteady flows, fluid instabilities etc. While most of fluid flows have been found to follow Newtonian dynamics and hence standard Navior-Stokes (NS) equations applies, a range of fluid (viz. polymeric and colloidal suspensions, cellular solids) have non - Newtonian dynamics. Such fluids have characteristics of both liquid and solid and are important from the perspective of their unique transport characteristics. Several models have been proposed for the understanding of such non - Newtonian fluids. The combination of viscous behavior and solid like elastic features (often termed as visco - elastic fluids) in some cases have been depicted by introducing a memory relaxation time in the model description. In recent years there have been a great deal of interest in understanding the behavior of visco-elastic fluids [142–146]. One important aspect is the study of the turbulent behavior of such systems as it plays a crucial role in determining the anomalous transport of the system. Experiments on turbulence on Polymeric flows of the system have been conducted. It is observed that turbulent power spectra of such fluids are from that of the hydrodynamic fluid [101, 102].

As the dusty plasma medium has also been found to reflect properties of fluid as well as solids at the intermediate range of coupling parameter Γ, a Generalized Hydrodynamic (GHD) description has been employed to study it. In the GHD prescription the dusty plasma system is assumed to mimic visco - elastic fluid behavior. Using this description, we have in the previous chapters provided numerical evidence of the existence of transverse shear waves, singular cusp structures and formation of short scales [94, 96, 98].

The formation of small scale structures observed in the previous chapter while studying the nonlinear evolution of shear flow driven KH instability in 2-D strongly coupled dusty plasma flows is in contrast with the phenomenon of inverse cascade in 2-D Navier Stokes fluids. It is, therefore, of interest to delve in a detailed study of the spectral cascade behavior of this system.

In this Chapter, we present our investigation on the evolution of random turbulent fluctuations. We choose to consider the simplified incompressible limit of the equation to limit ourselves mainly to the role of transverse shear waves (an attribute of elasticity in the medium) in such studies. The extraneous effects due to compressible fluctuations have been ignored at the moment. As the incompressible limit of GHD model assumes no density and charge fluctuations, the results obtained here would represent a wide range of fluid flows which could be explained using visco - elastic description. The Chapter has been organized as follows. A brief description of the governing equations for such an incompressible case and the numerical procedure adopted for the simulation studies have been provided in section 7.2. Section 7.3 contains the results obtained from the numerical simulation. The theoretical analysis and discussion has been provided in section 7.4. Section 7.5 contains the conclusion.

7.2 Governing equations

The complete set of governing equations are Eqs. (2.1,2.2,2.3) for the evolution of a strongly coupled dusty plasma medium through the Generalized Hydrodynamic (GHD) description.

In the limit of quasi-neutral and incompressible perturbations, we can ignore the continuity and Poisson's equation and we are left with the following equation

$$\left[1 + \tau_m \left(\frac{\partial}{\partial t} + \vec{v_d} \cdot \nabla\right)\right] \left[\left(\frac{\partial}{\partial t} + \vec{v_d} \cdot \nabla\right) \vec{v_d} + \frac{\nabla p}{n_d}\right] = \eta \nabla^2 \vec{v_d} \tag{7.1}$$

It is clear that in this limit, the model equations have no specific attribute connecting it specifically to the dusty plasma medium and it can in general represent any other visco-elastic system also, along with the case of dusty plasma medium.

For the purpose of numerical simulation we reduce the second order Eq. (7.1) in time to two coupled first order equations satisfying the following convective forms.

$$\left[1 + \tau_m \left(\frac{\partial}{\partial t} + \vec{v_d} \cdot \nabla\right)\right] \vec{\Psi} = \eta \nabla^2 \vec{v_d} \tag{7.2}$$

$$\left[\left(\frac{\partial}{\partial t} + \vec{v_d} \cdot \nabla\right) \vec{v_d} + \frac{\nabla p}{n_d}\right] = \vec{\Psi} \tag{7.3}$$

In the 2-D incompressible case, with the flow confined in the 2-D plane normal to the symmetry axis we can represent the velocity field by a scalar potential Φ, satisfying $\hat{z} \times \nabla \Phi = \vec{v_d}$. Here $\hat{z}$ is directed along the symmetry axis. Taking the curl of Eq. (7.3) we have

$$\left[\frac{\partial}{\partial t} + \hat{z} \times \nabla \Phi \cdot \nabla\right] \nabla^2 \Phi = (\nabla \times \Psi)_z = \left(\frac{\partial \Psi_y}{\partial x} - \frac{\partial \Psi_x}{\partial y}\right) \tag{7.4}$$

We can construct the following evolution equations for the square integral quantities by taking the scalar product of $\vec{v}$ with Eq. (7.3) and $\vec{\Psi}$ with Eq. (7.2)

$$\frac{1}{2}\frac{\partial}{\partial t} \int\int v_d^2 dxdy = \int\int \vec{v_d} \cdot \vec{\Psi} dxdy \tag{7.5}$$

$$\frac{1}{2}\frac{\partial}{\partial t} \int\int \Psi^2 dxdy = -\frac{1}{\tau_m} \int\int \Psi^2 dxdy + \frac{\eta}{\tau_m} \int\int \vec{\Psi} \cdot \nabla^2 \vec{v_d} dxdy \tag{7.6}$$

The evolution of these quantities are tracked during the course of numerical simulation for the purpose of determining the accuracy of the simulation. For the

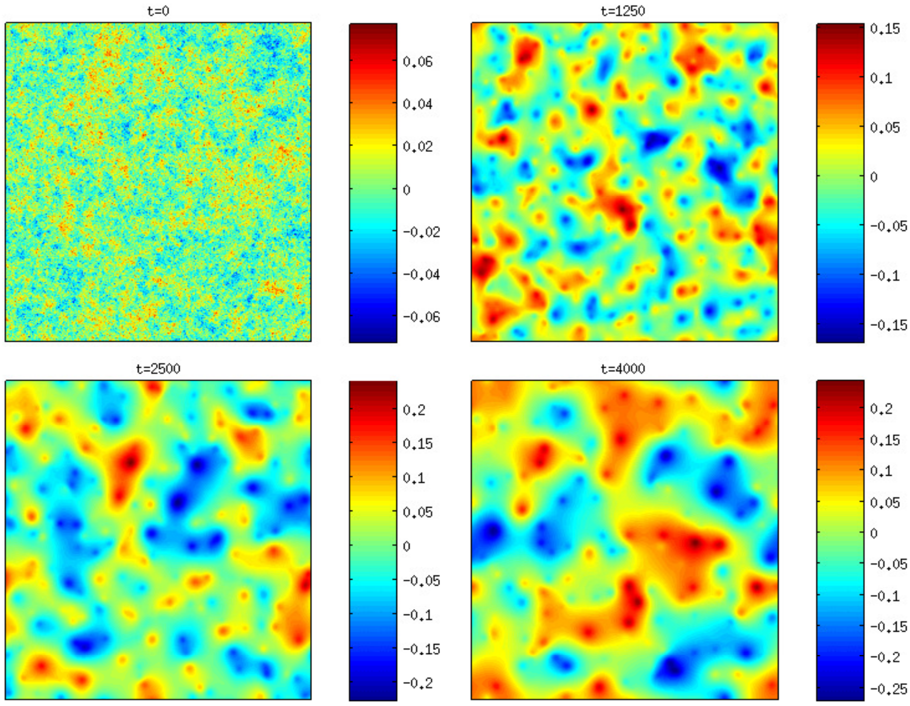

Figure 7.1: Evolution of phase randomized velocity potential for incompressible hydrodynamic fluids. The inverse cascade is evident as the smaller scales are coalescing to form large scale length structure.

purpose of simulation, a random initial condition for the incompressible flow in the 2-D plane is prescribed by choosing an initial spectrum for the field Φ according to the following two forms:

$$\mid \Phi_k \mid^2 = \frac{C}{(1+ \mid k \mid)^n} \tag{7.7}$$

$$\mid \Phi_k \mid^2 = Csech^2 \left(\frac{\mid k \mid - k_m}{4} \right) \tag{7.8}$$

In the first case, the power falls of monotonically with wave number (the rapidity of fall being governed by n) and in the latter case the peak of the initial spectrum can be chosen at any desired wavenumber determined by the value of k_m. The phase of the Fourier modes are chosen to be random. Here, C is constant which decides the amount of power being injected in system. In the simulations presented here, we have restricted to an initial choice of $\vec{\Psi} = 0$. These initial conditions are then evolved using the Eqs. (7.2,7.4) through a flux corrected scheme [107]. In the next section we present the details of some interesting observations obtained from numerical simulation studies.

7.3 Numerical observations

In Fig. 7.1 and Fig. 7.2, we show the constant contour plots of the velocity potential Φ for the hydrodynamics (HD) case ($\eta = \tau_m = 0$) and the GHD case of ($\eta = 5, \tau_m = 20$) respectively.

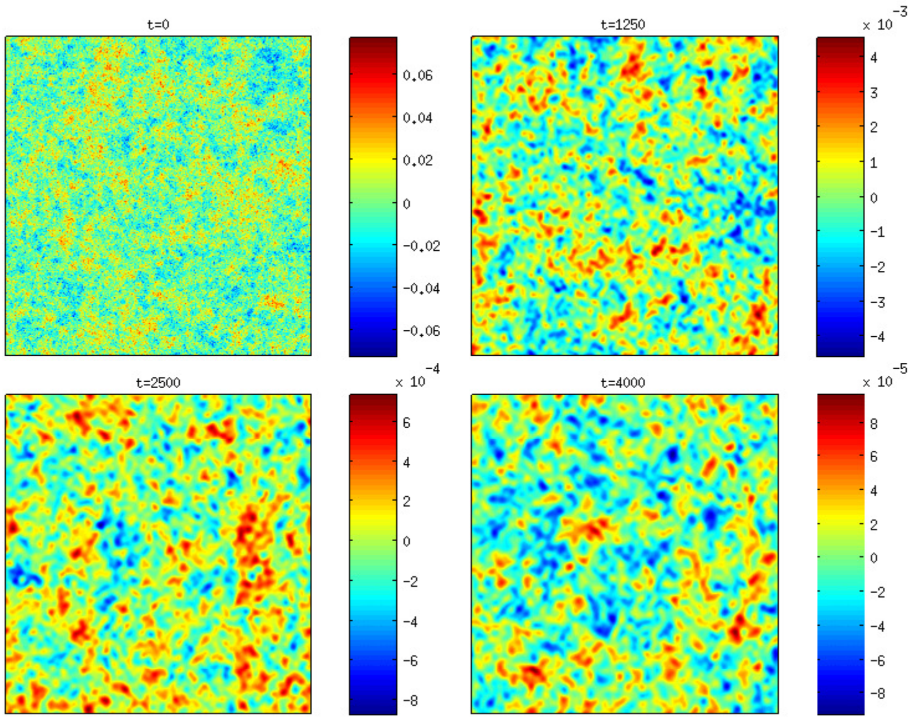

Figure 7.2: Evolution of phase randomized velocity potential for incompressible visco-elastic fluids. It could be seen that in contrast to hydrodynamic fluids, much shorter structures are present in this particular case. The parameters η and τ_m are 5 and 20 respectively.

It is clear that the evolution of the two cases show very different evolution characteristics. In the HD case, isolated fewer vortex structures are observed at later times. In GHD, the time asymptotic state shows a clutter of closely packed structures. We also monitored the evolution of averaged wavenumber in both the cases, which has been shown in Fig. 7.3. It is clear from the figure that in both HD and GHD cases the spectral cascade is towards longer scales. This is evident from the fact that the the mean square wave number reduces with time. This is expected and well known characteristics of the 2-D NS dynamics representing HD flows.

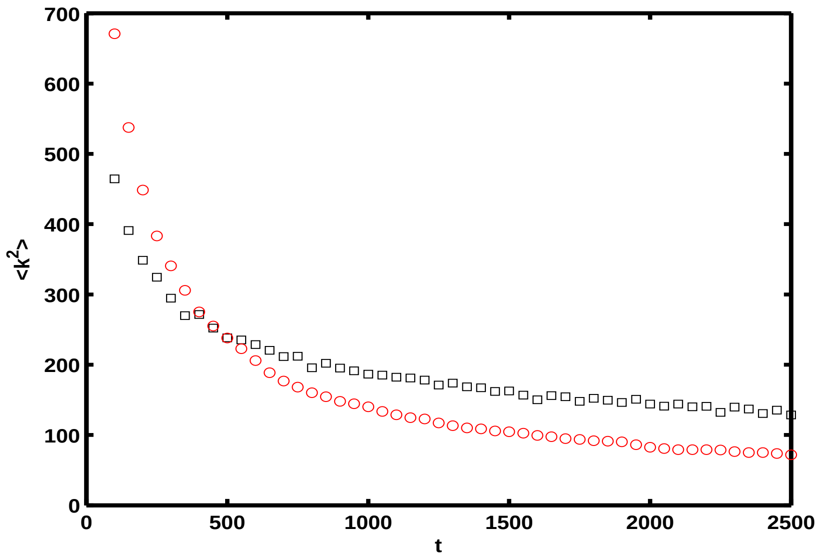

Figure 7.3: The plot of $< k >^2$ with time for the GHD case with ($\eta = 5$ and $\tau_m = 20$) (square) and for the incompressible fluid (circle). the initial random flow has been taken of the form given by Eq. (7.7) with $n = 2$.

We also provide a comparison of spectral power for the HD and GHD cases in Fig. 7.4 In the HD case a stationary power law spectrum with an index of $-5/3$ and -3 is clearly evident in the energy and vorticity cascade regimes. The GHD spectrum, however, is in stark contrast to the HD case. Any power law dependence if present is overwhelmed by the appearance of peaks in the spectrum at certain wave numbers. This indicates that the cascade process is severely inhibited at certain wave numbers, resulting in piling up of the spectral power at that location. The peaks are not sharp though and from the plots of Fig. 7.5 and Fig. 7.6, it is clear that their location shifts towards longer scale in the course of time. The evolved spectra is also dependent on initial choice of the spectrum.

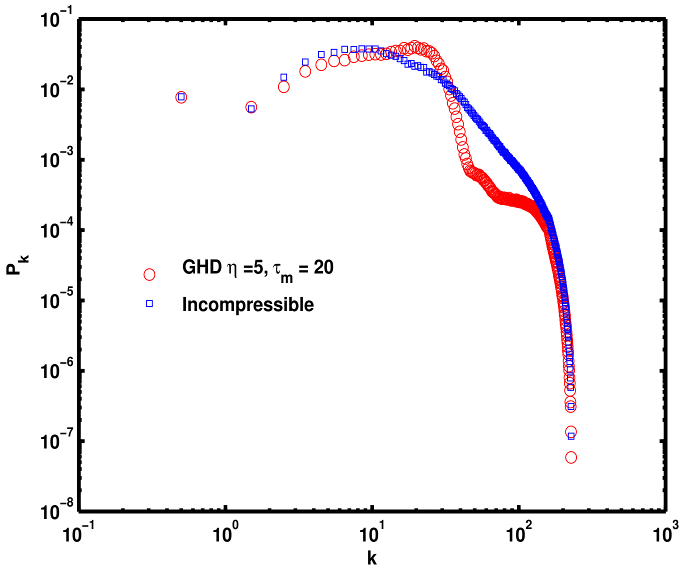

Figure 7.4: Comparison of power spectra for incompressible hydrodynamic fluid (blue box) with incompressible visco-elastic fluids (red circle).

We observe that the location of the peak depends on the choice of the parameter η/τ_m. In Fig. 7.7 we plot the power spectra for several cases with different values of the parameter η/τ_m. It can be seen that there is a definite shift of the spectra towards high k values as the value η/τ_m is reduced.

To summarize, the main observations of our simulations are (i) non universal character of the evolved spectrum for GHD, which shows strong dependence on the initial spectrum (ii) appearance of broad peaks which shift towards longer scales with increasing time (iii) with increasing η/τ_m the peak location again shifts towards long scales (iv) The peaks are dominant when the initial power content in shorter scales is high. In the next section we provide a discussion on these observations.

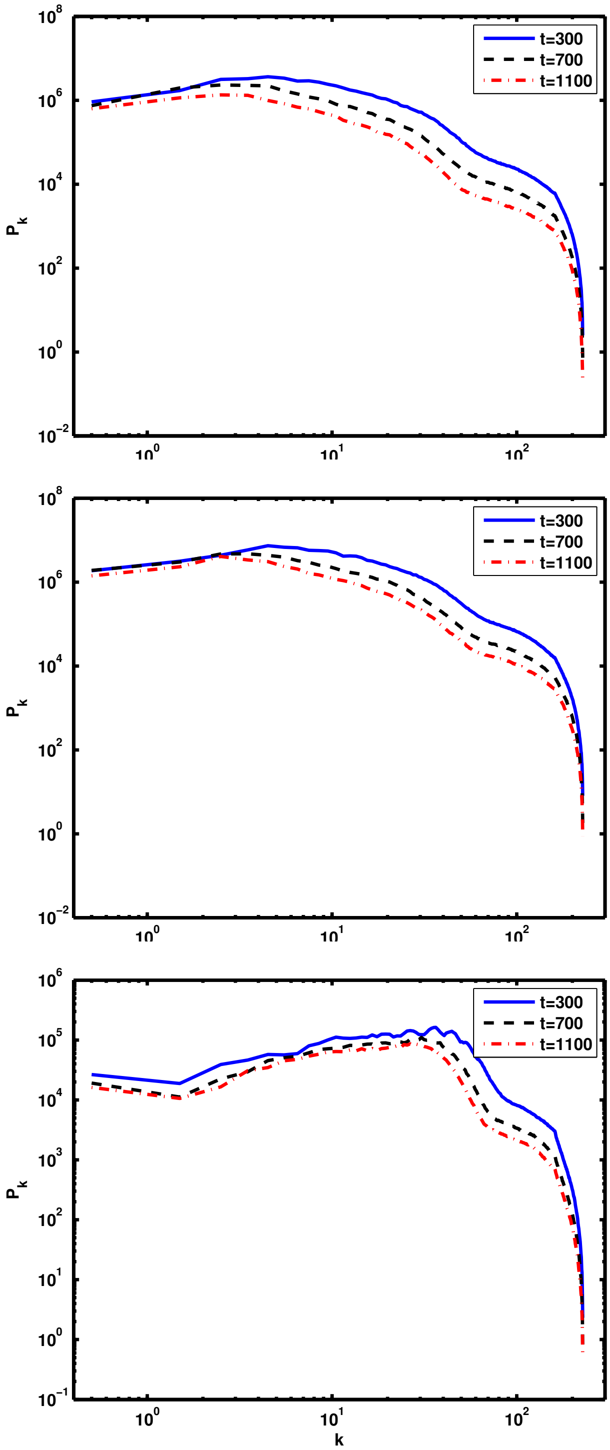

(a) $\mid \phi_k \mid^2 = Csech^2(\frac{|k|-20}{4})$

(b) $\mid \phi_k \mid^2 = Csech^2(\frac{|k|-30}{4})$

(c) $\mid \phi_k \mid^2 = Csech^2(\frac{|k|-90}{4})$

Figure 7.5: Power spectra for incompressible visco-elastic fluids with different initial form of spectrum mentioned alongside. For the subplots (a), (b) and (c), the initial power has been injected at $k_m = 20, 30$ and $k_m = 90$ respectively.

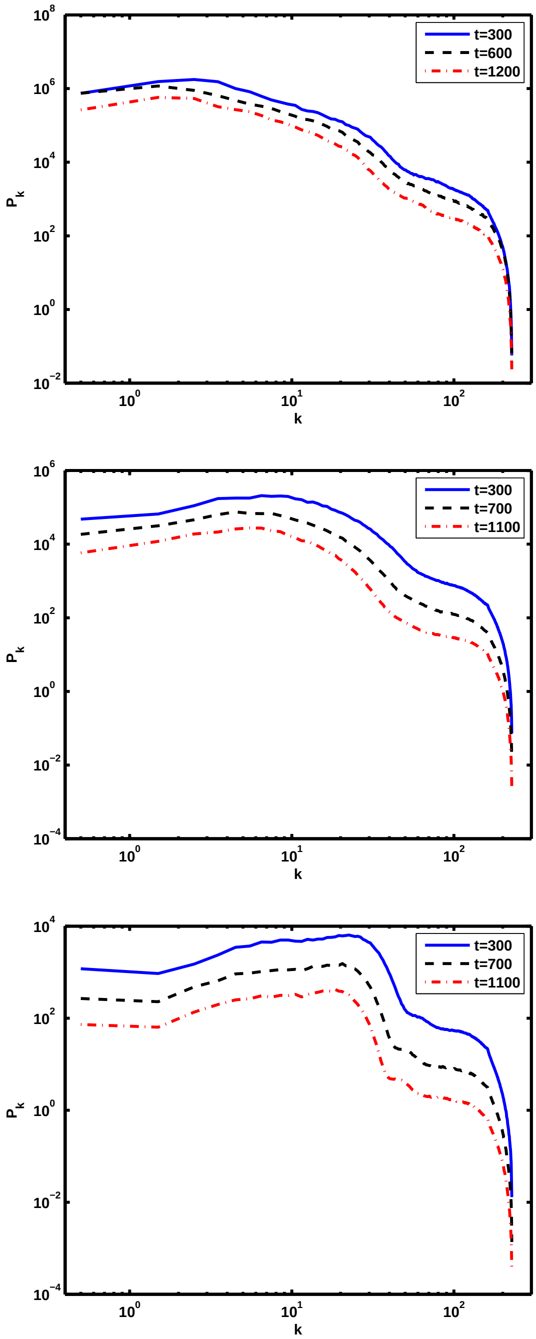

(a) $\mid \phi_k \mid^2 = \frac{C}{(1+|k|)^8}$

(b) $\mid \phi_k \mid^2 = \frac{C}{(1+|k|)^4}$

(c) $\mid \phi_k \mid^2 = \frac{C}{(1+|k|)^2}$

Figure 7.6: Power spectra with different initial form of spectrum (monotonically distributed power) mentioned alongside. For the subplots (a), (b) and (c), the initial power has been injected as given in Eq. (7.7) with $n = 8, 4$ and $n = 2$ respectively.

7.4 Discussion

A Hydrodynamic fluid in the incompressible limit is a scale free system as it does not support any normal mode and neither does it have any intrinsic length and/or time scale associated with it. In contrast, the incompressible GHD model employed in the present context supports transverse shear wave mode. There also exists a special time scale defined by the relaxation parameter τ_m in the system. In 2-D it is well known that the spectral cascade is towards long scales for the hydrodynamic system as it supports two non dissipative integral invariants. The GHD system does not support the second invariant related to the mean square vorticity integral. Thus the power cascade towards long scale is not necessary for this case. However, in the GHD system there is an inherent slow dynamics of HD medium occurring for time scales longer than the memory relaxation time τ_m. It is this aspect of dynamics which is responsible for a slow but preferential cascade towards longer scales. Thus while the inverse cascade is in general inhibited resulting in the appearance of peaks in the spectrum, there is a slow but yet susceptible transfer towards long scales resulting in the shift of the peaks towards longer scales.

In a similar fashion when the value of τ_m is chosen to be high, the HD dynamics would set in at even later times. The peak in the spectrum for higher values of τ_m is, therefore, found to occur preferentially at shorter scales. Similarly a dependence of the location of the spectral peak on η/τ_m is indicative of the role of the transverse shear wave on the spectrum.

7.5 Conclusion

The question of whether or not the natural modes and scales of the system have a role on turbulence has continued to remain an outstanding problem. Attempts have so far been made on the basis of identifying the differences predicted theoretically on the power spectral index of a stationary turbulence state. This has so far proved an extremely difficult exercise and has resulted in endless controversies without settling the issue one way or the other.

Against this backdrop we have shown that for the case of turbulence in Visco-Elastic medium governed by the Generalized Hydrodynamic equation, the quasi-

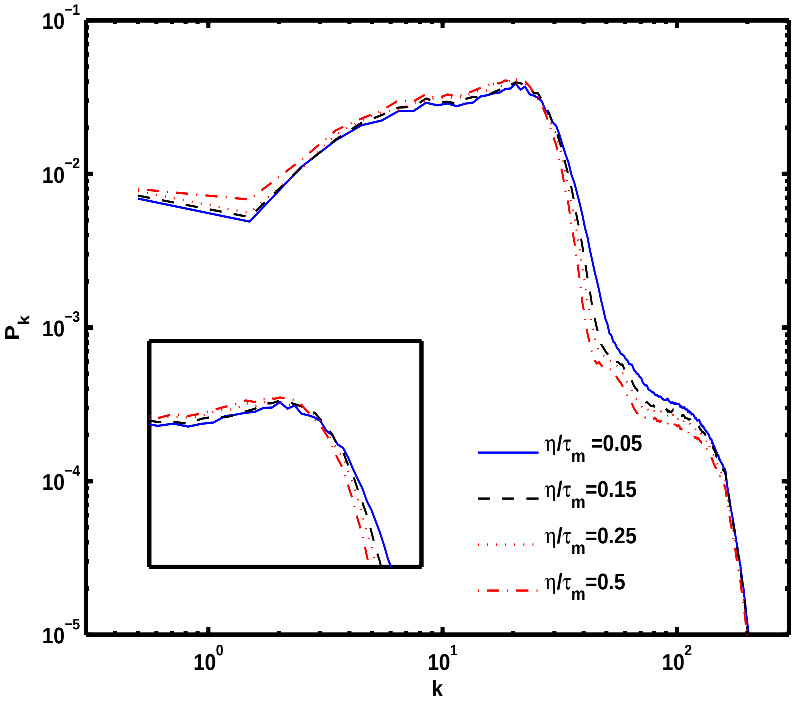

Figure 7.7: Power spectra plots with different value of η/τ_m for incompressible visco-elastic fluid.

stationary behavior of the turbulent spectrum provides ample evidence of the involvement of the memory relaxation time τ_m and the transverse shear wave in the spectral cascade process.

The appearance of shorter scales in 2-D for GHD system is also suggestive of enhanced transport and mixing properties of the GHD system vis. a vis the HD dynamics in 2-D.

8 Conclusion

The present thesis covers several novel phenomena in one and two dimensions associated with the dusty plasma medium in both weak and strong coupling regimes. A Generalized Hydrodynamic (GHD) fluid model coupled with Poisson's equation has been adopted for the purpose to describe the dusty plasma medium. The GHD model takes care of the visco - elastic properties of the medium in the strong coupling regime. Both analytical and numerical simulation studies have been done on the collective behavior of the dusty plasma medium in the two regimes of weak and strong coupling.

The summary of the interesting results obtained in this thesis has been presented in section 8.1. The future scope of the research studies carried out in this thesis have been listed point wise in section 8.2.

8.1 Main results of the Thesis

8.1.1 1-D studies

The 1-D coupled set of GHD and Poisson's equation was solved by using the flux corrected scheme and the Poisson solver respectively. The numerical code was benchmarked by reproducing the linear dispersion relation of the Dust Acoustic Wave (DAW) numerically.

We have made certain interesting observations pertaining to the characteristic nonlinear solutions for the coupled GHD and Poisson set of equations in one dimensions for the dusty plasma medium. These observations are summarized as below:

- **Observation of stable singular cusp structure in weakly coupled dusty plasma medium**

  The equations for the dusty plasma medium in the weak coupling limit reduce to the usual fluid equation for the charged dust fluid which is influenced by the scalar potential field through the Poisson's equation. It can be shown by using the reductive perturbative scheme, that in the limit of weak nonlinearity, the equations can be cast into a well known KdV form. Our simulations reproduce the characteristics properties of the KdV soliton solutions in the weak amplitude limit, thereby benchmarking the code in the nonlinear regime too.

  At higher amplitudes the exact analytical form of solutions can be obtained by constructing Sagdeev potential. At smaller amplitude the solutions of the Sagdeev potential are identical to KdV solutions. However, with increasing amplitude the form starts deviating from the KdV solutions. The Sagdeev potential provides an upper limit beyond which localized solutions propagating with constant velocity do not exist. This is due to the wave breaking at the limiting amplitude. At the limiting amplitude the structure has a singular cusp form for the density and velocity fields.

  We observe that by choosing an initial condition with amplitude higher than that provided by the Sagdeev limit, the evolution invariable deforms into two or more localized structures. The higher amplitude structures are found to be invariably the singular cusp solutions of the Sagdeev potential at the wave breaking limit. These solutions are observed to be fairly robust and evolve stably during the entire course of simulation (several hundreds of dust acoustic period).

  Our numerical observations have experimental relevance as such singular cusp structures have been observed in dusty plasma experiments by Teng *et al.* [1].

- **The new paradigm of Hunter Saxton (HS) equation for the Strongly coupled dusty plasma**

  The application of reductive perturbative approach to study the weakly nonlinear response of the strongly coupled dust fluid leads to an entirely new paradigm. The equation in this case do not reduce to the well known KdV form. They have an altogether different form from which it is apparent that periodic and all localized smooth solutions are not permissible in this particular case. In fact we have shown that in the limit when the elastic effects due to correlation dominate over the Boltzmann screening and dispersive effects, the equation takes the form of the Hunter Saxton (HS) equation. The HS equation is known to permit shock solutions which are either conservative or dissipative. This, therefore, offers an entirely new paradigm for the strongly coupled dusty plasma medium. The HS equations have been explored previously in context of the study of directors field in liquid crystals and we have first time predicted the applicability of such an equation in the context of dusty plasma medium.

The numerical simulations in 1-D with the complete set of coupled GHD and Poisson system with localized initial conditions are found to evolve and exhibit shock formation.

8.1.2 2-D studies

After carrying out a comprehensive investigation in 1-D, we have chosen to investigate the characteristics features exhibited by the dusty plasma medium in 2-D. We have chosen for this purpose to study the well known shear flow driven fluid Kelvin Helmholtz (KH) instability as well as turbulent characteristics for this medium. The important findings from our studies are as follows.

- **Compressible and dispersive effects on the nature of Kelvin-Helmholtz instability in weakly coupled dusty plasma medium**

  The growth rate as a function of wavenumber have been obtained by numerically finding the eigen value of the system for specific shear flow profiles. We have chosen to consider the case of a tangent hyperbolic profile of the shear flow in our studies. We observe that both compressibility and dispersive effects present in the case of dusty plasma medium reduce the growth rate of the KH mode.

We have also carried out perturbative analytical calculation to obtain the correction in growth rate due to the presence of compressibility. It is clear from such a calculation also that the presence of compressibility reduces the KH growth rate. The reason for this being that the free energy in the shear flow now finds an additional channel of release by the excitation of compressible modes in the system.

The nonlinear 2-D simulations with an initial shear flow profile shows the KH excitations. The linear growth rate obtained numerically from simulations are found to match with the eigen value estimates. In the nonlinear regime of the simulations the vortices get formed at the shear layer. The usual process of vortex coalescence is also observed in this case. The only difference in this case is that the coalesced vortices have an elliptical instead of the circular forms. The rotating elliptical structures in this case produce reversible oscillations in the perturbed kinetic energy evolution in the nonlinear regime. At each coalescence, however, an irreversible jump in perturbed kinetic energy is observed.

- **Existence of transverse shear waves in strongly coupled dusty plasma medium**

  The strongly coupled dusty plasma medium supports transverse shear wave in addition to compressible DAW's. However, the transverse nature of the mode requires two or higher dimension for its existence. We have simulated this mode numerically and have been able to verify the the linear dispersion characteristics of this particular mode. The phase velocity of the propagating waves are observed to match with the analytical expression, viz., $v_{ph} \sim \sqrt{\eta/\tau_m}$.

- **Shear flow instability in strongly coupled dusty plasma medium**

  The linear stability analysis of nonlocal KH mode for the 2-D sheared flow (the specific case of Tangent Hyperbolic sheared flow profile was studied) in the strongly coupled medium shows that the growth rate lies between the KH growth rates for the viscous and the inviscid hydrodynamic fluid. As the values of τ_m, the relaxation parameter is increased (i.e. with increase in coupling parameter Γ), we observe that the growth rate increases but continues to reside between the purely viscous and the inviscid hydrodynamic limits.

In addition to nonlocal KH mode instability, the shear flow in strongly coupled medium also supports a local instability. This is quite unlike the case of weakly coupled dusty plasma which does not support any growing local mode. It is also found that while v_0'' is responsible for the existence of KH instability, the v_0' is prime cause for local sheared flow instability. Here, $'$ indicates spatial derivative.

- **Phenomena of Recurrence in strongly coupled shear flow instability**

  The nonlinear regime of the sheared flow instability for the strongly coupled medium was studied by simulations. It is observed that in the nonlinear state the system exhibits an interesting interplay between vortex coalescence and its stretching followed by the KH instability repeatedly. This recurrence phenomena occurs for a couple of cycles and eventually it is followed by certain small scale vortex formation which are well separated from the original shear scale. The formation of small scale structures in this particular case is in distinct contrast to the inverse cascade behavior exhibited by ordinary fluids in 2-D.

- **2-D turbulence in Visco-Elastic fluids: A scale separation in the power spectra**

  The interplay between vortex coalescence and small scale formation observed in the context of KH instability suggests that the behavior of spectral cascade for the 2-D strongly coupled medium is distinct from the ordinary fluids. To study the phenomena of spectral cascade behavior we have studied the evolution of a given spectrum of random fluctuation. The evolved spectrum exhibits a power law, with a break in spectrum. The location of spectral break, however, is observed to evolve with time. Furthermore, the break is prominent when the initial spectral excitations are at short scales. These features can be understood by realizing the existence of two distinct time scale regime in the model. For time scales longer than the relaxation time τ_m, the GHD dynamics is similar to that of the ordinary fluid, exhibiting phenomena of inverse cascade. However, for shorter time scales the elastic nature of the fluid plays a predominant role. In this short time scale elastic limit the system does not respect the conservation of two invariants and direct cascade occurs. This is also apparent from the existence of local instabilities for the sheared system in the case of strong coupling. The interplay of these two dynamical features of the spectral cascade results in a spectral break.

8.2 Future scope of the work

The thesis results provide a direction towards lot of possibilities which could be explored in weakly as well strongly coupled plasmas. The formation of cusp structures, recurrence of vortex formation in sheared flow, the nature of turbulence are few of the interesting results predicted in strongly coupled dusty plasmas which needs to be verified by different possible experimental and numerical means. Here, we will present a point wise discussion over further possibilities of explorations in this particular area.

- The Generalized Hydrodynamic model is a phenomenological model which successfully explains many collective features of strongly coupled dusty plasmas. The model is a variant of *Maxwell's* model extensively used to explain visco-elastic fluids. In the present model, we have considered only one constant relaxation time scale. In actual dusty plasma medium or in other visco-elastic materials, multiple relaxation time scales are possible. Similarly, the viscosity which we have considered as a constant parameter could have a functional form depending on space and time. Inclusion of these properties will help us to look at more realistic view of dusty plasma as visco-elastic fluids.

- Present thesis assumes electrons and ions as inertialess species while studying the collective dynamics of dusty plasma medium, as the time scales and length scales for collective dynamics in these different species are well separated. But certain phenomena like dust void formation, dust rotation (observed in dusty plasma experiments) require the dynamics of ions to be included along with dust dynamics. For example, ion streaming is important for the formation of dust voids and the phenomenon of dust rotation occurs due to magnetized ions. These magnetized ions rotate fast and because of momentum transfer, dust also starts rotation [147, 148]. To understand such experimental observations in the strong coupling limit, one would need to incorporate ion dynamics along with the dust dynamic in the GHD and Poisson coupling.

- Throughout the thesis, the studies of dusty plasma medium assume the dust particles carrying constant charge. But in a realistic situation, the charge on dust species varies in time depending on a charging mechanism [57]. Inclusion of the mechanism of charge fluctuation may be interesting.

- In present thesis, we have employed GHD fluid model to study dusty plasma medium assuming the medium as visco-elastic fluid. Another way to study such medium is the particle approach (i.e. Molecular Dynamics). With the present computational facilities, realistic particle simulations are possible for dusty plasmas having typical density of the order $10^6 - 10^8/m^2$ in laboratory experiments. In such studies, the inter particle potential between dust particles has been taken of *Yukawa* potential form. The large scale simulations could be carried out to make a comparative study of the two approaches. Also, the particle studies will provide an opportunity to include the finite size effects of dust particles on the collective dust dynamics.

- Recently, experiments were performed to study turbulent flows in visco-elastic fluids [101]. Similar experimental studies could help us to understand the similarities and differences of dusty plasmas with visco-elastic fluids.

- The dusty plasmas were found to show exceptional similarities with polymer liquids in various experiments [149, 150]. The explorations to study such similarities opens up an entirely new domain of research.

Bibliography

[1] Lee-Wen Teng, Mei-Chu Chang, Yu-Ping Tseng, and Lin I. Wave-particle dynamics of wave breaking in the self-excited dust acoustic wave. *Phys. Rev. Lett.*, 103(2424):1–4, 2009.

[2] M. Schwabe, M. Rubin-Zuzic, S. Zhdanov, A. V. Ivlev, H. M. Thomas, and G. E. Morfill. Formation of bubbles, blobs, and surface cusps in complex plasmas. *Phys. Rev. Lett.*, 102(25):255005, Jun 2009.

[3] Anatoli P Nefedov, Gregor E Morfill, Vladimir E Fortov, Hubertus M Thomas, Hermann Rothermel, Tanja Hagl, Alexei V Ivlev, Milenko Zuzic, Boris A Klumov, Andrey M Lipaev, Vladimir I Molotkov, Oleg F Petrov, Yuri P Gidzenko, Sergey K Krikalev, William Shepherd, Alexandr I Ivanov, Maria Roth, Horst Binnenbruck, John A Goree, and Yuri P Semenov. Pke-nefedov: plasma crystal experiments on the international space station. *New Journal of Physics*, 5(1):33, 2003.

[4] P. Bandyopadhyay, G. Prasad, A. Sen, and P. K. Kaw. Experimental study of nonlinear dust acoustic solitary waves in a dusty plasma. *Phys. Rev. Lett.*, 101:065006, Aug 2008.

[5] A. Melzer, S. Nunomura, D. Samsonov, Z. W. Ma, and J. Goree. Laser-excited mach cones in a dusty plasma crystal. *Phys. Rev. E*, 62:4162–4176, Sep 2000.

[6] A Barkan, R.L. Merlino, and N. D'Angelo. Laboratory observation of the dust-acoustic wave mode. *Physics of Plasmas*, 2(1010):3563–3565, 1995.

[7] J. B. Pieper, J. Goree, and R. A. Quinn. Three-dimensional structure in a crystallized dusty plasma. *Phys. Rev. E*, 54:5636–5640, Nov 1996.

[8] Hunter John K. and Saxton Ralph. Dynamics of director fields. *SIAM J. APPL. MATH.*, 51(6):1498–1521, 1991.

[9] Gregor E. Morfill and Alexei V. Ivlev. Complex plasmas: An interdisciplinary research field. *Rev. Mod. Phys.*, 81(4):1353–1404, Oct 2009.

[10] P. K. Shukla. A survey of dusty plasma physics. *Physics of Plasmas*, 8(5):1791–1803, 2001.

[11] P. K. Shukla and B. Eliasson. *Colloquium*: Fundamentals of dust-plasma interactions. *Rev. Mod. Phys.*, 81:25–44, Jan 2009.

[12] Heinz M. Wiechen. Simulations of Kelvin-Helmholtz modes in the dusty plasma environment of noctilucent clouds. *Journal of Plasma Physics*, 73(05):649–658, October 2006.

[13] A.I. Ershkovich. Solar wind interaction with the tail of comet kohoutek. *Planetary and Space Science*, 24(3):287 – 291, 1976.

[14] Heinz M. Wiechen. Simulations of Kelvin-Helmholtz modes in partially ionized dusty plasmas comparing different charge numbers, charge polarities, and masses of the dust. *Physics of Plasmas*, 13(6):062104, 2006.

[15] O Havnes, T Aslaksen, TW Hartquist, and F Li. Probing the properties of planetary ring dust by the observation of mach cones. *Journal of geophysical*, 100:1731–1734, 1995.

[16] O. Havnes, F. Li, T.W. Hartquist, T. Aslaksen, and a. Brattli. Mach cones in dusty plasmas in planetary rings and in laboratory experiments. *Planetary and Space Science*, 49(2):223–229, February 2001.

[17] DA Mendis and M. Rosenberg. Cosmic dusty plasmas. *Annual Review of Astronomy and Astrophysics*, 32:419–463, 1994.

[18] N. D'Angelo and B. Song. The Kelvin-Helmholtz instability in dusty plasmas. *Planetary and Space Science*, 38(12):1577–1579, 1990.

[19] A. A. Mamun, P. K. Shukla, and R. Bingham. Dust-Alfvén Mach cones in Saturn's dense rings. *Journal of Experimental and Theoretical Physics Letters*, 77(10):541–545, May 2003.

[20] Q. Z. Luo, N. D'Angelo, and R. L. Merlino. The Kelvin-Helmholtz instability in a plasma with negatively charged dust. *Physics of Plasmas*, 8(1):31, 2001.

[21] A Piel and A Melzer. Dynamical processes in complex plasmas. *Plasma physics and controlled fusion*, 44:1–26, 2002.

[22] G. E. Morfill, H. M. Thomas, U. Konopka, H. Rothermel, M. Zuzic, A. Ivlev, and J. Goree. Condensed plasmas under microgravity. *Phys. Rev. Lett.*, 83:1598–1601, Aug 1999.

[23] J. Pramanik, G. Prasad, A. Sen, and P. K. Kaw. Experimental observations of transverse shear waves in strongly coupled dusty plasmas. *Phys. Rev. Lett.*, 88(17):175001, Apr 2002.

[24] P. Bandyopadhyay, G. Prasad, A. Sen, and P. K. Kaw. Experimental observation of strong coupling effects on the dispersion of dust acoustic waves in a plasma. *Phys. Lett. A*, 368:491, 2007.

[25] Aigen Li. Astrophysics: Cosmic crystals caught in the act. *Nature*, 459:173–176, 2009.

[26] Hubertus M. Thomas and Gregor E. Morfill. Melting dynamics of a plasma crystal. *Nature*, 379:806–809, Feb 1996.

[27] J.H. Chu and I Lin. Direct observation of coulomb crystals and liquids in strongly coupled rf dusty plasmas. *Phys. Rev. Lett.*, 72:4009–4012, 1994.

[28] Setsuo Ichimaru. Strongly coupled plasmas: high-density classical plasmas and degenerate electron liquids. *Rev. Mod. Phys.*, 54:1017–1059, Oct 1982.

[29] E. Schatzman. *White Dwarfs*. Amsterdam: North-Holland Publications, 1958.

[30] R. Kodama, P. A. Norreys, K. Mima, A. E. Dangor, R. G. Evans, H. Fujita, Y. Kitagawa, K. Krushelnick, T. Miyakoshi, N. Miyanaga, T. Norimatsu, S. J. Rose, T. Shozaki, K. Shigemori, A. Sunahara, M. Tampo, K. A. Tanaka, Y. Toyama, T. Yamanaka, and M. Zepf. Fast heating of ultrahigh-density plasma as a step towards laser fusion ignition. *Nature*, 412(6849):798–802, aug 2001.

[31] M. S. Murillo. Using fermi statistics to create strongly coupled ion plasmas in atom traps. *Phys. Rev. Lett.*, 87:115003, Aug 2001.

[32] T. C. Killian, S. Kulin, S. D. Bergeson, L. A. Orozco, C. Orzel, and S. L. Rolston. Creation of an ultracold neutral plasma. *Phys. Rev. Lett.*, 83:4776–4779, Dec 1999.

[33] G J Kalman, K I Golden, Z Donko, and P Hartmann. The quasilocalized charge approximation. *Journal of Physics: Conference Series*, 11(1):254, 2005.

[34] Kenneth I. Golden and Gabor J. Kalman. Quasilocalized charge approximation in strongly coupled plasma physics. *Physics of Plasmas*, 7(1):14–32, 2000.

[35] M. Rosenberg and G. Kalman. Dust acoustic waves in strongly coupled dusty plasmas. *Phys. Rev. E*, 56(6):7166–7173, Dec 1997.

[36] P Hartmann, Z Donkó, GJ Kalman, and S Kyrkos. Collective dynamics of complex plasma bilayers. *Physical Review Letters*, 245002(December):1–4, 2009.

[37] H. Ohta and S. Hamaguchi. Wave dispersion relations in yukawa fluids. *Phys. Rev. Lett.*, 84:6026–6029, Jun 2000.

[38] Bin Liu and J. Goree. Shear viscosity of two-dimensional yukawa systems in the liquid state. *Phys. Rev. Lett.*, 94(18):185002, May 2005.

[39] D Samsonov, J Goree, Hm Thomas, and Ge Morfill. Mach cone shocks in a two-dimensional Yukawa solid using a complex plasma. *Physical review. E, Statistical physics, plasmas, fluids, and related interdisciplinary topics*, 61(5B):5557–72, May 2000.

[40] Z Donkó and P Hartmann. Shear viscosity of strongly coupled Yukawa liquids. *Physical Review E*, page 026408, 2008.

[41] J Ashwin and R Ganesh. Kelvin Helmholtz Instability in Strongly Coupled Yukawa Liquids. *Physical Review Letters*, 215003(May):1–4, 2010.

[42] J Ashwin and R. Ganesh. Coherent Vortices in Strongly Coupled Liquids. *Physical Review Letters*, 106(13):135001, March 2011.

[43] N.N. Rao, P.K. Shukla, and M.Y. Yu. Dust-acoustic waves in dusty plasmas. *Planetary and Space Science*, 38(4):543–546, 1990.

[44] P K Shukla and V P Silin. Dust ion-acoustic wave. *Physica Scripta*, 45(5):508, 1992.

[45] B. Eliasson and P. K. Shukla. Dust acoustic shock waves. *Phys. Rev. E*, 69:067401, Jun 2004.

[46] P.K. Shukla and A.A. Mamun. Dust-acoustic shocks in a strongly coupled dusty plasma. *IEEE Transactions on Plasma Science*, 29:221–225, Apr 2001.

[47] N N Rao. Dust-acoustic kdv solitons in weakly non-ideal dusty plasmas. *Physica Scripta*, 1998(T75):179, 1998.

[48] P K Shukla and A A Mamun. Solitons, shocks and vortices in dusty plasmas. *New Journal of Physics*, 5(1):17, 2003.

[49] S. I. Popel, A. P. Golub', T. V. Losseva, A. V. Ivlev, S. A. Khrapak, and G. Morfill. Weakly dissipative dust-ion-acoustic solitons. *Phys. Rev. E*, 67:056402, May 2003.

[50] S. Hamaguchi and R. T. Farouki. Polarization force on a charged particulate in a nonuniform plasma. *Phys. Rev. E*, 49:4430–4441, May 1994.

[51] S. A. Khrapak, A. V. Ivlev, V. V. Yaroshenko, and G. E. Morfill. Influence of a polarization force on dust acoustic waves. *Phys. Rev. Lett.*, 102:245004, Jun 2009.

[52] P Bandyopadhyay, U Konopka, S A Khrapak, G E Morfill, and A Sen. Effect of polarization force on the propagation of dust acoustic solitary waves. *New Journal of Physics*, 12(7):073002, 2010.

[53] T.G. Northrop and T.J. Birmingham. Plasma drag on a dust grain due to coulomb collisions. *Planetary and Space Science*, 38(3):319 – 326, 1990.

[54] Leonardo Patacchini and Ian H. Hutchinson. Fully self-consistent ion-drag-force calculations for dust in collisional plasmas with an external electric field. *Phys. Rev. Lett.*, 101:025001, Jul 2008.

[55] S. Khrapak and G. Morfill. Basic processes in complex (dusty) plasmas: Charging, interactions, and ion drag force. *Contributions to Plasma Physics*, 49(3):148–168, 2009.

[56] A V Ivlev and G Morfill. Dust acoustic solitons with variable particle charge: Role of the ion distribution. *Physical Review*, 63:1–5, 2001.

[57] M R Jana, A Sen, and P K Kaw. Grain Charge Fluctuation Dynamics on Collective Modes in a Magnetized Dusty Plasma. *Physica*, 51:385–389, 1995.

[58] M S Murillo and I Introduction. Longitudinal collective modes of strongly coupled dusty plasmas at finite frequencies and wavevectors. *Physics of Plasmas*, 7(1):33–38, 2000.

[59] P. K. Kaw and A. Sen. Low frequency modes in strongly coupled dusty plasmas. *Phys. Plasmas*, **5**(10):3552–3559, 1998.

[60] M.S. Murillo. Static local field correction description of acoustic waves in strongly coupling dusty plasmas. *Phys. Plasmas*, 5:3116, 1998.

[61] D Winske and M S Murillo. Numerical simulation of dust-acoustic waves. *Physical Review E*, 59(2):2263–2272, 1999.

[62] M. S. Murillo. Critical wave vectors for transverse modes in strongly coupled dusty plasmas. *Phys. Rev. Lett.*, 85(12):2514–2517, Sep 2000.

[63] H. Ikezi. Coulomb solid of small particles in plasmas. *Physics of Fluids*, 29(6):1764–1766, 1986.

[64] Frank Melandsø. Lattice waves in dust plasma crystals. *Physics of Plasmas*, 3(11):3890–3901, 1996.

[65] A. A. Mamun and R. A. Cairns. Dust-acoustic shock waves due to strong correlation among arbitrarily charged dust. *Phys. Rev. E*, 79:055401, May 2009.

[66] W. (Lord Kelvin) Thomson. Hydrokinetic solutions and observations. *Philosophical Magazine*, 42(4):362–377, 1871.

[67] H.von Helmholtz. On the discontinuous movements of fluids. *Monthly Reports of the Royal Prussian Academy of Philosophy in Berlin*, 23:215–228, 1868.

[68] Guido T. Birk and H. Wiechen. Shear flow instabilities in magnetized partially ionized dense dusty plasmas. *Physics of Plasmas*, 9(3):964, 2002.

[69] A. Barkan, N. D'Angelo, and R.L. Merlino. Experiments on ion-acoustic waves in dusty plasmas. *Planetary and Space Science*, 44(3):239 – 242, 1996.

[70] J.B. Pieper and J. Goree. Dispersion of plasma dust acoustic waves in the strong-coupling regime. *Phys. Rev. Lett.*, 77:3137, 1996.

[71] H. R. Prabhakara and V. L. Tanna. Trapping of dust and dust acoustic waves in laboratory plasmas. *Physics of Plasmas*, 3(8):3176–3181, 1996.

[72] Y. Nakamura, H. Bailung, and P. K. Shukla. Observation of ion-acoustic shocks in a dusty plasma. *Phys. Rev. Lett.*, 83:1602–1605, Aug 1999.

[73] Y. Nakamura and A. Sarma. Observation of ion-acoustic solitary waves in a dusty plasma. *Physics of Plasmas*, 8(9):3921–3926, 2001.

[74] J. Heinrich, S.-H. Kim, and R. L. Merlino. Laboratory observations of self-excited dust acoustic shocks. *Phys. Rev. Lett.*, 103:115002, Sep 2009.

[75] D. Samsonov, G. Morfill, H. Thomas, T. Hagl, H. Rothermel, V. Fortov, A. Lipaev, V. Molotkov, A. Nefedov, O. Petrov, A. Ivanov, and S. Krikalev. Kinetic measurements of shock wave propagation in a three-dimensional complex (dusty) plasma. *Phys. Rev. E*, 67:036404, Mar 2003.

[76] D. Samsonov, S. K. Zhdanov, R. A. Quinn, S. I. Popel, and G. E. Morfill. Shock melting of a two-dimensional complex (dusty) plasma. *Phys. Rev. Lett.*, 92:255004, Jun 2004.

[77] S. Nunomura, D. Samsonov, and J. Goree. Transverse waves in a two-dimensional screened-coulomb crystal (dusty plasma). *Phys. Rev. Lett.*, 84(22):5141–5144, May 2000.

[78] H. Rothermel, T. Hagl, G. E. Morfill, M. H. Thoma, and H. M. Thomas. Gravity compensation in complex plasmas by application of a temperature gradient. *Phys. Rev. Lett.*, 89:175001, Oct 2002.

[79] A. Melzer, V. A. Schweigert, and A. Piel. Transition from attractive to repulsive forces between dust molecules in a plasma sheath. *Phys. Rev. Lett.*, 83:3194–3197, Oct 1999.

[80] T Nitter. Levitation of dust in rf and dc glow discharges. *Plasma Sources Science and Technology*, 5(1):93, 1996.

[81] H. Thomas, G. E. Morfill, V. Demmel, J. Goree, B. Feuerbacher, and D. Möhlmann. Plasma crystal: Coulomb crystallization in a dusty plasma. *Phys. Rev. Lett.*, 73:652–655, Aug 1994.

[82] A. Homann, A. Melzer, S. Peters, R. Madani, and A. Piel. Laser-excited dust lattice waves in plasma crystals. *Physics Letters A*, 242(3):173 – 180, 1998.

[83] A. Homann, A. Melzer, S. Peters, and A. Piel. Determination of the dust screening length by laser-excited lattice waves. *Phys. Rev. E*, 56:7138–7141, Dec 1997.

[84] G. S. Selwyn, J. Singh, and R. S. Bennett. In situ laser diagnostic studies of plasma generated particulate contamination. *Journal of Vacuum Science and Technology A: Vacuum, Surfaces, and Films*, 7(4):2758–2765, 1989.

[85] S. I. Krasheninnikov, Y. Tomita, R. D. Smirnov, and R. K. Janev. On dust dynamics in tokamak edge plasmas. *Physics of Plasmas*, 11(6):3141–3150, 2004.

[86] J Winter. Dust in fusion devices - experimental evidence, possible sources and consequences. *Plasma Physics and Controlled Fusion*, 40(6):1201, 1998.

[87] E. C. Harding, J. F. Hansen, O. A. Hurricane, R. P. Drake, H. F. Robey, C. C. Kuranz, B. A. Remington, M. J. Bono, M. J. Grosskopf, and R. S. Gillespie. Observation of a kelvin-helmholtz instability in a high-energy-density plasma on the omega laser. *Phys. Rev. Lett.*, 103:045005, Jul 2009.

[88] L. Ofman and B. J. Thompson. Sdo/aia observation of kelvin-helmholtz instability in the solar corona. *The Astrophysical Journal Letters*, 734(1):L11, 2011.

[89] A. K. Srivastava, R. Erdélyi, Durgesh Tripathi, V. Fedun, N. C. Joshi, and P. Kayshap. Observational evidence of sausage-pinch instability in solar corona by sdo/aia. *The Astrophysical Journal Letters*, 765(2):L42, 2013.

[90] U. Konopka, D. Samsonov, A. V. Ivlev, J. Goree, V. Steinberg, and G. E. Morfill. Rigid and differential plasma crystal rotation induced by magnetic fields. *Phys. Rev. E*, 61:1890–1898, Feb 2000.

[91] K. A. Pacha, J. R. Heinrich, S.-H. Kim, and R. L. Merlino. Observation of the taylor instability in a dusty plasma. *Physics of Plasmas*, 19(1):014501, 2012.

[92] Hermann A. Haus and William S. Wong. Solitons in optical communications. *Rev. Mod. Phys.*, 68:423–444, Apr 1996.

[93] J.F. Miramar Blazquer. Application of solitons to the study of laser propagation into a thermonuclear plasma in inertial confinement fusion. *Laser and Particle Beams*, 20:153–157, 0 2002.

[94] Sanat Kumar Tiwari, Amita Das, Predhiman Kaw, and Abhijit Sen. Observation of sharply peaked solitons in dusty plasma simulations. *New Juornal of Physics*, 14:063008, 2012.

[95] S. V. Bulanov, F. Pegoraro, A. M. Pukhov, and A. S. Sakharov. Transverse-wake wave breaking. *Phys. Rev. Lett.*, 78:4205–4208, Jun 1997.

[96] Sanat Kumar Tiwari, Amita Das, Predhiman Kaw, and Abhijit Sen. Longitudinal singular response of dusty plasma medium in weak and strong coupling limits. *Physics of Plasmas*, 19(1):013706, 2012.

[97] Sanat Kumar Tiwari, Amita Das, Predhiman Kaw, and Abhijit Sen. Kelvin–helmholtz instability in a weakly coupled dust fluid. *Physics of Plasmas*, 19(2):023703, 2012.

[98] Sanat Kumar Tiwari, Amita Das, Dilip Angom, Bhavesh G. Patel, and Predhiman Kaw. Kelvin-helmholtz instability in a strongly coupled dusty plasma medium. *Physics of Plasmas*, 19(7):073703, 2012.

[99] J.Frenkel. *Kinetic Theory Of Liquids*. Dover Publications, 1955.

[100] R. B. Bird, R. C. Armstrong, and O. Hassager. *Dynamics of Polymeric Liquids*. Wiley-Interscience Publication, 1987.

[101] A. Groisman and V. Steinberg. Elastic turbulence in a polymer solution flow. *Nature*, 405:53–55, 2000.

[102] Alexander Groisman and Victor Steinberg. Elastic turbulence in curvilinear flows of polymer solutions. *New Journal of Physics*, 6(1):29, 2004.

[103] Dandan Chen, Kenneth W. Desmond, and Eric R. Weeks. Topological rearrangements and stress fluctuations in quasi-two-dimensional hopper flow of emulsions. *Soft Matter*, 8:10486–10492, 2012.

[104] Yan Feng, J. Goree, and Bin Liu. Frequency-dependent shear viscosity of a liquid two-dimensional dusty plasma. *Phys. Rev. E*, 85:066402, Jun 2012.

[105] M. S. Murillo. Viscosity estimates of liquid metals and warm dense matter using the Yukawa reference system. *High Energy Density Physics*, 4:49–57, April 2008.

[106] Setsuo Ichimaru, Hiroshi Iyetomi, and Shigenori Tanaka. Statistical physics of dense plasmas: Thermodynamics, transport coefficients and dynamic correlations. *Physics Reports*, 149(2-3):91 – 205, 1987.

[107] J.P. Boris, A.M. Landsberg, E.S. Oran, and J.H. Gardner. Lcpfct - a flux-corrected transport algorithm for solving generalized continuity equations. Technical Report NRL Memorandum Report 93-7192., Navel Research Laboratory, 1993.

[108] F. Verheest. *Waves in Dusty Space Plasmas*. Kluwer Academic, Dordrecht, 2000.

[109] A.A. Mamun P.K. Shukla. *Introduction to Dusty Plasma Physics.* Institute of Physics, Bristol, 2002.

[110] R L Merlino, A Barkan, C Thompson, and N D'Angelo. Experiments on waves and instabilities in dusty plasmas. *Plasma Physics and Controlled Fusion*, 39(5A):A421, 1997.

[111] A. V. Volosevich and C.-V. Meister. Nonlinear electrostatic structures in collisional dusty plasmas. *Contributions to Plasma Physics*, 42(1):61–65, 2002.

[112] Farah Aziz, Hitendra K Malik, Sebastian Enge, Lars Stollenwerk, and Ulrich Stroth. Experimental and simulation studies on soliton generation in a double-plasma device: role of fast ions. *Plasma Physics and Controlled Fusion*, 53(6):065012, 2011.

[113] H. Ikezi, R. J. Taylor, and D. R. Baker. Formation and interaction of ion-acoustic solitions. *Phys. Rev. Lett.*, 25:11–14, Jul 1970.

[114] Zhijun Qiao and Xin Brian Qiao. Cusp solitons and cusp-like singular solutions for nonlinear equations. *Chaos Solitons and Fractals*, **25**(1):153, 2005.

[115] D. Farina and S. V. Bulanov. Relativistic electromagnetic solitons in the electron-ion plasma. *Phys. Rev. Lett.*, 86(23):5289–5292, Jun 2001.

[116] W. Masood, H. A. Shah, N. L. Tsintsadze, and M. N.S. Qureshi. Dust alfven ordinary and cusp solitons and modulational instability in a self-gravitating magneto-radiative plasma. *The European Physical Journal D - Atomic, Molecular, Optical and Plasma Physics*, 59:413–419, 2010. 10.1140/epjd/e2010-00180-x.

[117] Z. Ehsan, N. L. Tsintsadze, G. Murtaza, and H. A. Shah. Two types of lower-hybrid waves in dusty plasmas and cusp solitons. *Physics of Plasmas*, 16(2):023702, 2009.

[118] Miklos Porkolab and Martin V. Goldman. Upper-hybrid solitons and oscillating-two-stream instabilities. *Physics of Fluids*, 19(6):872–881, 1976.

[119] L Kavitha, P Sathishkumar, T Nathiyaa, and D Gopi. Cusp-like singular soliton solutions of jaulent-miodek equation using symbolic computation. *Physica Scripta*, 79(3):035403, 2009.

[120] M. Jaulent and I. Miodek. Nonlinear evolution equations associated with 'enegry-dependent schrodinger potentials'. *Letters in Mathematical Physics*, 1:243–250, 1976. 10.1007/BF00417611.

[121] Brian O Storey. *private communication.* Jan. 25 2007.

[122] B. M. Veeresha, S. K. Tiwari, A. Sen, P. K. Kaw, and A. Das. Nonlinear wave propagation in strongly coupled dusty plasmas. *Phys. Rev. E*, **81**(3):036407, Mar 2010.

[123] Roberto Camassa and Darryl D. Holm. An integrable shallow water equation with peaked solitons. *Phys. Rev. Lett.*, 71:1661–1664, Sep 1993.

[124] Hunter J. K. and Zheng Y. On a completely integrable nonlinear hyperbolic variational equation. *Physica D*, 79:361–386, 1994.

[125] W Hereman, P P Banerjee, and M R Chatterjee. Derivation and implicit solution of the harry dym equation and its connections with the korteweg-de vries equation. *Journal of Physics A: Mathematical and General*, 22(3):241, 1989.

[126] P. G. Drazin. *Introduction to Hydrodynamic Stability.* Cambridge University Press, UK, 2002.

[127] S. Chandrasekhar. *Hydrodynamic and hydromagnetic stability.* Oxford: Clarendon Press, 1961.

[128] Akira Miura and P. L. Pritchett. Nonlocal Stability Analysis of the MHD Kelvin-Helmholtz Instability in a Compressible Plasma. *Journal of Geophysical Research*, 87(A9):7431–7444, 1982.

[129] A. Otto and D. H. Fairfield. Kelvin-Helmholtz instability at the magnetotail boundary: MHD simulation and comparison with Geotail observations. *Journal of Geophysical Research*, 105(A9):21175–21190, 2000.

[130] William Blumen. Shear layer instability of an inviscid compressible fluid. *Journal of Fluid Mechanics*, **40**(04):769–781, 1970.

[131] R. L. Merlino, A. Barkan, C. Thompson, and N. D'Angelo. Laboratory studies of waves and instabilities in dusty plasmas. *Physics of Plasmas*, 5(5):1607–1614, 1998.

[132] D. Samsonov, J. Goree, Z. Ma, A. Bhattacharjee, H. Thomas, and G. Morfill. Mach Cones in a Coulomb Lattice and a Dusty Plasma. *Physical Review Letters*, 83(18):3649–3652, November 1999.

[133] N. D'Angelo. Current-driven electrostatic dust-cyclotron instability in a collisional plasma. *Planetary and Space Science*, 46(11-12):1671 – 1676, 1998.

[134] G.T. Birk, H. Wiechen, A. Kopp, and H. Lesch. The magnetization of protoplanetary discs. *Monthly Notices of the Royal Astronomical Society*, 339(2):455–459, 2003.

[135] Neeraj Jain, Amita Das, Predhiman Kaw, and Sudip Sengupta. Nonlinear electron magnetohydrodynamic simulations of sausage-like instability of current channels. *Physics of Plasmas*, 10(1):29, 2003.

[136] A. Ng, P. Celliers, G. Xu, and A. Forsman. Electron-ion equilibration in a strongly coupled plasma. *Phys. Rev. E*, 52:4299–4310, Oct 1995.

[137] P. K. Shukla, A. A. Mamun, and D. A. Mendis. Nonlinear ion modes in a dense plasma with strongly coupled ions and degenerate electron fluids. *Phys. Rev. E*, 84:026405, Aug 2011.

[138] T. Pohl, T. Pattard, and J. M. Rost. Coulomb crystallization in expanding laser-cooled neutral plasmas. *Phys. Rev. Lett.*, 92:155003, Apr 2004.

[139] V. E. Fortov, I. T. Iakubov, and A. G. Khrapak. *Physics of Strongly Coupled Plasma.* Clarendon Press, Oxford, 2006.

[140] G. K. Batchelor. *An Introduction to Fluid Dynamics.* Cambridge University Press, 2000.

[141] L. G. Leal P. H. Steen M. Samimy, K. S. Breuer. *A Gallery of Fluid Motion.* Cambridge University Press, 2003.

[142] Anne Le Goff, Pablo Cobelli, and Guillaume Lagubeau. Supershear rayleigh waves at a soft interface. *Phys. Rev. Lett.*, 110:236101, Jun 2013.

[143] L. Pan, A. Morozov, C. Wagner, and P. E. Arratia. Nonlinear elastic instability in channel flows at low reynolds numbers. *Phys. Rev. Lett.*, 110:174502, Apr 2013.

[144] M. Brust, C. Schaefer, R. Doerr, L. Pan, M. Garcia, P. E. Arratia, and C. Wagner. Rheology of human blood plasma: Viscoelastic versus newtonian behavior. *Phys. Rev. Lett.*, 110:078305, Feb 2013.

[145] Piotr Habdas, Eric R. Weeks, and David G. Lynn. Squishy materials. *The Physics Teacher*, 44(5):276–279, 2006.

[146] R. S. Lakes. Viscoelastic measurement techniques. *Review of Scientific Instruments*, 75(4):797–810, 2004.

[147] M. Kretschmer, U. Konopka, S.K. Zhdanov, H.M. Thomas, G.E. Morfill, V.E. Fortov, V.I. Molotkov, A.M. Lipaev, and O.F. Petrov. Particles inside the void of a complex plasma. *Plasma Science, IEEE Transactions on*, 39(11):2758–2759, 2011.

[148] J. Goree, G. E. Morfill, V. N. Tsytovich, and S. V. Vladimirov. Theory of dust voids in plasmas. *Phys. Rev. E*, 59:7055–7067, Jun 1999.

[149] Eric R. Weeks. *Microscopy of soft materials.* Cambridge University Press, October 2010.

[150] Nabiha Saklayen, Gary L. Hunter, Kazem V. Edmond, and Eric R. Weeks. Slow dynamics in cylindrically confined colloidal suspensions. *AIP Conference Proceedings*, 1518(1):328–335, 2013.